Electrospun, Proton-Conducting Nanofiber Mats for use in Advanced Direct Methanol Fuel Cell Electrodes

by

Matthew S. Perrone

A Thesis

Submitted to the Faculty of the

WORCESTER POLYTECHNIC INSTITUTE

In partial fulfillment of the requirements for the

Degree of Master of Science

in

Chemical Engineering

Approved by:

_____

Dr. Ravindra Datta, Professor of Chemical Engineering, Major Advisor

_____

Dr. David DiBiasio, Professor of Chemical Engineering, Department Head

Table of Contents

Table of Figures

List of Tables

Table of Images

Abstract

For fuel cells to become commercially viable in a wider range of applications, the amount of catalyst must be reduced. One crucial area of the fuel cell assembly is the anode and cathode; these layers allow fuel and exhaust gases to diffuse, provide conduction paths for both protons and electrons, and house sites for electrocataytic reactions. Despite their multi-functionality and importance, these layers have received little attention in the way of engineering design. While Nafion and catalyst loading has been studied, the electrode layer is still considered a two-dimensional structure. By understanding the current electrode limitations, available materials, and interactions at the sites reaction sites, an intelligent, deliberate design of the anode and cathode layer can be undertaken. A three-dimensional, fibrous mat of continuous, networked proton-conducting fibers can decrease mass diffusion limitations while maintaining proton conductivity.

Nafion can be formed into these types of fibers via the fabrication technique of electrospinning. By forcing a solution of Nafion, solvent, and carrier polymer through a small nozzle under high electric voltage, the polymer can be extruded into fibers with nanometer-scale diameters. The ability to control the fiber morphology lies with solution, environmental and equipment properties. In order to successfully fabricate Nafion nanofibers, we looked to both existing methodologies as well as mathematical models to try to predict behavior and fabricate our own nanofibers. Once fabricated, these mats are assembled in a membrane-electrode assembly and tested with both methanol and hydrogen as fuel, with performance compared against known data for conventional MEAs.

We have been able to successfully electrospin Nafion® nanofibers continuously, creating fiber mats with fiber diameters near 400nm as verified by SEM. These mats were tested in a direct methanol fuel cell (DMFC) application as cathodes, and showed improved performance with a dilute methanol feed compared to conventional MEAs with equivalent Nafion and catalyst loading. An MEA fabricated with twin electrospun electrodes was compared against an equivalent conventional MEA, showing the same performance enhancement using a dilute methanol fuel.

Introduction

Fuel Cell Overview

Fuel cells have been attracting attention in recent decade as energy converting devices with a high degree of scalability; fuel cells can be designed to power small devices such as laptops to entire hospital complexes by splitting hydrogen gas into protons and electrons, and using the electrons as a source of electricity. Fuel cells have inherently high efficiency (utilizing 60% of the fuel's energy; internal combustion engines are ~20-30% efficient) and produce few, if any, emissions. Present concern of high energy demands, fossil fuel depletion, and environmental pollution make fuel cells an attractive alternative. In the past decade, there is a considerable rise in research in fuel cells compared to alternatives. This trend is seen in Figure 1.
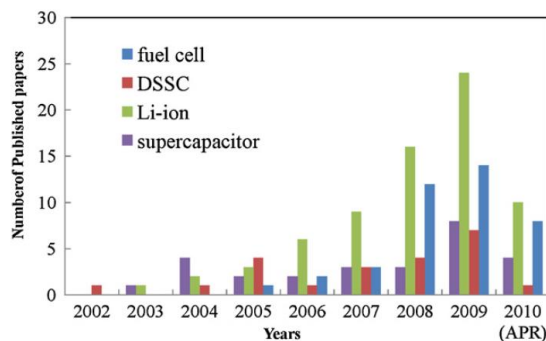
Figure 1: Number of published papers in alterative fuel storage focus areas[1]

Direct methanol fuel cells (DMFCs), using a potentially renewable, liquid methanol fuel which is easily stored and transported, simplifies low-temperature fuel cell systems compared to those based on H_2 fuel. The basic DMFC, in operation, is shown in Figure 2.

---

[1] (Dong, Kennedy, & Wu, 2011)

Fuel Gas Flow (Methanol)

O₂ Flow

Electrons

Gas Diffusion Layer (GDL) Carbon Cloth

Anode

Nafion® Proton Exchange Membrane (PEM)

Cathode

Gas Diffusion Layer (GDL) Carbon Cloth

Methanol

Protons

Oxygen

Carbon Dioxide

Water
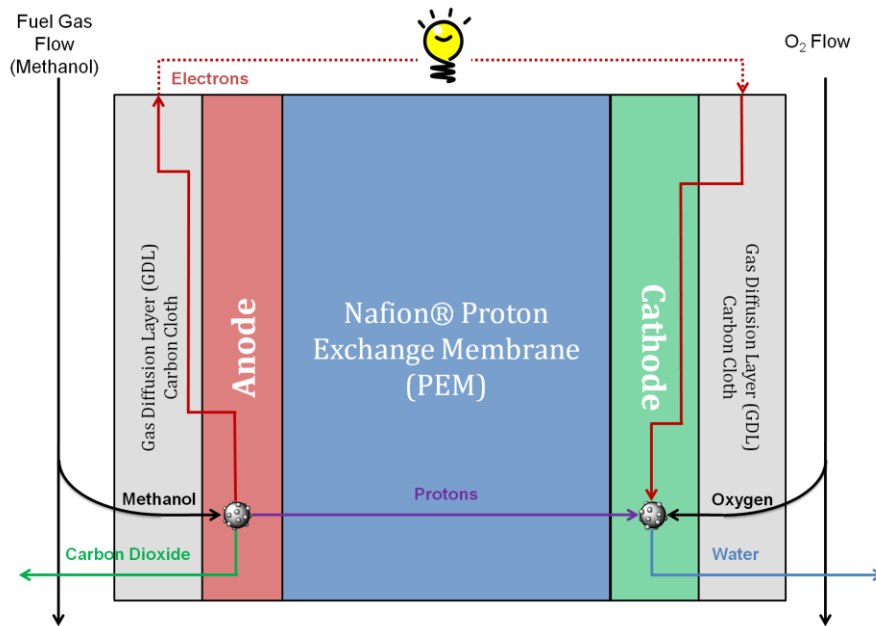
Figure 2: Basic schematic of a PEM fuel cell running MeOH conditions

Moving from left to right, a fuel gas, in our case of operation methanol (MeOH), is fed into the system. As it passes, some of the methanol will diffuse into the cell, traveling first through the gas diffusion layer (GDL) and into the anode, an electrode. In the electrode, the gaseous fuel species finds and active site on a catalyst particle and a hydrogen species is split into a proton and a pair of electrons. The protons, able to cross through the membrane, do so, while the electrons are forced around an external path, which is seen as an electric current with a measurable potential. The electrons are introduced back into the fuel cell, traveling from a current collector to the GDL and into the cathode by conduction, with the protons traveling across the membrane to reach the cathode. In the cathode, the electrons and the protons find an available catalyst particle and, combining with oxygen, reforms into water.

As described, electrode has three tasks. First, it must house catalyst particles for the reduction of the fuel gas to occur. Second, it must provide electron-conducting material so

the electrons can be transported out of the anode into the GDL to the external path. Third, the electrode must contain proton-conducting material, as the protons must travel inwards to contact the membrane and be transported across.

Current Limitations

For fuel cells to become commercially viable in a wider range of applications, the amount of catalyst must be reduced. One crucial area of the fuel cell assembly is the multi-functional the anode and cathode; these layers allow fuel and exhaust gases to diffuse, provide conduction paths for both protons and electrons, as well as house catalytic sites for proton/electron separation. Despite their importance, these layers have received little attention in the way of design; the electrode layer is still considered a two-dimensional structure.

By understanding the current gas diffusion limitations, available materials, and molecular interactions at the reaction sites, an intelligent, deliberate design of the anode and cathode layer can be undertaken.

A novel approach to the electrode morphology is to make a mat of continuous Nafion® nanofibers; this would potentially decrease the mass diffusion limitations of fuel and exhaust through the electrode, increase triple-phase interfaces, and utilize more Nafion® by mass, compared to a traditional scattered, gel-globule structure as long, thin fibers have a much higher surface area / volume ratio. A representation of an MEA utilizing these fibers is shown in Figure 3.
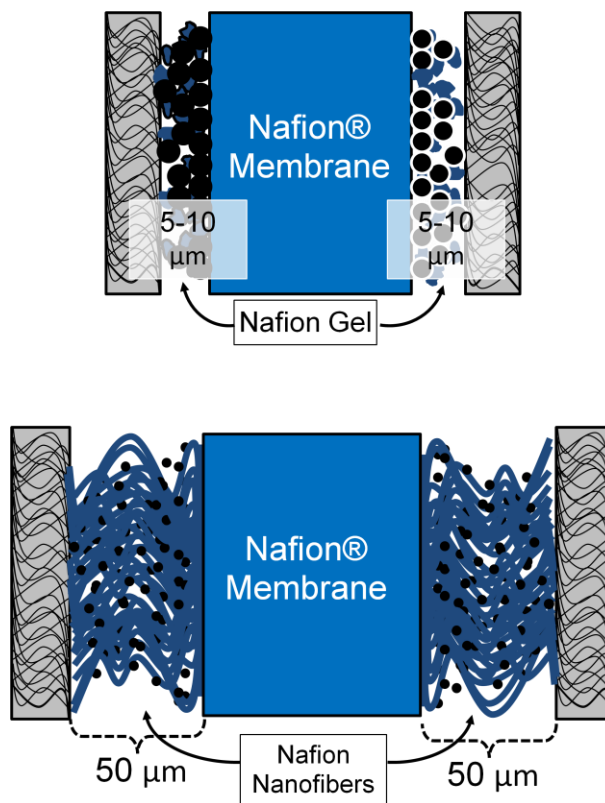
Figure 3: A basic schematic of a conventional DMFC with a traditional 2D electrode (top) and the proposed MEA, using 3D electrospun electrodes (bottom)

By forcing a solution of Nafion, solvent, and carrier polymer through a small nozzle under high electric voltage, the polymer can be electrospun into fibers with nanometer-scale diameters. This process is called electrospinning. The ability to control the fiber morphology lies with solution, environmental and equipment properties.

Goals

First, the repeatable, controllable fabrication of continuous, high-purity Nafion® fibers with an ideal diameter of 400nm (highest proton conductivity) needs to be achieved. Upon fabrication, assemble these fibers into a fibrous mat upon typical GDL material (carbon cloth with MPL) with a footprint of 5 cm^2 for single cell testing and comparison to other MEAs (lab and commercial) under both H_2/O_2 and MeOH feed conditions.

Literature Review

Direct Methanol Fuel Cells History

Early Developments[2]

While fuel cells are a fairly modern topic, the ideas behind such work, and the knowledge of phenomena behind the performance of fuel cells, has been around for nearly two centuries. Early work in Britain in 1800 led to the electrolysis of water; splitting two water molecules into two molecules of diatomic hydrogen gas and a single diatomic oxygen. Shortly thereafter, around 1832, Michael Faraday started to explore the ideas of electrolysis, and postulated Faraday's first two laws of electrolysis, which lead to Robert Grove's experiments in 1838. Grove discovered that by partially immersing two platinum electrodes into a bath of sulfuric acid, with the non-immersed ends fixed into sealed containers of hydrogen and oxygen, a current flow was achieved, and water would accumulate in the gas containers. Hooking these up into a series, his "Gas Battery" was formed, and is evidence of the first fuel cell, though the term was coined in 1889 when further experimentation was done.

As the centuries progressed, and such names as Friedrich Ostwald and Francis Bacon pushed the field of study along both theoretically and experimentally, fuel cells first started to be seen commercial applications in the 1950s. Used sparingly, due to cost, some notable examples are use on the Apollo spacecraft and a 1008-cell Allis Chalmers Tractor, able to produce 15kW at 1V per cell using a fuel gas mixture of mostly propane. These notable uses have found their way into various museums since.

---

[2] (Ortiz-Pivera, Reyer-Hernandez, & Febo, 2007)

Fuel cells have evolved, with many various types existing today, tailored for particular fuels as well as operating conditions. Proton exchange membrane (PEM) fuel cells are typically H_2/O_2 fed and run al low temperatures below 100°C. Molten carbonate fuel cells (MCFC) utilize molten salts at high temperature as an electrolyte, and have been operated on hydrogen, carbon monoxide, a slew of hydrocarbons and simulated coal gasification products. Solid oxide fuel cells (SOFC) use a hard, non-porous ceramic electrolyte and run at very high temperatures, 1800°F. Alkaline fuel cells (AFC) utilize a electrolyte of potassium hydroxide and operate around 160°F, but must be run with pure H_2/O_2, as it is susceptible to carbon contamination. Lastly, there are direct methanol fuel cells (DMFC) which utilize methanol as a fuel, and utilize Nafion® polymer, a perflourosulfonic acid (PFSA), as the electrolyte membrane.

Use of Methanol as Fuel

While there are a large number of fuel cell types, direct methanol fuel cells are fairly new, with research starting to pop up in the early 90's. The attractiveness of methanol as a fuel lies with its inherently high efficiency as a fuel in fuel cells, as well as its easy storage, transportation, and temperature the fuel cell needs to be operated at. Seen as a replacement for traditional Li-ion batteries, the DMFC can run for long periods of time, and can be instantaneously recharged by simply replacing the fuel cartridge, which could, if commercialized, be disposable or refillable.

Introduction of Nafion into the Electrode Layer

Nafion, a perflourosulphonic acid (PFSA), conducts protons via the sulfuric groups studded along the polymer backbone. The Nafion polymer is shown, chemically, in Figure 4.
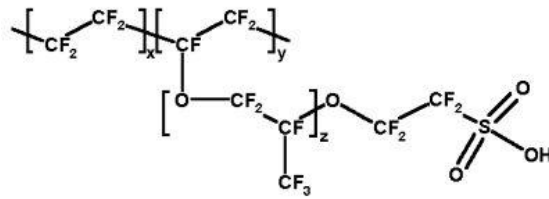
While Nafion was first utilized as a fuel cell membrane during the early development of PEMFC, the use in the electrode layer to aid in proton conduction (to wick away protons, aid in reaction kinetics and to fully utilize the catalyst) was not until the early 1990s, as this is when research for new electrode catalyst structures was developed, including a recast ionic polymer binder to aid in construction[3,4].

Kinetics and Catalysis of DMFC

Overview of reactions

Catalyst layer composition of the anode and cathode has developed to the point where they are not symmetrical; they are optimized for the task each electrode must complete. Typically, the anode catalyst consists of platinum and ruthenium and is carbon supported. The cathode catalyst usually only contains platinum, and is not always carbon supported. The carbon support allows for more efficient dispersion of the catalyst particles through the electrode layer. As methanol diffuses through the GDL and into the anode, the first step of the reaction is the oxidation of methanol into carbon monoxide, with the four protons and four electrons existing as free species; this is shown in equation 1.

$$CH_3OH \rightarrow CO + 4H^+ + 4e^- \tag{1}$$

---

[3] (Gottesfeld & Wilson, 1992)
[4] (Kosek, 1994)

The byproduct of this reaction, carbon monoxide, is a known catalyst poison for platinum. To eliminate the poison generated on the platinum surface, a different catalyst must be used. Ruthenium, Ru, has been introduced at a 1:1 ratio with Pt. The presence of Ru to water, which is present in an aqueous MeOH feed, will decompose water into a hydroxide radical; this radical can then react with an adsorbed CO molecule on the surface of a neighboring Pt atom, oxidizing the CO into CO_2, which can be wicked away from the cell as an exhaust gas that is much less toxic and poisonous. This reaction sequence is seen in equations 2 and 3.

$$H_2O \rightarrow OH\bullet + H^+ + e^- \tag{2}$$

$$CO + OH\bullet \rightarrow CO_2 + H^+ + e^- \tag{3}$$

The resulting overall half-reaction, is shown in equation 4.

$$CH_3OH + H_2O \rightarrow CO_2 + 6H^+ + 6e^- \tag{4}$$

As the electrons freed in the anode reaction are carried from the electrode, into the GDL, and around the outside path to do electrical work, the protons are selectively transported through the membrane to the cathode. Upon both species reaching the cathode, the reduction half-reaction occurs in the presence of oxygen, resulting in the formation of water, as seen in equation 5.

$$^3/_2\, O_2 + 6H^+ + 6e^- \rightarrow 3H_2O \tag{5}$$

The two half-reactions, when combined, form the overall reaction in equation 6. During the conversion of methanol, consumption of oxygen and production of carbon dioxide and water, six electrons were freed and used for external power.

$$CH_3OH + {}^3/_2O_2 \rightarrow CO_2 + 2H_2O \qquad\qquad (6)$$

Limiting factors

A methanol-fed fuel cell's operation is based upon this reaction; however, the ability to utilize the full potential of this reaction sequence has yet to be achieved, due to a plethora of limitations, be it physical, chemical or electrical. The reaction, according to thermodynamics, is able to produce 1.2V without current drawn, know as open circuit voltage (OCV). In fuel cell operation, this theoretical maximum in never achieved, due to limitation in construction, catalyst utilization, fuel crossover and limitations of reaction kinetics. The use of hydrogen fuel can produce and OCV value greater than 1 from an MEA, but never reaching the maximum 1.2V. The use of methanol as a fuel, on the other hand, has an average OCV of 0.65V. This decrease is attributed to a variety of limitations, mostly attributed to fuel crossover, but also includes factors such as electrical resistance of the fuel cell materials, inadequate utilization of the catalyst, and non-homogeneity of the electrode layers that effect a larger MeOH molecule than the smaller diatomic hydrogen.

There is a distinct ability for the fuel, introduced on the anode side, to travel through the electrode without reacting (no available reaction sites from too little loading, or by taking a path without encountering a particle) and reach the anode/membrane interface. While the membrane selectively diffuses protons, other species can "cross over" to the cathode side and react there, driving the reaction in the opposite direction. Hydrogen gas, while a small molecule, does not have a high affinity to crossover; methanol, on the other hand, is already dissolved in water. Even if neat methanol is used, the membrane, made of Nafion, must be humidified to some extent, as the relative humidity of the membrane

directly affects proton conductivity, with optimal values between 70-90%. Thus, methanol can dissolve into the water which is humidifying the membrane, and leach into the cathode. This results in a lower OCV and poorer performance. Membranes, such as PBI, have been developed to combat methanol crossover, but at the compromise of decreased proton conductivity[5].

Analysis of a DMFC can be done in a variety of ways, many of which investigate only individual components of the fuel cell's performance, such as the identifying the percentage of catalyst utilized or the location of the Nafion in the electrode. To understand a fuel cell's performance as a whole system, an individual MEA can be tested as a single cell, and, by selecting the fuel, temperature, and feed conditions, the cell will be able to generate electricity. By drawing current from the cell and monitoring the voltage of the circuit, done in a discrete fashion, a polarization plot can be obtained. This "sweep" of current draws, selecting a current and waiting for the cell voltage to reach steady state, is known as galvinostatic polarization. An example of a polarization plot is shown in Figure 5[6].

---

[5] (Pintauro, Wycisk, & Lee, 2005)
[6] (Rosenthal, 2009)
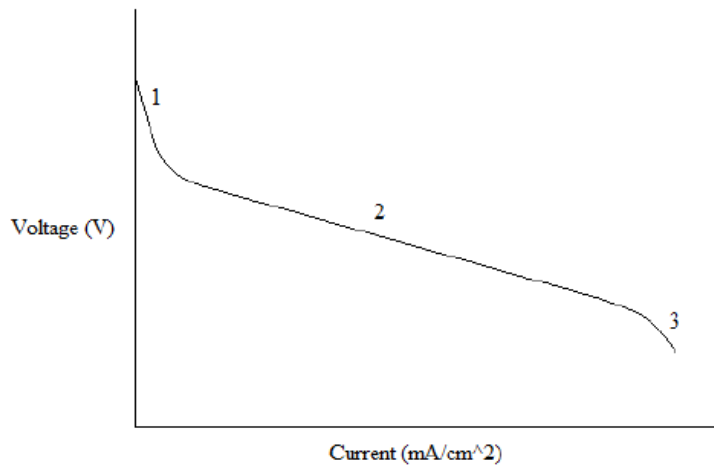
Figure 5: Example of a galvinostatic polarization plot of a fuel cell

The resulting plot can be interpreted and related to various aspects of the fuel cell and its performance. Polarization plots are typically split into three distinct sections. The first section, labeled with a "1", is at very low current draw. This drop in performance is attributed to the activation polarization of the electrodes; the activation energy needed to drive the reaction forward is low, and thus the reaction rate is limited by kinetics. The second region, "2", is dictated by the resistance of the fuel cell. Ohm's law states that V=IR; as V and I are plotted, the slope of this section is attributed to the total resistance of the MEA. A thicker membrane, a denser electrode, or worse conduction will all result in a faster-declining slope in region 2. The third region starts at what is known as the "mass transport knee"; at these high current densities, the ability for the fuel cell to transport fuel into the electrode and exhaust gases to be removed will be limited. This can be caused by construction, as well as the fact that pores of the GDL and electrode are being filled with more and more material. When this limit is reached, the performance drops rapidly. This is seen in section 3.

Ru corrosion and migration[7]

Ruthenium was introduced as a catalyst to the anode of DMFCs to help convert carbon monoxide to carbon dioxide and water, as seen in the previous section. While attributed to decreasing the methanol oxidation overpotential to ~0.25V at 70°C , the introduction of an active, dissimilar (to platinum) metal in nanoparticle form has repercussions. Ruthenium, which is not as noble as platinum, can detach from the carbon nanoparticle support (the catalyst particles tend to be ~5nm particles supported on a ~35nm carbon sphere) and migrate from the anode to the cathode. Stability analysis is common in higher temperature fuel cells, where materials are questioned about thermal tolerance for long durations. Low-temperature fuel cells are just starting to be analyzed for potential instabilities; in the case of DMFC, ruthenium crossover. As DMFC are known to undergo performance degradation over time without a complete explanation, one aspect may be Ru crossover, and this was investigated by a team at Los Alamos National labs.

Using 22cm^2 active-area MEAs, the catalysts were applied to the membranes (both N117 and N1035 were used) directly, or from Teflon in the decal-coating method. These cells were tested using 3M methanol with excess dry air. The electrodes and MEAs were tested with cyclic voltammetery (CV) to measure the active electrochemical surface area, x-ray fluorescence to test for Pt and Ru compositions and loadings, and x-ray diffraction (XRD) to characterize the crystal structure, purity and size of any material, potentially Ru containing, from the cathode half-MEA.

---

[7] (Piela, Eickes, Brosha, Garzon, & Zelenay, 2004)

The results of CV indicate that, after being in operation for 6 months and operated under reverse voltage conditions at times, the Pt/Ru surface of the anode began to resemble a plain Pt surface; the cathode surface, on the other hand, began to take on significant resemblance to the Pt/Ru reference case. While this was done under reverse voltage, which is not a typical operating condition, it was proven that the ruthenium is able to migrate across the membrane. To study this phenomenon further, half-cells were tested to prove the contamination of the cathode had originated from the anode.

Two half-cell tests were done. The half cells, one cathode (GDL, cathode and N1035) and one anode (GDL, andove and N1035) resemble a full-thickness N117 MEA when pressed together. In the first test, both anode and cathode were catalyzed with Pt only. After operation under standard conditions, it was found that, via CO stripping and CV, that the cathode surface was characteristic of a pure Pt surface. To compare, a new but identical anode, loaded with Pt/Ru, replaced the pure-Pt anode. Without drawing current, the cell was humidified and fuel was run as it had before. When the cathode was checked with CV and CO-stripping techniques, it was found to be heavily contaminated with a number of Ru phases and Pt/Ru alloys. This "current-less" migration indicates that the ruthenium will migrate if the cell is not in operation.

To test the Ru migration during operation, the same type of test was run, with the anode supplied with methanol and the MEA held at gradually increasing potentials over the course of two hours. The cathode was then tested in the same manner, and a clear, proportional trend of Ru contamination on the cathode and magnitude of current drawn was seen. These MEAs were then run in a H_2/air environment, and a clear decrease in

performance was seen, showing that this migration does affect the performance of the fuel cell.

This crossover could be caused to a thermodynamic instability of Ru, or attributed to the mobile nature of unalloyed Ru search for a way to oxidize into the thermodynamically favorable RuO_2 phase. This field is currently under study, and has even seen a fair share of modeling to help elucidate the reasons for this performance-degrading migration, as this decrease in performance over the lifetime of a cell could decrease the overall commercial DMFC lifetime by several thousand hours[8].

Catalyst Supports and the Electrode Layer

Nafion Loading

In order for the forward reduction reactions to take place in the anode, the electrons must be wicked away to the GDL and the protons transported to, and through, the membrane. The only place where the electrocatalytic reaction can occur is at the interface between a catalyst particle, the membrane electrolyte and the fuel gas. Traditionally, the only place where this is true is at a thin, 2D layer where the catalyst contacts the membrane. The introduction of proton-conducting polymer into the electrode layer increases the utilization of catalyst, and therefore performance, by constructing more of these triple-phase interfaces[9]. With the main focus of driving down cost by using less catalyst, optimizing the amount of Nafion impregnated into the electrode layer is vital. Too

---

[8] (Kulikovsky, 2011)
[9] (Ticianelli, Derouin, Redondo, & Srinivasan, 1988)

little, and the catalyst is under-utilized; too much, and the Nafion both fills pores in the electrodes as well as cast thin films over the catalyst, increasing the ionic resistance of the electrode and encapsulation of potential reaction sites, resulting in a decrease in performance[10]. This optimization has been studied for the past decade, with various results being reported. Moving through the literature chronologically, the amount of Nafion used in the electrodes can be checked, and the progression of thought can be seen.

A 1997 article from a Korean group studied Nafion loading in both H_2/O_2 and H_2/air systems of low platinum-loading electrodes, averaging 0.4 mg·cm^{-2}. These electrodes were hot-pressed to a Nafion 115 membrane and tested on a 1 cm^2 single cell. It was found that there was an increase in performance until a Nafion loading of 1.3 mg·cm^{-2} was reached; after which, for loadings of 1.3, 1.9, 2.1 and 2.7 mg·cm^{-2}, performance was diminished as loading increased. The use of cyclic voltammetery and impedance spectroscopy identified the 1.3 mg·cm^{-2} loading as the optimal amount. In addition, the group sited the main role in determining the overall cell performance tended to be related to mass transport, and this was seen in the H_2/air system at high current densities, where the mass transport dictates performance[11].

An Italian research team published results in 1999 regarding the effect of Nafion loading of fuel cell cathodes. Finding the steady-state galvinostatic polarization of the electrode, as well as testing with both CV and electrical impedance spectroscopy (EIS), the group was able to identify an equation for optimum Nafion content, represented as a

---

[10] (Staiti, Poltarzewski, Alderucci, Maggio, & Giordano, 1994)
[11] (Lee, Mukerjee, McBreen, Rho, Kho, & Lee, 1998)

function of the catalyst loading (L_{Pt}) and the weight % of metal supported on carbon (P_{Pt}), seen below.

$$ \underline{\hspace{1cm}} \qquad \underline{\hspace{1cm}} $$

In the testing done by this research group, it was found that the optimal amount of Nafion is 0.67 mg·cm^{-2}; however, based upon the relationship given (empirically derived when comparing other data collected by fellow researchers), this equation was developed. For a catalyst where P_{Pt} = 0.6 (60%), amd the catalyst loading is 0.4 mg·cm^{-2}, the resulting Nafion loading is 0.373 mg·cm^{-2}. With ten times the catalyst loading, 4 mg·cm^{-2}, the predicted Nafion loading is 3.73 mg·cm^{-2}; in their work, it was found that both of these loadings would be outside the bounds of successful performance. The 0.373 mg·cm^{-2} loading would not be high enough to fully utilize the catalyst, where the 3.73 mg·cm^{-2} would be too high, prematurely inducing the mass transport losses seen at high current densities. This relationship was developed during a time where the catalyst weight percent, when compared to the XC-72 support, was only 20wt%; modern 60wt% catalysts may be incompatible with this equation[12].

2001 brought a Korean research groups experimentation to print, examining the optimal composition of polymer by using AC impedance spectroscopy. At this point in time, it was fairly novel to fabricate a thin Teflon layer onto the surface of the carbon paper used as a GDL, and then deposit the catalyst upon it. In this study, the carbon cloth underwent a hydrophobic treatment, and then a PTFE/carbon film was applied to that to create catalyst

---

[12] (Antolini, Giorgi, Pozio, & Passalacqua, 1999)

supporting layer, aiming to prevent the catalyst from falling into the carbon cloth and blocking pores.

The AC impedance method was used to examine the frequency response of the cathodic oxygen reduction reaction. A 1 cm^2 test bed was used, and Nafion 115 was the membrane of choice. The PTFE/carbon loading was varied between 0.1 and 0.4, and the total amount of this loading was varied between 1.5 mg·cm^{-2}, 3.5 mg·cm^{-2}, and 10 mg·cm^{-2}. It was found that the 3.5 mg·cm^{-2} loading performed the best during fuel cell testing, with the optimal PTFE/carbon loading to be 0.3. The AC impedance spectroscopy results indicate that the 3.5 mg·cm^{-2} has the least resistance, corresponding to a more active surface area. The impedance plots also indicate the PTFE/carbon loading of 0.3 was optimal over the range tested. With catalyst loading at 0.4 mg·cm^{-2}, this translates to an optimal Nafion concentration of 0.8 mg·cm^{-2}, twice the loading of the catalyst[13].

A 2003 study from a pair based in the University of Newfoundland also studied the effect of Nafion and catalyst loading on overall fuel cell performance. Identifying the importance of the humidity the cell is run at, and the need to keep this variable well controlled, the fuel cells fabricated in this study were tested using EIS with three distinct ranges. First, at low overpotentials (low current densities in a cell) where mass transport is not a significant limiting factor, as the interfacial charge transfer resistance is the main contributor to the cell's impedance. Over the medium overpotential range, the transport of protons, oxygen, fuel and water will primarily contribute to the observed overpotential. At high overpotentials, the fuel or oxygen transport in the GDL become the major factor, as

---

[13] (Song, Cha, & Lee, 2001)

17 | P a g e

seen by the significant drop in performance at high current densities, or the mass transport "knee".

The EIS results demonstrated that, at a Nafion loading of 0.9 mg·cm^{-2}, there was the highest measured Pt utilization, found to be 76%, as well as the lowest ohmic resistance (0.1 Ohm/cm^2). Even at these optimal conditions, there is nearly a quarter of the catalyst particles isolated either ionically or electronically from the cell; this was believed to be deposition in the pores of the carbon paper backing, but could also be due to catalyst encapsulation by the polymer. Also, the use of EDX, a spectroscopy technique which a CsCl solution is used to exchange ions with Nafion, can be used to show the Nafion dispersion in the MEA. The tests were redone using a "bi-layer" electrode, with low Nafion loading near the membrane (0.3 mg·cm^{-2}) and higher loading towards the GDL (0.6 mg·cm^{-2}). It was found that a high loading of Nafion showed good utilization of catalyst near the electrode, but fell rapidly as approaching the GDL. The lower loadings of Nafion near the GDL showed poor bonding of polymer to the electrode, calling into question the importance of the dispersion of Nafion over the electrode layer;[14].

A 2004 paper from South Korea continued this study of Nafion loading, varying both the catalyst loading and the Nafion loading of the electrodes made. Three platinum loadings of 0.5, 0.25, and 0.1 mg Pt/cm^2 were fabricated with varying amounts of Nafion, ranging from 15wt% Nafion to 60wt% Nafion. These electrodes were then assembled onto a Nafion 115 membrane and tested at 80°C. The resulting performance verified that at low Nafion

---

[14] (Li & Pickup, 2003)

loadings, performance was poor; at higher loadings of Nafion, especially with lower catalyst loading, the performance also decreased.

The optimal performance was seen with the highest catalyst loading, with a proportionally high loading of Nafion. It was concluded that the optimum loading for a 0.5 mg·cm^{-2} loading of Pt is 20% Nafion; for 0.25 mg·cm^{-2} Pt loading the optimal Nafion is 40%, and with a low loading of catalyst, 0.1 mg·cm^{-2} of Pt, 50% Nafion is required, with the highest performing cell being the 0.25 mg·cm^{-2} Pt / 40 wt% Nafion electrode. These particular results were nearly equal between the N117 and N1035 membrane, potentially removing membrane thickness as a variable for electrode performance[15]. A separate South Korean team published findings in the same edition of Electrochemica Acta, comparing equivalent weight of the Nafion used in the electrodes; even in low humidity, the performance was very similar despite the chain length of the polymer used[16].

There was a flurry of activity on this subject starting in 2008, with many articles published in the International Journal for Hydrogen Energy, all focused on the optimization of the Nafion found in electrodes of PEMFC; some, the continuation of work from studies mentioned this far.

The use of a Nafion gradient through the electrode, as opposed to a homogenous dispersion, was studied. CV, EIS and standard cell polarization, were used to find that a low loading throughout the entire electrode showed a reduction in performance throughout the entire polarization curve. However, a gradient from 33% Nafion to 23% Nafion improved performance, especially at high current densities, with a maximum current density as high

[15] (Sasikumar, Ihm, & Ryu, 2004)
[16] (Ahn, Lee, Heung, Hong, & Oh, 2004)

as 1600 mA/cm² at 0.388V. A homogenous 33 wt% Nafion electrode reached this same current density at 0.272V. This improvement is cited as the result of low Nafion content near the GDL, leading the researches to believe the lower loading near the GDL surface improves water management in the electrode[17].

EIS, CV and linear scan voltammetery (LSV) were used in a study to examine Nafion loadings, from 0-2.0 mg·cm^{-2}, in a catalyst with 0.5 mg·cm^{-2} of Pt. Resistances with EIS and a polarization plot showed the Nafion loading of 1 mg·cm^{-2} to be optimal. The specific activity of the Pt, indicating how active the Pt is, hit a maximum at this 1 mg·cm^{-2} value, with no improvement seen thereafter. At these higher loadings, however, degradation in performance was seen at high current densities. This was attributed to the developing belief that there is significant blocking of pores at the electrode/GDL interface, amplifying the existing issues of transport limitations at high current densities[18]. These results were somewhat verified; a separate ground found optimal performance was measured using an electrode with a loading of 0.5 mg·cm^{-2} inside the electrode layer, paired with a 1.0 mg·cm^{-2} Nafion loading on the membrane/electrode interface: these results were published in the same volume[19].

Another flurry of activity was seen in 2010, mainly in the International Journal for Hydrogen Energy. The first paper of note studied the optimization of the catalyst/ionomer loading in the electrodes. It was found that, when standard loadings of Pt/C were used (0.4 mg·cm^{-2} of 45 Pt wt% Pt/C), the catalytic activity was not directly proportional to the electrochemically active surface area (EAS), demonstrating the importance of ionic

---

[17] (Kim K. , et al., 2008)
[18] (Lai, Lin, Ting, San-Der, & Hsueh, 2008)
[19] (Lee & Hwang, 2008)

conductivity through the electrode layer. To investigate these effect of high loadings with varied cell operation, the stoichiometry of the air to the cathode. At high ionomer content, there was a much more immediate drop in performance when flowrate was decreased; this points to clear mass diffusion limitations at high ionomer loadings.

With the combined results of EAS, CV, and polarization, it was found that 30 wt% Nafion was ideal when paired with a 0.4 mg·cm^{-2} catalyst loading[20]. Electrodes tested over a wide range of Nafion contents, from 0 to 1.6 mg·cm^{-2}, were found to perform best a 0.4 mg·cm^{-2} Nafion, paired with a catalyst loading of 0.2 mg·cm^{-2} Pt by techniques such as CV, EIS and SEM. Interestingly, the deposition procedure gave rise to polyaniline (PANI) nanofibers in the catalyst layer, and this nanofiber presence seemed to improve the homogeneity of the catalyst in the electrode, though this was done mostly visually via SEM and not corroborated by any other technique[21].

A very intriguing and comprehensive parametric study of the cathode catalyst layer was performed by an Iranian research group; while the scope of the modeling is outside the focus of this paper, it examines six structural parameters on the performance of the cathode: platinum and carbon loadings, ionomer volume fraction, extent of GDL/cathode layer crossover/sharing, GDL porosity and catalyst layer thickness. It is important to note that, when the Pt comprises more than 30% the mass of the electrode, the cost effectiveness of the entire system decreases dramatically[22].

---

[20] (Kim, et al., 2010)
[21] (Zhani, Gharibi, & Kakaei, 2010)
[22] (Khajeh-Hosseini-Dalasm, Kermani, Moghaddam, & Stockie, 2010)

A DMFC application was published in early 2011, demonstrating that a decrease in the Nafion aggregate size in the ink benefits both the catalyst and Nafion utilization; this improvement manifests as higher performance visually in the polarization plot. These tests were done with a 4 cm² single-cell MEA. The catalyst ink prepared at 80°C showed a considerable increase in maximum power density (32 mW/cm²) compared to those prepared at lower temperatures (29 mW/cm² at 50°C, 23 mW/cm² at 25°C). There was a sharper peak in Nafion particle size distribution occurring at a smaller diameter as the temperature in preparation increased[23].

Carbon Supports

As this study investigates a novel material morphology for a catalyst support, carbon supports of various nanomorphologies have been proposed in the past decade, with a surge coming in the past five years, most likely due to the increased focus on fabrication of these nanostructures for different applications. Carbon nanostructures such as coils, ribbons and tubes offer a very high surface area to volume ratio, as well as being continuous structures, allowing for high electron conduction. Their stability under aggressive environments further promotes their use in a fuel cell, especially one using methanol as a fuel.

One of the earliest papers used solid-phase-synthesized carbon nanocoils in a DMFC. These coils, verified by XRD to be highly graphitized (002 plane dominating), had a crystallite size of 5.5 nm. These coils, when loaded with the equivalent weight of 60wt% 1:1

---

[23] (Yuan, et al., 2011)

Pt/Ru catalyst, show a significant improvement in the specific methanol electrooxidation current, as seen in Figure 6.
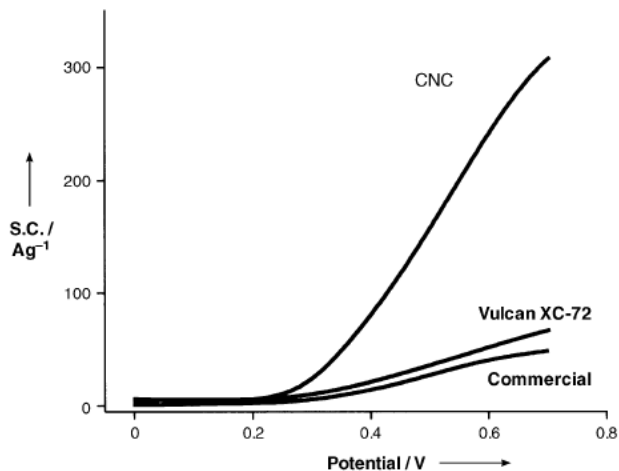
Figure 6: Specific methanol electroxidation over a variety of catalyst supports

This increase in electrocatalytic activity of the methanol oxidation is the main factor cited as the reason for the increase in fuel cell performance, seen in Figure 7. However, the continuous electron-conducting phase may lessen the resistance of the electron flow through the electrode to the gas diffusion layer; this decrease in overall resistance should manifest as a less negative slope in the middle region of the polarization plot, and there is evidence of this[24].

---

[24] (Hyeon, Han, Sung, Park, & Kim, 2003)
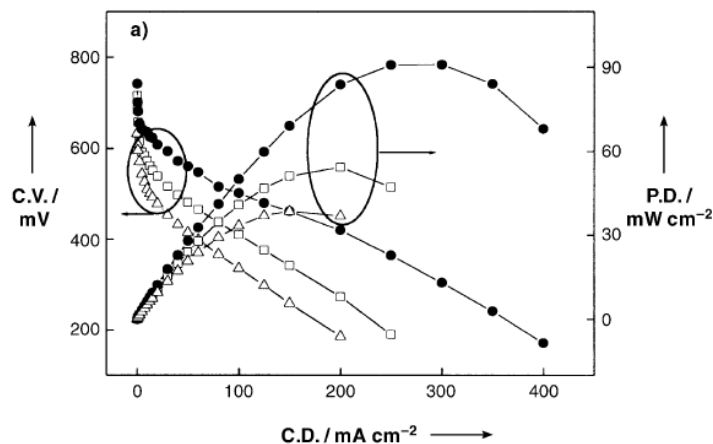
Figure 7: Polarization plot of DFMC performance with carbon nanocoils (filled circle), Vulcan XC-72 (open square), and commercial catalyst on optimized carbon (open triangle)

The use of carbon nanotubes, both single-walled and multi-walled, was evaluated in 2005 by a research team from Brazil. While high performance was achieved with both types of carbon nanotubes, the increase in performance was slight over the existing Vulcan XC-72 support. Despite this, the power densities of these experiments were shown to exceed 100 mW/cm^2 at 90°C, and the nanotubes withstood testing of H$_2$ poisoned with 100ppm CO without a significant decrease in performance[25].

Carbon nanofibers were evaluated for DMFC use in a 2007 study, utilizing a novel poly(vinylpyrrolidone) grafting surface additive. The various carbon nanostructures were fabricated with their respective techniques, and tested for conductivity. The conductivities of these structures are shown in Figure 8. The PVP coating was shown to increase the electrocatalytic performance compared to typical acid-catalyzed carbon nanostructures. This increase was between 17-463% based upon CV and other testing techniques[26].

---

[25] (Carmo, Paganin, Rosolen, & Gonzalez, 2005)
[26] (Hsin, Hwang, & Yeh, 2007)
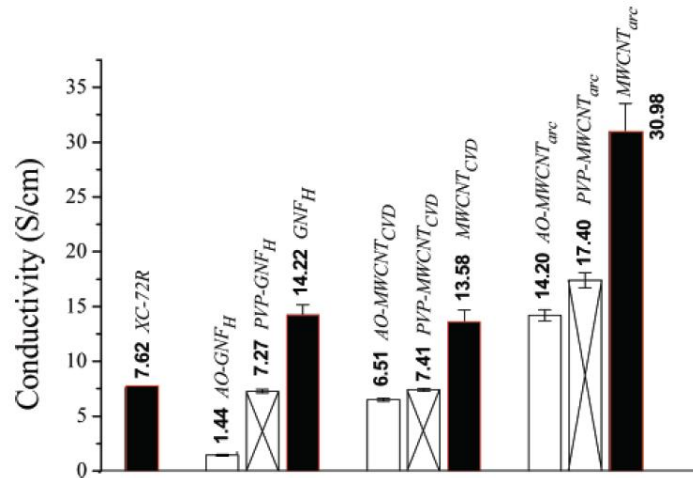
Figure 8: Conductivity of a variety of carbon structures

The use of electrospun polyacrylonitrile (PAN), the precursor to carbon fiber, was tested for use as a catalyst support for PEMFC in 2009. The fibers, having a rough surface with an average diameter, determined by SEM, of 250nm. The fibers are slightly porous, having a pores of 2.36nm compared to the pores of XC-72, which were measured to be 10.92nm. The increased performance, shown in Figure 9, is attributed to the more favorable structure, and this was verified with the obtained Pt utilization: 69% for Pt/e-CNF with only 35% for Pt/XC-72[27].

---

[27] (Park, Ju, Park, Jung, Yang, & Lee, 2009)
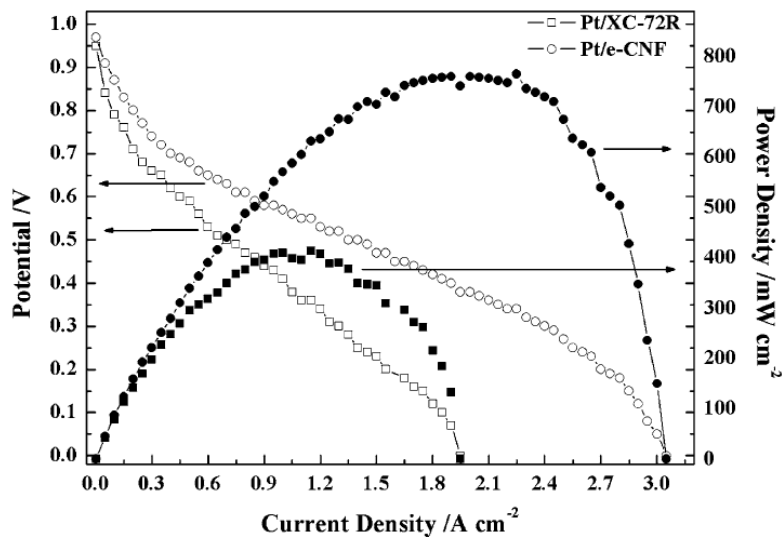
Figure 9: Polarization plot comparing carbon supports; the traditional XC-72 (squares) are significantly outperformed by the carbon nanofibers (circles)

While these are a small selection of studies from the literature, a review article published in 2009 provides a very comprehensive source for the comparisons of traditional carbon structures, blacks and graphite, to novel materials such as mesoporous carbons. gels, carbon nanotubes, carbon nanocoils and a variety of nanofibers, both pure and of a composite nature. The mechanical strength of the material, as well as the electrical conductivity make a good candidate for a catalyst support, and the variety of morphologies, especially those with porous character (many of which can have pore sizes tailored), show promise. The ideal catalyst support would have a high surface area, good electrical conductivity, suitable porosity for fuel and exhaust gas flux, and stability; many carbon structures offer these. In addition, a fuel cell's environment, particularly in DMFC, will provide plenty of polar and non-polar substances for the dissolution of a material that is not resilient. A review of the types of materials reviewed can be seen in Table 1[28].

---

[28] (Antolini, Carbon supports for low-temperature fuel cell catalysts, 2009)

Table 1: Comparison of carbon catalyst support morphologies and thier properties

Carbon material	Specific surface area (m² g⁻¹)	Porosity	Electronic conductivity (S cm⁻¹)	Supported catalyst properties
Vulcan XC-72R	254	Microporous	4.0	Good metal dispersion low gas flow
OMC	400–1800	Mesoporous	0.3×10^{-2}–1.4	High metal dispersion High gas flow Low metal accessibility
Carbon gels	400–900	Mesoporous	>1	High metal dispersion High gas flow High metal accessibility
CNT	400–900 (SWCNT) 200–400 (MWCNT)	Microporous (SWCNT) Mesoporous (MWCNT)	10–10^4 depending on nanotube alignment 0.3, 3 (functionalized MWCNTs)	Good metal dispersion high gas flow Low metal accessibility high metal stability
CNH, CNC	150	Micro/mesoporous	3–200	High metal dispersion high gas flow
ACF	>1000	Microporous	13	Good metal dispersion low gas flow High metal stability
CNF	10–300	Mesoporous	10^2–10^4	High metal dispersion High gas flow High metal stability
BDD	2	–	1.5	Low metal dispersion Low metal stability High metal stability on BDD/Nafion

Electrospinning

Introduction

The use of electrospinning to form continuous, small-diameter polymer fibers was born of the need to control sub-micron fiber diameter for various applications, from composite materials to filtration media, mostly in a porous mat morphology[29]. There are a variety of ways to construct micron and sub-micron fibers; material can be commonly formed by drawing, template synthesis, phase separations, self-assembly and electrospinning. Each manufacturing technique has respective pros and cons, and can only be utilized when matched with the proper material[30]. Drawing, or dry spinning, is able to produce very long, nanoscale fibers, but is limited to viscoelastic material that can undergo

---

[29] (Dotti, Varesano, Montarsolo, Aluigi, Tonin, & Mazzuchetti, 2007)
[30] (Huang, Zhang, Kotaki, & Ramakrishna, 2003)

large deformations while still being cohesive enough to withstand the stresses involved with the process. Template synthesis uses a porous membrane as a guide, and the fibers are grown into fibers; this can be used for many materials, such as metals and semiconductors, but is difficult, requires a tailored membrane, and cannot make single fibers. Self-assembly requires individual components to organize themselves into patterns; while possible, it is not energetically favorable for most materials, and is time consuming even when the properly done, with bamboo-type carbon nanotubes being one example[31].

The process of electrospinning is fairly simple; a solvated solution of material, in this case a polymer, is forced out of a fine needle tip, a spinneret, at a slow flowrate (from 0.5 to 10 mL/h). The needle is charged with a variable amount of electric potential; as the polymer is electrostatic ally active, the droplet of polymer, at the tip of the needle, will need to discharge that electricity to the nearest grounded source. To capture this, a grounded plate or collection drum is placed in front of the needle at varying lengths. The polymer then travels towards this grounded collection plate. If the polymer is sufficiently tangled, the strands of polymer leaving the tip will draw other polymer strands out; this creates a fiber wrapped in a solvent sheath. As the solvent evaporates, the fiber solidifies. If this is done too quickly, the fiber will become brittle and break; too slow, and the polymer chain will never thin out properly. A typical electrospinning apparatus is shown in Figure 10. The portion labeled 1 is the oscillating syringe pump, 2 is the nozzle / spinneret, 3 is the high-voltage supply, 4 and 5 are optional excitation plates typically used with stable electrospun fibers to modify the path the fiber takes whilst being spun, and 6 is the grounded collection plate.

---

[31] (Thostenson, Ren, & Chou, 2001)
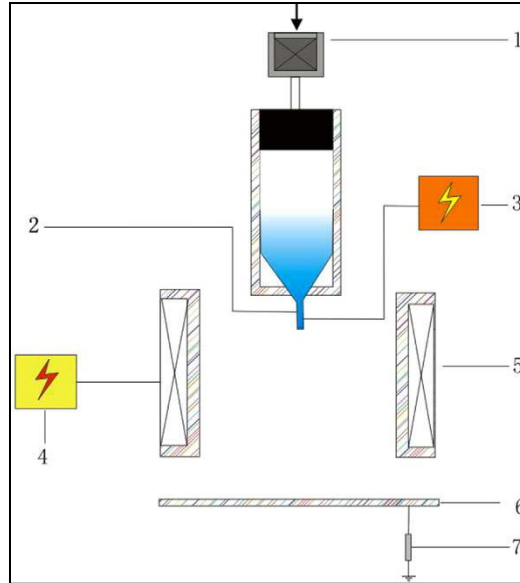
The resulting fiber is nearly two orders of magnitude less than the initial diameter at the tip of the needle. This is due to the rate at which the solution travels to the collection plate. The higher the rate of travel, either due to an increased flowrate or electric potential, the more fiber will be extruded. This interface, where solution is pumped and solution is lost to the collector in the form of fiber, is the droplet at the tip of the needle. This is called the Taylor Cone, named after Sir Geoffrey Ingram Taylor, a pioneer in electrospinning in the 1960's. The Taylor cone, and an electrospun jet of material, can be seen in Figure 11.

Figure 11: A stable Taylor cone; the top of the image is at the needle/droplet interface

---

[32] (Xu, 2009)

The functionality of a fiber, in most cases, if a function of the fiber's diameter. Traditional fiber-spinning processes, where a thick, viscous liquid is extruded through holes in a plate or through a thin needle, are typically limited to a lower bound of 5 micrometers in diameter, and this is only possible with very stable polymers. Electrospinning processes, for polymer solutions, can generate fibers, with consistency, in the range of 10 nm to 10 µmeters in diameter. As this production method has matured, textile, medical and a wide range of engineering applications, once limited to a narrow realm of material choices, are able to tailor a material to a task using both the chemical properties as well as morphology.

Nafion Electrospinning

Nafion, as described before, is a perflourosulfonic acid compound, containing both hydrophobic and hydrophilic portions. This ionic character prevents PFSAs from dissolving into normal organic solvents. Instead, the acid chains will cluster, with the hydrophobic head retreating inwards and the hydrophilic tail emerging to face the solvent. These aggregates are referred to as micellar solutions, and the dynamics of these solutions in various solvents has been studied[33]. Due to this behavior, the polymer chains, made up of the perflourinated backbone and pendant sulfonic groups, will not entangle to make long chains. These long chains are vital to create nanofibers, as the structure is highly dependent on the concentration and homogeneity of the Nafion solution. Inadequate entanglements

---

[33] (Szajdzinska-Pietek, Wolszczak, Plonka, & Schlick, 1999)

will lead to aggregate clusters of Nafion unable to form continuous fibers and thus be electrosprayed, as droplets, onto the collection surface[34].

To achieve the necessary entanglements, a carrier polymer is introduced. The role of the carrier polymer is to break these micellar dispersions by both physically entangling the molecules, as well as creating a localized environment to coax the hydrophobic portions away from each other. In the case of Nafion, long-chain (and therefore high molecular weight) polymers can be used, with those capable being polyethylene oxide (PEO), poly(acrylic acid) (PAA) or poly(vinyl alcohol) (PVA). In early studies, as well as with the attempt of including particles or colloids into an electrospinning solution, the only way to successfully electrospin Nafion was to utilize very high loadings in solution, up to 25wt%, of carrier polymer[35,36]. In the case of proton conductivity, the inclusion of a carrier polymer, which is not proton conducting, will severely hamper performance, only adding resistance to proton flow. Over the past few years, the necessary concentration of carrier polymer has decreased into a much more manageable 1-3%, with some, using ultra-high molecular weight carrier polymers, achieving fibers with less than 0.1 wt% PEO[37,38].

The properties of a material, both chemical and mechanical, will change with a fiber's diameter, requiring fine control of a fiber's diameter for any application. One example of a fiber's diameter being a function of an important characteristic is the relationship between a perflourosulphonic acid (PFSA) fiber and its intrinsic proton conductivity. A 2010 paper by a research group from Drexel University found a general

---

[34] (Celebioglu & Uyar, 2012)
[35] (Laforgue, Robitaille, Mokrini, & Ajji, 2007)
[36] (Zhou, Liu, Dai, & Xiao, 2010)
[37] (Choi J. , Wycisk, Zhang, Pintauro, & Lee, 2010)
[38] (Dong, Gwee, Salas-de la Cruz, Winey, & Elabd, 2010)

correlation between fiber diameter and proton conductivity, shown in graphical format in Figure 12. The smallest diameter of smooth nanofiber that could be produced without surface abnormalities was found to be 400nm; this fiber boasted a proton conductivity of 1.5 S/cm, nearly an order of magnitude more than typical bulk Nafion of the same equivalent weight[39]. It is important to note that, as a target, the Department of Energy has set the conductivity requirement for membranes to be 0.1 S/cm [40].
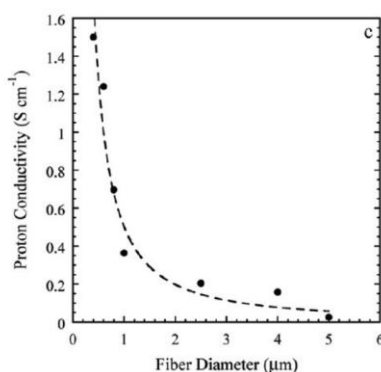
Figure 12: Proton Conductivity of Nafion nanofibers as a function of fiber diameter

Additional research has shown that the ideal diameter is 400 nm; while not explicitly tested for, this seems to be the lower limit of producing smooth nanofibers with consistent morphologies without electrospraying (evidence of an unstable / unsustainable electrospinning process)[41].

The draw of the high-proton conduction has beckoned many into the electrospinning of Nafion, many for fuel cell applications as a membrane. While this increase in conductivity would be very beneficial, the inherent porous nature of a nanofiber membrane would be disastrous for methanol crossover. Some attempts to reduce this

---

[39] (Dong, Gwee, Salas-de la Cruz, Winey, & Elabd, 2010)
[40] (Garland & Kopasz, 2007)
[41] (Ballengee & Pintauro, 2011)

potential for crossover is to fill the tortuous paths with an inert material, or, in some cases, another proton conducting material such as polyphenolsulpone[42]. The common methodology is to electrospin the proton conducting polymer with a sulfonated filler (such as silsesquioxane), weld the intersecting fibers together to improve proton conduction, compact the mat to increase the volumetric density, and impregnating the processed nonfiber network with an uncharged polymer, reinforcing the structure mechanically and limiting the amount of ionic swelling that can occur. In addition, this will fill pores, limiting the diffusion of fuel gas through the membrane, decreasing in the dreaded effect of crossover[43].

The most critical aspects of a Nafion nanofiber, as mentioned, is fiber diameter and purity. There is a distinct trade off between the two; however, no matter that the ratio between the two are, there is the overarching problem of ensuring the solution fabricated is able to be electrospun. If a solution is too thin, or does not have enough PFSA content, there will be little entanglement between the chains, no matter how high the carrier polymer loading, with a higher carrier polymer loading decreasing the purity of the resulting fiber. A fiber will not be formed, as the polymer molecules are spaced too far apart to entangle and connect, so only small droplets will be ejected, pulsed out from the spinneret tip; this process has been dubbed electrospraying, and is evidence of a solution that is either too thin or deficient in polymer loading to be electrospun.

On the other had, a solution which is too viscous will not be able to travel through the needle to the spinneret tip quickly enough, resulting in the solution hardening in the

---

[42] (Ballengee & Pintauro, 2011)
[43] (Choi J. , Wycisk, Zhang, Pintauro, Lee, & Mather, 2010)

needle and causing a jam, or simply dribbling out and being unable to form a stable Taylor cone. It is known that a thicker solution, with the polymer chains more densely packed and entangled, will result in a thicker fiber, with equipment variables remaining *ceteris paribus.* This phenomenon is demonstrated well in a 2010 paper, using PFSA with PAA as a copolymer; this is seen in Figure 13; note the presence of electroprayed material at low loadings, with thicker fibers at higher loadings. While not reported, it is certain that these solutions also show a proportional trend with polymer content and viscosity, a trend that is demonstrated in a different paper by the same research group, as seen in Figure 14.
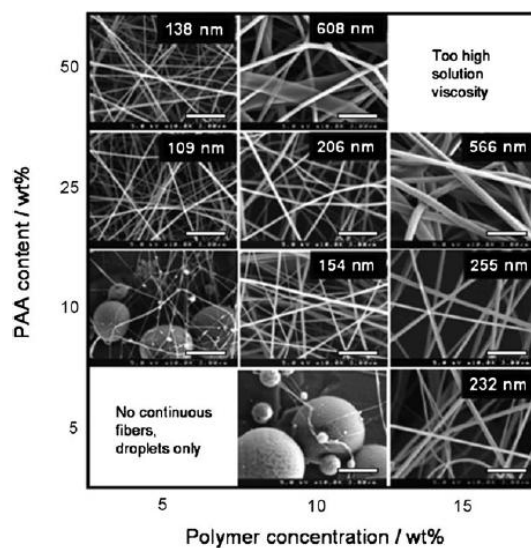
Figure 13: Fiber morphology of electrospun PFSA/PAA with varied polymer content[44]

---

[44] (Choi J. , Wycisk, Zhang, Pintauro, Lee, & Mather, 2010)
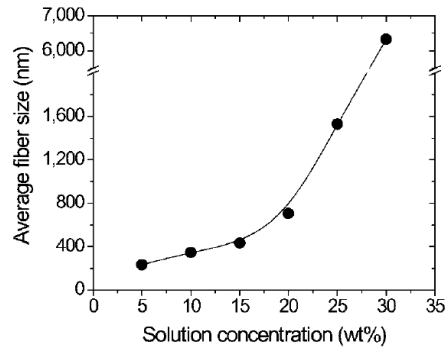
Figure 14: Solution concentration of PFSA/PAA and the diameter of the resulting fiber[45]

For the experimental work to be done in this project, the literature can be reviewed for existing experimental procedures for creating 400nm Nafion fibers, using a variety of copolymers and electrospinning apparatuses. In addition to the setup, the experimental procedures used for these experiments can be evaluated and compared, selecting the proper starting point for the in-house electrospinning planned for this work.

It is noted that Nafion is in a family of chemicals where, as it contains long chains of variable length which are both hydrophobic and acid containing groups, the molecule is limited as transport and mechanical properties are linked; an optimization of one will degrade the other. Low viscosity with few intermolecular interactions may be ideal for electrospinning continuously; however, will yield a material with low mechanical strength, and vice-versa. These observations were made by a research group studying the micro-scale interactions of highly-sulfonated polystyrene (PS). Polystyrene is a very stable polymer which is readily electrospun with ease; sulfonating the molecules was done to attempt to emulate the properties of Nafion, and identify the differences between the two, PS and Nafion[46].

---

[45] (Choi J. , Wycisk, Pintauro, Lee, & Mather, 2010)
[46] (Subramanian, Weiss, & Shaw, 2010)

A 2010 work for electrospun membrane work used PFSA with PAA in various concentrations in a 2:1 1-propanol/water (by weight) solvent. The PAA was 450kDa, and PFSA content was varied from 5-15%. These test results, with corresponding average fiber diameter, are shown in Table 2[47].

Table 2: PFSA/PAA Electrospinning Results

PFSA/PAA (wt/wt)	Total polymer concentration (wt%)	Voltage (kV)	SCD[1] (cm)	Solution flow rate (mL/hr)	Average Fiber Diameter (nm)
50/50	5	6	8	0.15	138
50/50	10	7	8	0.15	608
75/25	5	7	8	0.15	109
75/25	10	8	8	0.15	206
75/25	15	10	8	0.15	566
90/10	10	8	8	0.15	154
90/10	15	12	8	0.15	255
95/5	15	12	8	0.15	232

Nafion electrospinning, using both PVA and PEO, was done with a focused effort on elucidating the proton conductivity of the fiber morphologies. In this study, it was found that the use of PVA provided higher conductivity than PEO, but is attributed to the fact that PVA-based fibers had superior mechanical properties when swollen in water. The use of high-magnification SEM brought forth not only fiber diameters for each sample, but a distribution of size compared to both solution and distance to the collector. These are seen in Figure 15. In addition, the conductivities that were measured, as seen in Table 3, are slightly lower than extruded Nafion 115, as well as cast Nafion/PVA films.

---

[47] (Choi J. , Wycisk, Zhang, Pintauro, Lee, & Mather, 2010)
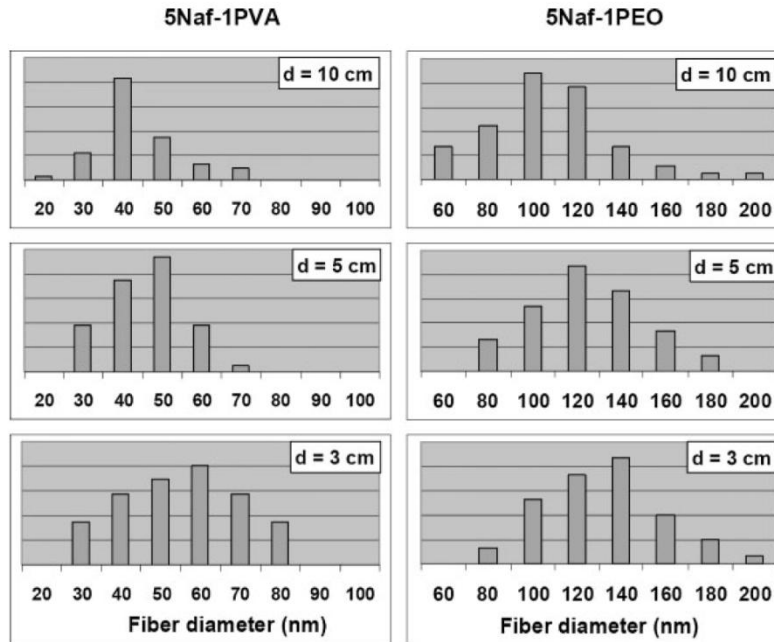
Figure 15: Fiber diameter distribution of Nafion/PVA and Nafion/PEO fibers

Table 3: Results of the 2007 Study on Nafion with PVA/PEO

Sample Type		Observed Morphology	Conductivity	Water Uptake
			$S \cdot cm^{-1}$	%
Nafion 115		Extruded film	7.3×10^{-2}	36 ± 5
Nafion (5 wt.-%) + PVA Series				
PVA sol. concentration	PVA fiber content			
wt.-%	wt.-%			
0.25	4.8	Spheres	3.5×10^{-3}	112 ± 10
0.50	9.1	Spheres + ultrathin fibers	4.3×10^{-3}	115 ± 7
0.75	13.0	Beaded nanofibers	8.7×10^{-3}	118 ± 8
1.00	16.7	Nanofibers + few beads	1.7×10^{-2}	125 ± 5
1.00	16.7	Cast film	3.0×10^{-2}	50 ± 7
1.25	20.0	Nanofibers + few beads	1.6×10^{-2}	127 ± 6
1.50	23.1	Nanofibers + scarce beads	1.4×10^{-2}	140 ± 6
2.00	28.6	Nanofibers	1.0×10^{-2}	155 ± 4
Nafion (5 wt.-%) + PEO Series				
PEO sol. concentration	PEO fiber content			
wt.-%	wt.-%			
0.50	9.1	Spheres + ultrathin fibers	3.5×10^{-3}	255 ± 15
1.00	16.7	Nanofibers	5.9×10^{-3}	400 ± 35

It is important to note that the carrier polymer solution concentration, in the most left-hand column, does not match up with the weight percent found in the fiber. However, the carrier polymer weight percent is in percent of solution, not percent compared to the Nafion loading. The first PEO solution, for example, is 0.5 wt%; the Nafion loading is 5 wt%, so the Nafion to PEO ratio is 10:1; thus, the resulting 9.1 wt% PEO in the electrospun fiber seem to be correct.

In 2009, a group investigated the effect of changing the carrier polymer of the solution, using PEO, PVA and/or PVP (polyvinyl propanol). The experimental setup was varied in a similar way as those who have electrospun before 8-12cm collection distance, 7.5-15kV, and a low flow rate from 0.1 to 1 mL/h. While diameter was not investigated, it was determined that PVP/Nafion had the best compatibility, but all tests were done with the Nafion to carrier polymer ratio lower than one, making the results mean little for a high-purity application[48].

A 2010 group from the Yuan Ze University in Taiwan explored the use of a nanocomposite fiber membrane for DMFC applications by forming a Nafion/PVA structure (10wt%PVA) on a pure PVA crosslinked support. The Nafion solution was 5wt% in a mixture of water, propanol, ethanol and methanol, and was tested with PVA. The electrospun solution was 12wt% polymer, with the polymer 10wt% PVA. The equipment was run using a 20mL syringe with an inside diameter of 0.8mm, a tip-to-collector distance of 20cm, a flowrate of 1.2mL/h at 20kV, and the resulting fibers were not tested for diameter, but appear to be close to 1000nm, or 1μm. The mats, however, were measured

---

[48] (Bajon, Balaji, & Guo, 2009)

for thickness, and were found to be spun to 50µm thickness, proving a dense mat can be made via electrospinning[49].

A fairly comprehensive study of Nafion paired with PAA was done in 2008 out of Drexel. Over the course of this particular study, 1100EW, 5wt% Nafion in a 3/1 by volume isopropyl alcohol / water solvent was paired with a 450kDa PAA polymer, with the polymer loading in the solutions ranging from 12 to 25%. The electrospinning equipment was set to run from between 0.5 and 5 mL/h, through a needle with an inside diameter of 0.047 in, with collection distance between 10 and 25 cm and a voltage of 10-25kV; the system was capable of producing 50kV. While the results are posted in Table 4, it is important to note that this work verified the assumption that an increase in carrier polymer had yielded a decrease in conductivity; note the exponential factor at which it increases as PAA content approaches zero, seen in Figure 16.

Table 4: Electrospinning variables and results for Nafion/PAA

PAA content (%)	electric field (kV/cm)	observation
100	16/18	fiber mat
66	10/20	fiber mat
50	12/24	fiber mat
25	17/25	fiber mat
16	18/28	fiber mat, few beads
12	15/25	fiber mat, few beads
8	15/24	beaded fibers
5	16/21	beads

---

[49] (Lin, et al., 2010)
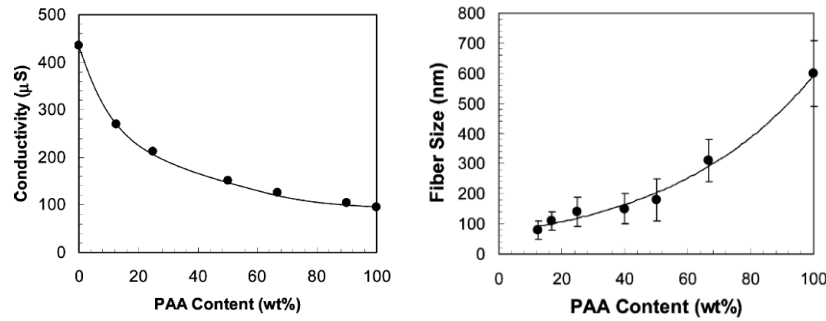
In an attempt to model fiber diameter, experimental work was done in parallel to evaluate the model. Aiming for high purity, the group used PEO at various molecular weights with Nafion. While the modeling will be discussed later, the basic solution mixture, with the fiber diameters produced, is shown in Table 5.

Table 5: Average nanofiber diameter of Nafion/PEO electrospun under various conditions[50]

Average Nanofiber Diameter	Solution Properties	Electrospinning Conditions	Relative Humidity at 25°C
300 nm	15 wt%, 2-propanol/water, 300 kDa PEO	4.5kV, 0.2 mL/hr, 5 cm	20%
500 nm	20 wt%, 2-propanol/water, 300 kDa PEO	4kV, 0.2 mL/hr, 6 cm	40%
700 nm	25 wt%, 1-propanol/water, 400 kDa PEO	4kV, 0.4 mL/hr, 5 cm	30%
900 nm	25 wt%, 1-propanol/water, 400 kDA PEO	4kV, 0.6 mL/hr, 6 cm	30%

Recently, a Nafion solution was electrospun using multi-walled carbon nanotubes (MWCNT) for electrodes in micro-scale actuators. This is not the first time MWCNTs have been used as supports for polymers, but this electrospun electrode assembly is novel. A 20 wt% Nafion solution, in water, was diluted down to 5 wt% with a 1:1 by weight 1-propanol/water solvent. 1 polymer wt% of 400kDa PEO was added, and stirred for 12

---

[50] (Ballengee & Pintauro, 2010)

hours. It was successfully electrospun through a 21 gauge needle, with voltage varied between 10 -12kV to a 10cm collection distance at a flow rate of 0.2 mL/h[51].

A 2011 study tested Nafion/PVA nanofibers for potential use in DMFC as a composite membrane. The results are shown in Table 6; however, pay special notice to both the water uptake and the conductivity; we see that, compared to individual fibers, their conductivity is much less, even when compared to commercially available N117.

Table 6: Nafion/PVA membrane testing for use as PEM Electrolyte for DMFC

Membrane	Thickness (μm)	Water uptake (%)	IEC (meq g^{-1})	λ (mol H$_2$O)/(mol SO$_3$H)	$\sigma^{95\,°C}$ (S cm^{-1})
Nafion/PVA	19 ± 1	26.4 ± 0.1	0.47 ± 0.1	42	0.012
Nafion/PVA	26 ± 2	19.3 ± 0.1	0.33 ± 0.1	44	0.012
Nafion/PVA	39 ± 3	27.9 ± 0.1	0.45 ± 0.1	47	0.016
Nafion/PVA	47 ± 3	25.8 ± 0.1	0.58 ± 0.1	34	0.025
Nafion/PVA	61 ± 3	22.9 ± 0.1	0.57 ± 0.1	30	0.010
Nafion/PVA	97 ± 5	35.8 ± 0.1	0.55 ± 0.1	49	0.007
Nafion®	18 ± 1	27.0 ± 0.1	0.93 ± 0.1	22	0.015
Nafion®	28 ± 1	27.0 ± 0.1	0.93 ± 0.1	22	0.027
Nafion®	37 ± 1	27.0 ± 0.1	0.93 ± 0.1	22	0.034
Nafion®	46 ± 1	27.0 ± 0.1	0.93 ± 0.1	22	0.035
Nafion®	60 ± 2	27.0 ± 0.1	0.93 ± 0.1	22	0.049
Nafion®	95 ± 2	27.0 ± 0.1	0.93 ± 0.1	22	0.070
Nafion 117 (commercial)	216 ± 4	21.5 ± 0.1	0.91 ± 0.1	18	0.096

On the note of high-purity fibers, the goal of achieving very pure nanofibers was pursued by the Drexel research group. By using ultra-high molecular weight carrier polymer, 8000 kg/mol PEO, which is normally unable to be spun by itself due to high degrees of hydrogen bonding with the solvent used, the group was able to spin fibers that were verified by x-ray scattering microscopy to be 99.9% pure. While conductivity increased as purity increased, the diameter did not; at 98% the fibers were ~150 nm, while the highest purity fibers were measured to be 400nm. There was shown to be a linear increase in diameter of fibers with purities of 98, 98.5, 99, 99.5 and 99.9 %. This finding has

---

[51] (Lee Y. , 2011)

pushed the idea that 400nm is the ideal target, as it has the highest conductivity of 1.5 S/cm, but it is also a function of high purity fibers[52].

While not modeling, a very through investigation of how certain variables effect the resulting fiber radius of an electrospun Nafion nanofiber has been reported. This morphological control is vital; if the tailoring of the electrospun fiber is needed, as it is for proton conduction, the knowledge of how each variable, though related to each other, must be gained. By electrospinning various Nafion/PEO blends and modifying only one variable at a time, the magnitude of the affect of that change can be clearly identified. The results, while procured from different solutions (1-propanol instead of 2-propanol/ water as a solvent), utilize the same solution for each specific test; thus, the change shown in each chart is of that variable only being modified.
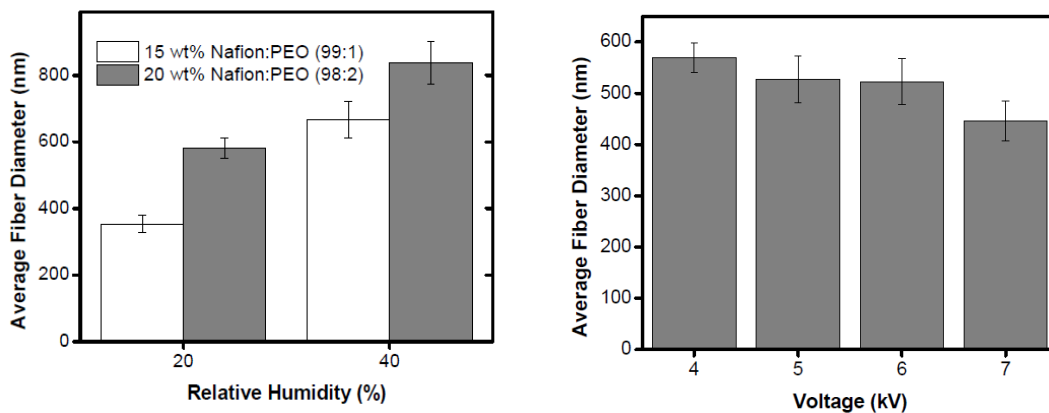
Figure 17: Effect of humidity and electric potential on fiber diameter

---

[52] (Dong, Gwee, Salas-de la Cruz, Winey, & Elabd, 2010)
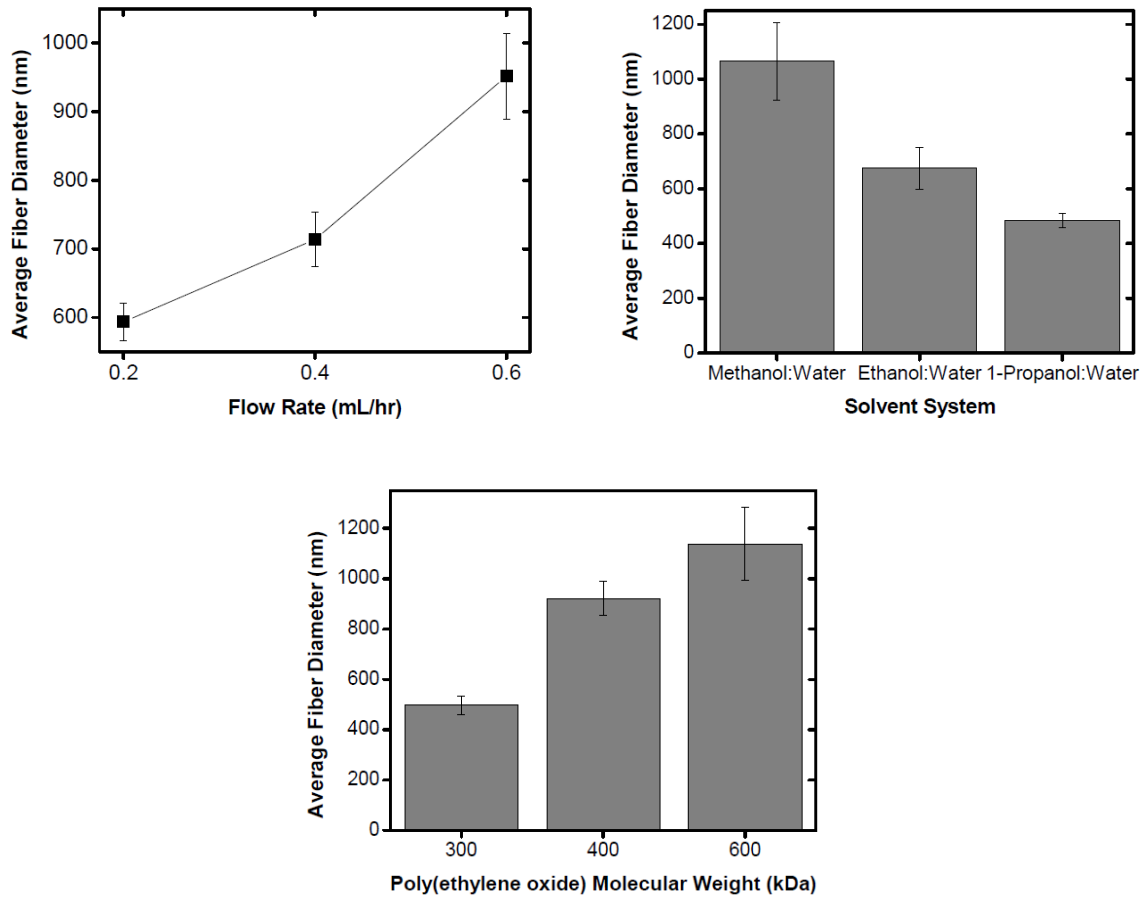
Figure 18: Effect of flow rate and solvent package and PEO molecular weight on fiber diameter

The results shown are clear, and also give insight when scrutinized. The weight of the PEO seems to have a great deal of influence; however, when compared to the super high-purity fibers made in the previous study above, they utilized a 8000kDa PEO molecule, under drastically different electrospinning conditions. However, this trend is still to be taken into consideration when choosing the correct PEO weight. While humidity seems to play a more important factor in the presence of beaded fibers or the lack thereof, the solvent system chosen plays a much larger role. This is believed to be due to the fact that the lighter solvents, which give rise to thicker fibers, are evaporating much too quickly from the surface of the fiber. If this occurs, the fiber can expand in diameter, swelling in the process, as there is no solvent sheath to compress it. A heavier solvent, like 1-propanol,

stays on the fiber surface for longer, and does not allow the fiber to expand; in fact, the pressure of liquid solvent sheath will keep the fiber diameter lower for longer distances between the tip and collector[53].

Modeling

Electrospinning Process

Background

The electrospinning process, while mechanically simple, is a very complex process with many factors interacting to obtain the resulting fiber. As there are many applications of which small, high-purity nanoscale fibers could be used, especially due to the very high surface-to-volume ratio, understanding the phenomena that occur has drawn a significant amount of focus from various researchers, spanning Material Science, Physics, and Chemical, Mechanical and Electrical engineering.

If these fundamental concepts can be harnessed and understood, there is the potential to quantitize and model the system. If an adequate model for electrospinning can be developed, the time consuming and resource-intensive process of trial-and-error with solution can be mitigated, to a point. In addition, the results of the modeling may elucidate points of leverage in the system; what are the important parameters, and how can they be changed to modify the resulting fiber.

---

[53] (Ballengee & Pintauro, 2010)

Nafion Electrospinning

Nafion, being a very conductive polymer, has been focused upon, especially as the main means, if not the only way, of fabricating these fibers is through electrospinning. In order to predict behavior through modeling, two main targets are given. First, modeling the system to see the effect on the resulting fiber radius. Second, the system can be modeled to examine the dynamic behavior, modeling the system as it travels though space.

Modeling Target: Fiber Radius

One attempt of modeling the electrospinning process to find the affects on nanofiber diameter was performed by C.J Thompson *et al.* from a research site in Akron, Ohio. The premise of his work was to establish the effects of 13 material and operating parameters on the final fiber diameter. Isolating each variable and testing is prohibitive; many solution properties are intrinsically linked; one example being polymer concentration and viscosity. Due to the difficulty and time required to analyze the process experimentally, a purely mathematical approach was taken. The group selected an existing model from a large batch of candidates as seen in Figure 19.

[11]	Straight electrified jet, viscous Newtonian or shear-thinning power-law liquid
[12,13]	Linear stability analysis of small capillary and bending perturbations of electrified viscous Newtonian jet
[10]	Analysis of terminal diameter of a thinning electrified jet at the last stage of bending. The model does not account for viscoelasticity, solvent evaporation and polymer solidification. As a result, a disproportionately large role is attributed to surface tension
[14]	Straight electrified jet of viscoelastic liquid
[1,2,8,9]	Linear and nonlinear model (small and large perturbations) of the dynamics of single and multiple bending jets in electrospinning of polymer solutions. The model accounts for solution viscoelasticity, electric forces, solvent evaporation and solidification, surface tension and jet–jet interactions. It explains the physical mechanism of electrospinning and describes all the stages of the process

- [11] Spivak AF, Dzenis YA. Asymptotic decay of radius of a weakly conductive viscous jet in an external electric field. Applied Physics Letters 1998;73:3067-9.
- [12] Hohman MM, Shin M, Rutledge G, Brenner MP. Electrospinning and electrically forced jets. I. Stability theory. Physics of Fluids 2001; 13:2201-20.
- [13] Hohman MM, Shin M, Rutledge G, Brenner MP. Electrospinning and electrically forced jets. II. Applications. Physics of Fluids 2001;13:2221-36.
- [14] Feng JJ. Stretching of a straight electrically charged viscoelastic jet. Journal of Non-Newtonian Fluid Mechanics 2003;116:55-70.
- **[1]** Reneker DH, Yarin AL, Fong H, Koombhongse S. Bending instability of electrically charged liquid jets of polymer solution in electrospinning. Journal of Applied Physics 2000;87:4531-47.
- **[2]** Yarin AL, Koombhongse S, Reneker DH. Taylor cone and jetting from liquid droplets in electrospinning of nanofibers. Journal of AppliedPhysics 2001;90:4836-46

Figure 19: List of possible models and sources of said models

The model selected was one developed in 2000 to account for most parameters found while electrospinning, such as equipment, solution, and ambient variables. The linear and nonlinear components allow one to remove the restrictive assumption that all changes are nearly infinitesimally small or very large, as well as account for the full bending profile a jet will undergo.

The model itself consists of three conservation equations; these are the charge, momentum, continuity equations that govern the system. To start, a baseline was created by giving all parameters realistic values characteristic of a low-viscosity polymer solution. Once the base case was modeled, each variable was changed over a wide range, typically orders of magnitude, of values above and below the base case setpoints. After each modification, the resulting fiber radius was used to generate plots to visualize the effect of the change. The equations, and the variables to be changed, are shown in Figure 20.

$$\frac{\partial \lambda f}{\partial t} = -j_{ev}$$

$$\rho \frac{\partial \lambda f \mathbf{V}}{\partial t} = \tau \frac{\partial P}{\partial s} + \lambda |k| P n + \lambda |k| (\pi a \sigma - q_{el}) n - \lambda e \frac{U_0}{h} \mathbf{k}$$

$$e\lambda = e_0 \lambda_0$$

- λ = Geometrical Stretching ratio
- $f = \pi a^2$ = cross sectional area
- a = cross sectional radius
- ρ = liquid density
- **V** = Velocity Vector
- **P** = the longitudinal force in the jet cross-section (of viscoelastic origin)
- U0/h = the outer electric field strength (U0 the potential difference, h the inter-electrode distance)
- σ = surface tension
- k = local curvature of the jet axis
- e = charge per unit jet length
- q_{el} is the net Coulomb force acting on a jet element
- j_{ev} (>0) is the flux describing mass loss due to solvent evaporation from the jet surface

Figure 20: Conservation equations and the variables used in modeling

To start, a baseline was created by giving all parameters realistic values characteristic of a low-viscosity polymer solution. Once the base case was modeled, each variable was changed over a wide range, typically orders of magnitude, of values above and below the base case setpoints. After each modification, the resulting fiber radius was used to generate plots to visualize the effect of the change. A handful of the graphical representations are Figure 21.
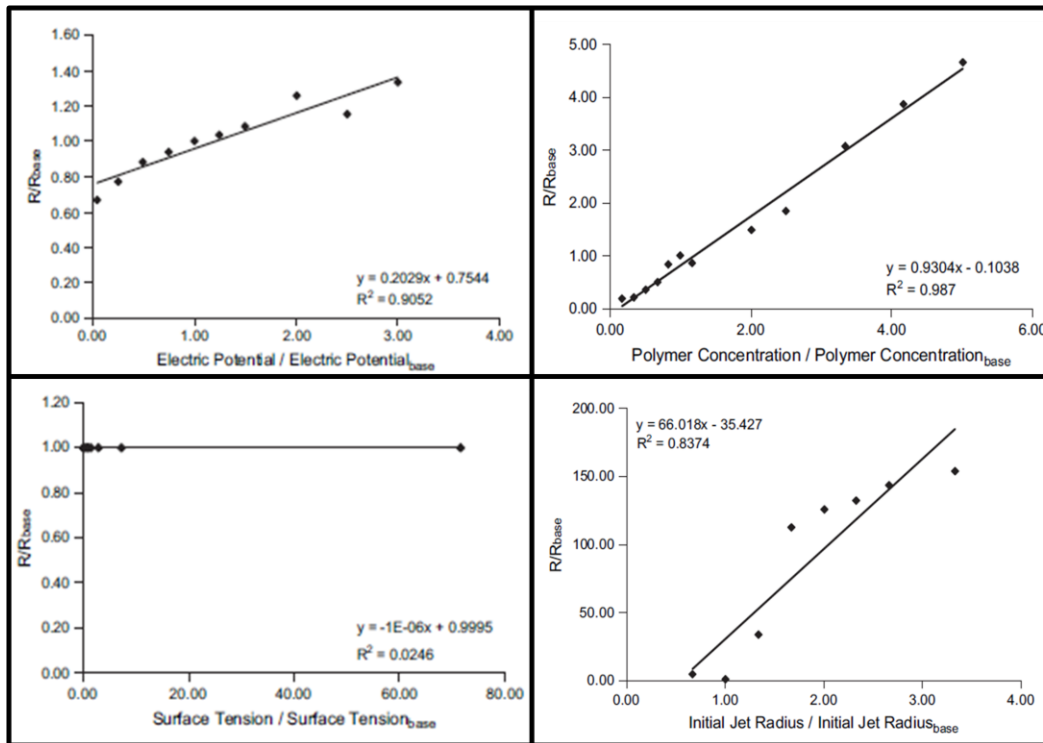
Figure 21: Sampling of results from discrete variable modification

From the data, regressions, linear, exponential and power-law, were performed to get a best-fit characteristic. The variables that are found to have the largest influence on the radius are the volumetric charge density, the distance from the nozzle to collector, the initial jet radius, the relaxation time[54], and the elongational viscosity. Moderate effects were seen with the initial polymer concentration, solution density, electric potential, perturbation frequency, and solvent vapor pressure. There were only slight effects seen with changes in relative humidity, surface tension, and vapor diffusivity. Solution pH, charge polarity and pressure were omitted from the model. These are summarized in Table 7. The text in blue are controllable through the equipment, the variables in green are those

---

[54] Relaxation time measures a material's ability to relax elastically from any pre-stressed state

controllable through the solution, and those in black are inherent properties of either the material or the solution made.

Table 7: Magnitude of influence of electrospinning variables

Largest Influence	Moderate Influence	Slight Influence
Volumetric Charge Density	Initial Polymer Concentration	Relative Humidity
Distance from Nozzle to Collector	Solution Density	Surface Tension
Initial Jet Radius	Electric Potential	Vapor Diffusivity
Relaxation Time	Perturbation Frequency	
Elongational Viscosity	Solvent Vapor Pressure	

These results show that, in terms of fiber radius, the most influencing parameters that can be controlled are the spinneret-to-collector distance and the initial jet radius, which can be changed by simply changing the plate distance and the gauge of needle used, respectively. The moderate influences that can be equipment controlled are the electric potential. The solution's properties, which are all a function of polymer concentration, see a moderate influence, and the solvent vapor pressure can be changed by substituting a different solvent package. It is interesting to note that surface tension, which is shown later on to change the path at which a fiber takes, does not influence the diameter of the resulting fiber. Either this is true, or one model is limited in understanding the actual impact on the system.

One point to note is that there are the actual limitations of the polymer solution and the ability for it to be electrospun; as we have seen in many attempt to electrospun Nafion, the slight changes in carrier polymer loading and initial concentration have vast affects of morphology, oftentimes being to thick to extrude or too thin to produce continuous fibers.

This study also provided a data set of radius vs. distance from the collector. The chart is shown in Figure 22.
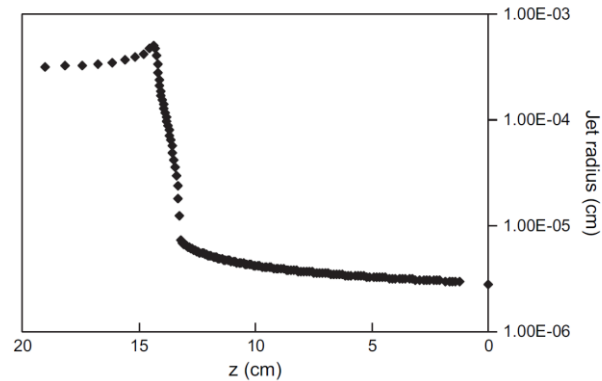
This result shows a constant radius once emitted from the Taylor cone, then a slight increase in diameter before thinning out nearly two orders of magnitude over span of a centimeter. This behavior can be compared to experimental results from other studies, and can be compared to the morphological changes seen when the jet starts to have the bending instability to form a concentric path[55].

Modeling Target: Dynamic Behavior

The dynamic behavior of the electrospinning process will not be immediately concerned with how the fiber changes over time, but the location of the fiber over time. This branch of electrospinning modeling is done to investigate what happens to a strand of nanofiber, in space, as it travels to make contact with the collection plate. One main research group in Poland has been looking at this problem for nearly a decade, with their first work being published in 2005, and, using both mathematical principals and actual

---

[55] (Thompson, 2007)

electrospinning experiments monitored with a high-speed camera, a great deal of insight has been gained.

When approaching the problem of a series of point charges in a system, Earnshaw's thermo states that "A collection of point charges cannot be maintained in a stable stationary equilibrium configuration solely by the electrostatic interaction of the charges". In the case of electrospinning, this implies that treating each fiber as discrete points will result with an unstable equilibrium; the electrostatic interactions will prevent the equilibrium state from being stationary. If the background electric field is considered static, the fiber considered a perfect insulator of electric current, and we treat the polymer solution as a viscoelastic medium with a constant elastic modulus, the system can be modeled as a series of discrete resistors win a long chain. The physical implications can be covered by applying a mass conservation equation as well as a total stress balance along a differential length of the fiber. In addition, columbic, electric, and mechanical forces such as momentum must be conserved[56].

With these baselines given, the boundary conditions of the problem must be established. While the background field is conserved perfectly axial and uniform, the issue arises when dealing with the first bead of fiber. This is taken care of by saying a small initial perturbation is used to position the first bead, and it is kept stationary. While not perfect, this does represent the electrospinning process well, as the polymer does originate from the Taylor cone which is fixed in space.

---

[56] (Yarin, Kataphinan, & Reneker, 2005)

However, this model requires a discrete length for each resistor; what happens as the length of the resistor goes to zero? It is found that this 1-D discretized model is not consistent, as the electrostatic force exerted by a fiber portion to another discrete fiber portion, assuming a constant charge density, will go to infinity; this problem has been approached by the Polish team, to work around this. They identify that the charges do no sit in a linear, point-to-point way, but the charge, rather, migrates to the surface to create a ring charge around the fiber. The resulting columbic forces between neighboring rings are substantially weaker than the point-charges. With this substitution, the longitudinal stress on a fiber, due to the travel through space, is limited and also finite, something the point-charge model failed to incorporate.

This next iteration in the model utilizes a random perturbation of the initial position, surface tension effects, and a more accurate sphere-plate capacitor configuration for the background field. The comparison between these two models, schematically, is shown in Figure 23.
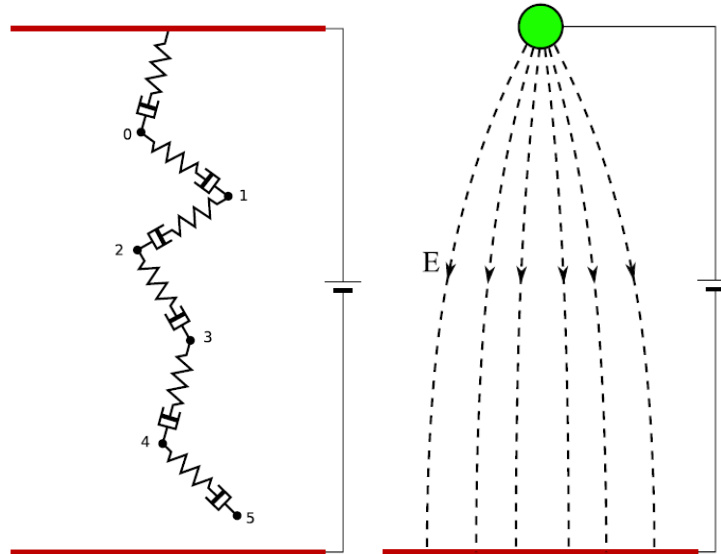
Figure 23: Point-to-point modeling vs. continuous modeling shown schematically

From this model, a basic rheological system can be introduced, with all solution properties given a value such as density, viscosity, surface tension and columbic charge; equipment variables, as well, are all given a base reference case. From this, the properties can be modified and the resulting electrospinning trial can be performed. One such example, a six-fold decrease in surface tension, can be see in Figure 24.
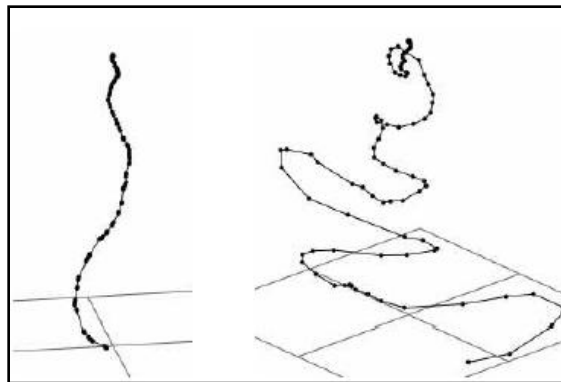
Figure 24: Effect of surface tension on dynamic electrospinning behavior in a modeled environment

This exact model, however, does have shortcomings. The rheological model is very idealized for a solution, and does not incorporate the intermolecular forces that are present in polymeric solutions. In addition, there is no electrical conduction between the ring charges, only electrostatic implications. Evaporation is also omitted, as the rate of solvent

evaporation over the course of the material being electrospun is not clear, though it has been shown that heavier organic solvents require more time to evaporate[57].

This research group published again in 2009, with improvements made. Importantly, short-range electrostatic forces are evaluated with slender-body analytical approximations; a hierarchical force evaluation algorithm is used for long-range interactions and has been coupled with a boundary element condition of solving discreetly. This change is visually depicted in Figure 25, with the red double line being the fiber, with discrete ring charges along the length; as seen, the individual ring charges interact with each other, but they way in which they act has been further refined to more accurately model the behavior. This model was compared qualitatively to experimental data done in an electrospinning chamber of 1 cubic meter with a pure PEO polymer solution.
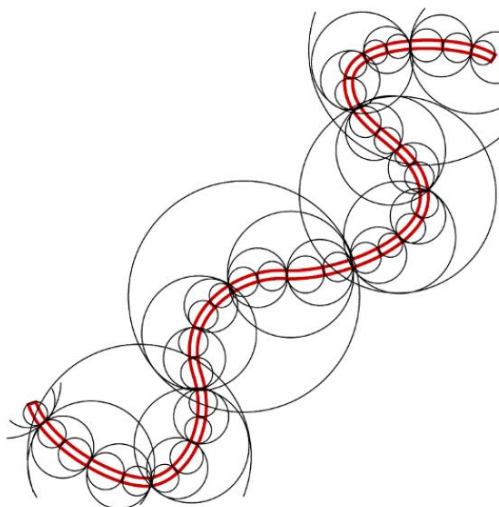
Figure 25: Discrete ring-charges and the interaction between neighboring charges using both short-range and long-range methods

The results, while not a complete match, did estimate when and when not the electrospinning would result in a fiber, as well as showing similar trends in the effects of

---

[57] (Barral & Kowalewsi, 2006)

charge density and applied electric potential[58]. In addition, other materials were tested, such as PAN and PEO, as well as a simple glycerol/water mixture. Utilizing the high speed camera, it is clear that the strong viscoelastic properties, as well as intermolecular forces of attraction, are crucial for the performance of the electrospinning. This is seen with images seen in Figure 26.
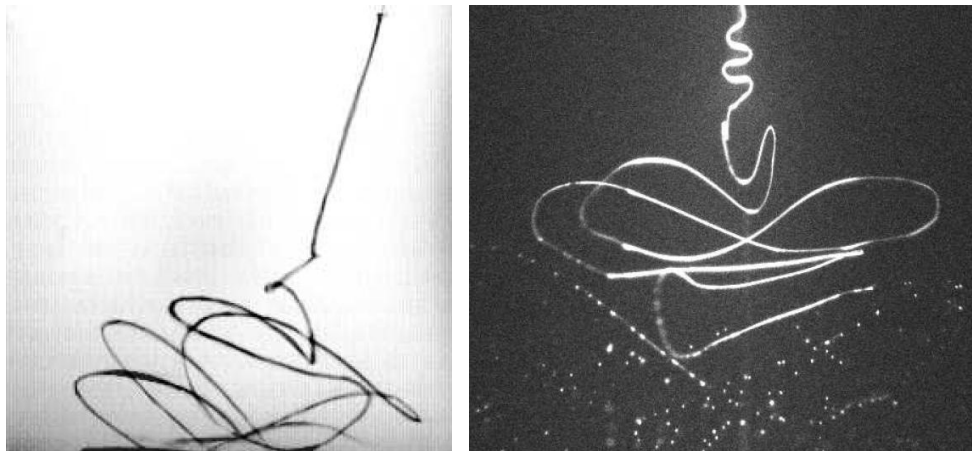
Figure 26: Comparisons of the electrospinning profiles of PEO in water/alcohol (left) and 88% glycerol in water. The tip-to-collector distance seen here is 40 mm

While certainly not the only modeling that has been done, these well-developed, iterative studies give a general overview of the approach taken, while including both modeled results and comparison to actual systems[59].

---

[58] (Kowalczyk & Barral, 2009)
[59] (Shutov & Astakhov, 2006)

Experimental

Nafion® Electrospinning

Experimental Design

As previous experimental studies have shown, the ideal radius of a PFSA polymer fiber is 400nm for optimal proton conductivity. Through various modeling endeavors, as well as experimental trials, we are able to elucidate the critical solution variables. These variables, such as the solution viscosity, weight percentage of Nafion and carrier polymer, the molecular weight of the carrier polymer and the solvent package (which determines the rate of solvent evaporation), must be controlled tightly. The equipment variables heavily influence the resulting fiber's morphology, and those with the most influence have been found to be the applied electric potential, the distance between the spinneret tip and collection plate, and the initial fiber diameter. By controlling the space in which the experiments are conducted, we can eliminate most variation caused by environmental variables such as temperature and relative humidity.

The series of electrospinning experiments were designed to find the values of solution and equipment variables that:

1. Produce high-purity (97% and higher) fibers near 400nm in diameter

2. Can be electrospun continuously for long durations of time

3. Can be deposited to achieve coverage of 5 cm^2 for use in a single-cell PEMFC test bed

To achieve this, the knowledge gained from previous trials was evaluated to determine baseline values for our initial solutions. By starting with a Nafion solution in ethanol, crystalline PEO (400kDa) and various solvents, solutions were fabricated. The main variables were Nafion loading (5-15%) carrier polymer loading (1- 5 polymer wt%), and solvent package (ethanol, 1-propanol, 2-propanol & blends).

The electrospinning equipment was also varied, modifying the variables with the highest influence to see the effect on fiber morphology. Tip-to-collector distance (8-30cm), electric potential (5-18.5 kV), and flow rate (0.05-0.75 $^{mL}/_{hour}$) were varied. As the solutions were already fabricated, these equipment variables could be fine-tuned during the experiment, allowing us to find an optimal set of experimental conditions for each solution prepared.

Continuous Electrospinning

In order to control the deposition of the electrospun nanofibers in a 5cm^2 area, various methods were proposed. As the fiber travels towards the collection plate, the electrostaticly unstable polymer jet will start to follow a conical path. The larger the distance the fiber has to travel to deposit on the collection plate, the farther from the center the fiber will deposit. The fiber, as it travels along this path, will also undergo morphological changes, namely an increase in diameter, after the initial thinning at the needle tip. As the solvent starts to evaporate, the fiber will then expand; as the solvent is lost, the polymer will then dry, and can potentially become brittle and break.

The longer the distance between the collection plate, the larger both the footprint of deposition and fiber diameter will be. If the collection plate is placed very close to the tip of

the spinneret, it will decrease the size of the footprint where the fibers are deposited, but we may not be able to achieve the proper fiber diameter. In addition, the shorter tip-to-collector distances may not allow for the proper formation of the spiral, and could also promote build up of fiber at one point, and not be spread over the area. This build up can will act as electrical resistance between the needle tip and the collection plate, and, at short distances, can cause erratic fiber behavior.

Charge-Density / Localized electrospinning

To sidestep these difficulties, a small collection plate was suggested. As this was unable to be implemented, layers of non-conductive Teflon pieces were placed over the collection plate, with cut-outs of a $5cm^2$ area in the center. As the fiber follows the path of least electrical resistance, the fiber should tend to deposit near the center, where the there is no impedance by Teflon. To ensure the GDL was in contact with the collection plate (as we had just added space between the center of the GDL and the plate), small squares of aluminum foil were added in the center to promote electrical conductivity between the GDL and the collection plate.

Collection Plate treatment

Initial testing for fiber radius were done by covering the collection plate with bare carbon cloth; while GDL material (actual carbon cloth with a carbon microporous layer) was used when the actual to-be-tested fiber mats were created, these initial tests did not warrant the use of the GDL material. In addition, there was no need to control the deposition area, so no Teflon inserts were used.

Soft-Baking for Mechanical Strength

Other researchers fabricating electrospun Nafion mats utilize a post-production step of "fiber welding", or "soft-baking". The fibers, as spun, overlap, but do not have any mechanical bonding between them. These fiber crossovers, if linked together, could create a crosslinked structure instead of a simple overlapping mat. This crosslinked structure has two immediate benefits. First, the welded junctures can transport protons across, as opposed to forcing a proton to travel on the same fiber, even though it may require more energy. Second, this structure will have much more mechanical strength, as the fibers are physically bonded into a networked structure.

To achieve this, an electrospun PFSA mat is typically exposed to DMF vapor at 70°C for anywhere from one to eight hours. Due to time constraints and the lack a controlled environment, this was not attempted. If this was to be done, a careful amount of DMF is to be used, under very precise temperature and time measurements. If overexposed to DMF, the fibers will not just melt into each other at areas where fibers are crossed, they will all melt, losing the rigid, smooth fiber morphology and melt into a solid mat[60].

Electrospinning

Solution Methodology

The solutions to be electrospun were mixed to control Nafion loading, carrier polymer loading, and solvent loading. Solvent loading was a particular area of concern, as the Nafion is pre-dissolved in ethanol, and solvent can be lost to the environment (low vapor pressures) if not stored carefully. As solvent content cannot be tested for, the

---

[60] (Ballengee & Pintauro, 2010)

amounts of each component added to the solution must be done diligently and recorded carefully. To achieve higher Nafion weight loadings (above our initial concentrations), a solution was mixed and then left, uncapped in a fume hood, to evaporate solvent until the proper weight of solvent was lost. While the rate of solvent loss could be accelerated by adding heat, this caused the Nafion in solution to crystallize, separating from the solution in a clump.

To achieve a homogenous solution, it must be mixed. As these solutions were made in very small quantities due to cost (>10mL), the components were dissolved in a common solvent before being mixed. The PEO was in a crystalline form, and must be miscible with the solvent systems we have chosen (methanol, ethanol, 1- and 2-propanol); therefore, it was tested and found to be only partially miscible in methanol, ethanol and water, with near complete miscibility in 1-propanol and 2-propanol. Therefore, a bulk solution of PEO was made, with a solvent of 1:1 1-propanol/HOH, at a loading of 0.025g PEO / 1g solution.

The components were mixed together in small 10mL vials with sealed caps. To aid in homogenous mixing, the solutions were initially sonocated for 10 minutes, and shaken vigorously for 2-3 minutes to ensure settling, and thus separation, did not occur.

Viscosity

Before electrospinning the solutions, they were tested for viscosity with a Brookfield V-III cup-and-plate viscometer, a standard rheometer found in academia and industry. By loading a small sample of material into the cup and compressing it with the plate, it is spread into a thin layer. By spinning the plate at a set value for RPM, the viscometer is able to detect the shear strain and give a value for viscosity. It is important to

note that the rheometry of polymers has been widely studied, but most polymer solutions are not ideal; there is a tendency for solutions to be fixotropic; this sensitivity to shear stress will be seen in experiments as a value for viscosity to be higher at a low shear rate (low RPM), but much lower at a high shear rate (high RPM). To alleviate for this, the rheometer was calibrated using Brookfield's calibration solution at the beginning of the run and verified at the end of the run; while the viscometer is most accurate in the middle range of its torque range, this was ignored to ensure there was no difference in shear stress between our samples.

PEMFC Testing

Experimental Design

To determine the overall performance of the MEAs that are fabricated, single-cell testing was done. While there is a multitude of testing that can be done to a fuel cell for various individual fuel cell components, such as electrical impedance spectroscopy (EIS) of an surface to determine resistances and cyclic voltammetery (CV) of an electrode surface to determine the active catalytic sites, single-cells testing will evaluate the entire MEA as a system. These single-cell tests are performed by taking an MEA of known construction, feeding in a fuel to the anode and a oxygen-containing stream to the cathode, and drawing current from the assembly while monitoring the current draw and the resulting voltage of the circuit. With this data, one can plot voltage (y-axis) vs. current density (x-axis), and use the resulting plot to analyze the cell's performance. By plotting the power density vs. current density, one can see the maximum power output the device can achieve. Both of

these plots can be analyzed to deduce the properties of the MEA and their ability to generate power over a wide range of current draws.

In this project, the single-cell MEA is constructed and tested with a variety of feed conditions and operating temperatures. By testing different MEAs under equivalent conditions, direct comparisons can be made between the several MEAs; this is important as there is currently a loose understanding of how to exactly optimize a fuel cell for performance. Membrane thickness, GDL material, MPL fabrication, electrode catalyst and ionic binder loadings, and even operating conditions are not agreed upon over the wide range of literature. Because of this, keeping our fabrication techniques equal and testing under identical conditions is vital to being able to clearly identify the variable changed as the source of the difference in performance.

Preparation and Construction

Procedure of Fabricating an MEA

An MEA can be created in a variety of ways. Because the electrode must be fabricated, the method of doing so and the surface at which it is deposited can be changed. While the literature shows evidence of some methods over others with respect to the performance of the resulting electrodes, no method is clear-cut as to creating a better performing MEA. Typically, the discussion of "improved" performance lies in the porosity of the electrode layer and MPL.

The first way to fabricate an electrode layer is known as the Decal Transfer method; this method was first reported in 1992 by Wilson and Gottesfeld, though there have been

many reports of modified thin-film decal transfer methods[61]. The electrode is constructed onto a surface with little adhesion, typically Teflon. The Nafion can be cast onto the Teflon, or it can be mixed with catalyst particles and cast as an ink. Once this is done, the entire layered system is hot pressed, which adheres the electrode layers to the membrane. After the hot-pressing has been completed, the Teflon can be peeled away, keeping the electrode firmly in place on the membrane. The resulting structure can be referred to as a catalyst-coated membrane, or CCM. This process is outlined in Figure 27. The GDL can then be adhered to the external surfaces of the electrode and used in a fuel cell application.
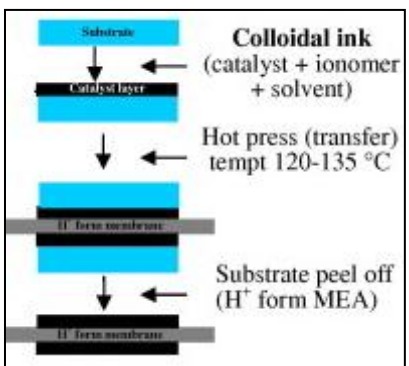
Figure 27: Schematic of catalyst-coated membrane fabrication via the decal method[62]

The second major method of forming an MEA is by creating a catalyst-coated substrate, or CCS, and hot-pressing it to the activated/protonated membrane. In this method, the catalyst, ionic binder, and solvent form an ink, and this ink is applied to the GDL. This can be done by painting the ink onto the GDL's MPL surface or, more commonly, airbrushed on the surface and dried. Once the GDL has the electrode structure, it can be applied to membrane via the same hot-pressing that occurs in the CCM procedure. Once hot-pressed, the MEA can then be used in an fuel cell assembly. Some claim that this

---

[61] (Saha, Paul, Peppley, & Karan, 2010)
[62] (Krishnan, et al., 2010)

method ensures more homogenous deposition of the electrode layer, but it has not been established that this method will constantly provide a better-performing MEA.

Introduction

While an in-depth explanation of the procedure used to fabricate the membrane-electrode assembly (MEA) can be found in Appendix B, this section explains the logic and basic procedure for preparing the MEAs used in this study. The gas diffusion layer (GDL) is prepared, and then coated with a catalytic ink to form the electrode layer upon the surface of the GDL. Once an anode and cathode are made on their respective GDL, an activated, 8cm x 8cm, Nafion membrane is placed between the two electrodes and pressed at 275°F (135°C), for 2-3 minutes under pressures ranging from 1300psi to 5000psi, depending on catalyst loading and membrane thickness.

Gas Diffusion Layer Preparation

The gas diffusion layer (GDL) material chosen for a majority of the MEAs constructed was ETEK-LT1400K carbon cloth, treated with a carbon MPL on one side. The GDL is prepared by cutting out the proper sized piece and establishing a weight. Once this is done, it can be airbrushed with the catalytic ink.

Electrode Fabrication

he electrode fabrication employs the use of a sprayable ink, containing the electrode material, and an airbrush to deposit the electrode material onto the GDL. The inks mixed with both the catalyst loading and Nafion/Catalyst ration as design specifications. To make an electrode with a $4\text{mg}\cdot\text{cm}^{-2}$ catalyst loading and a Nafion/catalyst weight ratio of 33%, the proper amount of catalyst (as well as a 20% margin of loss during the spraying process)

must be added, as well as the correct amount of Nafion. As the Nafion is a solution (labeled as 10wt% in ethanol, tested and found to be 13.58% Nafion in ethanol), the correct ratio must be observed. This leads us to choose 25mg of catalyst, and add ~60.75mg of Nafion solution. To make solution the proper viscosity for spraying, the catalyst is first mixed into 10mL of water, with 10mL of ethanol mixed afterwards, and then the Nafion solution. This ensures that the active sites on the catalyst do not react violently with the ethanol in either the Nafion solution or the pure ethanol.

Once this has been mixed in a small Erlenmeyer flask, it is covered and placed in a sonocated bath for at least hours; this time duration has been shown to achieve the smallest agglomerate size of Nafion; shorter times will produce a solution with large clusters of Nafion, with longer durations yielding little improvement over the two-hour testing. In addition, the sonication bath was not temperature controlled, but there is evidence to suggest that sonication at elevated temperatures, up to 80°C, will decrease the Nafion aggregate size (from a wide dispersion at 25 °C to a sharp peak at ~25nm at 80 °C) and, therefore, increase performance (a 14mW/cm^2 peak power density increase with a higher limiting current density)[63] .

This mixture is then poured into the feed hopper of the airbrush. The GDL to be coated is placed vertically, with one edge slightly being help by a clip apparatus. To reduce the amount of catalyst lost due to solvent running off the GDL as it is airbrushed, a convective heat source is used to dry the ink as it is applied; past work has sprayed ink and

---

[63] (Yuan, et al., 2011)

dried the ink in separate steps; we have blended the steps together to decrease time and diminish losses due to excess solvent building up on the GDL surface and running off.

As the electrode layer builds up, it will gain the mass of the solvent, catalyst and Nafion. As periodic points in time, the GDL is taken and dried in a furnace at 80°C; this is done to drive off most of the solvent. Once dried, the GDL can be weighed and, based upon the amount and ratio of Nafion and catalyst, as well as the initial GDL weight, we can calculate a loading. If we have not reached our target ($4mg \cdot cm^{-2}$), we continue the deposition process until it has been reached. Once made, the GDLs can be stored in a dark environment in a sealed container, and used at a later date, once the membrane has been activated.

Membrane Activation

The membrane, a cast sheet of Nafion polymer, is used in the PEM fuel cell to prevent fuel crossover, as well as promote proton conductivity. Nafion, as perfloursulphonic acid, promotes proton conduction via the sulfonic groups the polymer contains. To ensure that these sites are active and able to be utilized in the fuel cell, it must be activated. This process ensures the membrane is clean of any surface impurities, is activated, and is clean and ready to be used in the fuel cell.

The roughly 5cm x 5cm square is first boiled in water for a half an hour, to get the membrane up to temperature and ready. Then, it is boiled in hydrogen peroxide for another half hour; this is done to oxidize any surface impurities the membrane may have accumulated in storage, or in the lab environment. The membrane is then returned to the lightly boiling water to clean off any peroxide, and is then boiled in 0.5 M sulfuric acid for

an hour: this activates the membrane to achieve better proton conduction. Once this is done, it is then cleansed in boiling water until it is ready to be used.

Hot-Pressing

Once the membrane is activated and we have a proper cathode and anode, the membrane is placed between the two electrodes. This "sandwich" is then bookended by Teflon, and then by a thin aluminum caul plate and an equivalent tool plate. This is then placed into a Carver press, pre-heated to the correct temperature, and then pressed between both platens for the specified time. Once the time is up, the MEA is removed from the press, is allowed to cool, and then carefully removed from the Teflon sheets. The MEA is inspected to ensure there is proper adhesion between all layers, and that there have been no pockets of air captured. Once this inspection is done, the MEA is then packaged, sealed, and put aside for later use.

Break in Procedure

While an MEA is able to be used immediately after it has been hot-pressed, most will need to undergo a break-in period; testing an MEA immediately after its fabrication will not indicate its maximum potential for generating power. While many different procedures have been developed and adapted to various fuel cell applications (membrane type, catalyst type, stack vs. single cell, etc.), the literature concerning single-cell Nafion-based MEAs was focused upon. Despite this focus, there are still a wide range of procedures. As finding an optimal break-in cycle is a project in itself, one must be chosen and carried through with all MEAs to eliminate variation.

One major factor that contributes to poor fuel cell performance is the active amount of catalyst. Even if the anode layer contains a large amount of catalyst, the catalyst sites will need to be active. While platinum, one material used as catalyst, is somewhat noble, the ruthenium found in the anode can oxidize easily; such oxidation can happen in ambient air or even in aqueous solutions. As we prepare and activate our membrane in aqueous solutions, it is very likely some of the catalyst has been oxidized at some point; between the synthesis of the actual catalyst nanoparticles, the storage for long periods of time in plastic containers, and exposure to ambient air, these nanoparticles have a very high likelihood of being partially oxidized. This phenomenon was tested; 1:1 Pt/Ru black (unsupported) catalyst particles, were procured from a supplier. As received, they were found to have a very narrow size distribution near 5nm. These particles were either oxidized (treatment in flowing humidified air for one hour at 100°C) or reduced (treatment in flowing H_2 for one hour at 100°C), and tested for both a change in size, as well as for performance. The size was seen to increase, with the distribution of both the oxidized and reduced particles being fairly even over the 5-20nm range. To discern performance, electrodes were made; equal weight of catalyst was mixed with Nafion as the binder, placed on a rotating disk electrode and immersed in 1M sulfuric acid. With the electrode in the presence of 0.5M methanol, cyclic voltammetery was performed to measure the ability for the electrode to oxidize methanol. These results are seen in Figure 28.
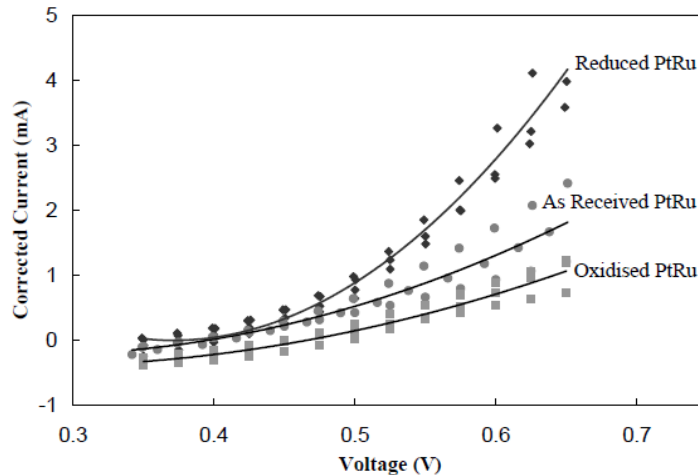
Figure 28: CV results comparing the ability of reduced, as-received and oxidized Pt/Ru black catalysts to oxidize MeOH.[64]

As shown, even low-temperature exposure to dry H_2 has a fairly profound effect upon performance. In light of this, we will be using a dry H_2 anode feed during the break in period.

In addition to choosing a feed, the cell must be broken in by physical use; typically, keeping a cell at OCV may be detrimental, as it can promote catalyst migration. In addition, excess feed must be utilized; as an MEA is first used and current is drawn, the fuel cell will react. If there is not enough feed material to oxidize, other fuel sources within the MEA can be broken down to keep up with the current demand. One such internal fuel source can be the carbon catalyst support; while this phenomenon will typically manifest as a negative voltage as current is drawn, this may not always be the case.

To allow for proper break in, the fuel cell is set up to run with unhumidified hydrogen on the anode side and dry air on the cathode side. The cell is then alternated every 30 minutes between no current draw (OCV) and a current draw of 100mA/cm² over

---

[64] (Hill, 2003)

the course of five hours. With a 5cm² test bed, we will be drawing 500mA, or 0.5A. These types of cyclic procedures are fairly common,

Testing Conditions

In order for our MEAs to be tested and compared against each other (and to existing literature values), the test station used allowed for the control our major variables, listed below.

1. Fuel and oxygen feed flow rates and pressures
2. Temperature of the liquid methanol feed stream to the fuel cell (methanol only)
3. The temperature at which the fuel cell operated
4. The temperature of our bubble-through humidifier (hydrogen/oxygen runs only)
5. The amount of current being drawn from the single cell
6. The concentration of the methanol feed (methanol only)

While values for these variables can be optimized for a specific fuel cell, this study is primarily focused on the affect of catalyst loading, Nafion loading, and temperatures over a typical range of operating conditions seen by DMFC. While not a comprehensive study, the main test station variables modified were the operating temperature, the feed flow rates, and the feed pressures/concentrations. A group of undergraduate students at WPI studied the effect of these major variables on both Nafion and PBI membranes on the exact setup utilized in this project. It was found, via their study, that for a 5cm² Nafion-117 MEA, with a 4mg·cm⁻² Pt/Ru on C anode and a 2 mg·cm⁻² Pt/C cathode, it was found that operating the

cell with 2.5M MeOH fuel with a 7 psig oxygen stream to the cathode was found to produce optimal performance[65].

The testing conditions saw a temperature range between 50°C to 90°C, with methanol flow rates ranging from 1mL/min to 5mL/min, with hydrogen and oxygen pressures ranging from near atmospheric to 10 psi, with thy hydrogen run in both a humidified and unhumidified state. While all system variables are reported with each set of results, it is to note that the 70°C, 1.5mL/hr MeOH flowrate with 7psig oxygen to the cathode was the standard testing protocol. For a hydrogen feed, it was humidified (with the humidifier temperature set to 75°C) and run near 5psig.

MEAs Fabricated and Tested

The MEAs that were fabricated were designed and created to selectively investigate different aspects of the MEA variables on performance. The major variables are listed below.

1. Membrane material (Nafion, PBI, etc. and thickness)
2. Catalyst Type (Pt/C, Pt/Ru on C, etc.)
3. Catalyst loading of Anode and Cathode ($1mg \cdot cm^{-2}$ – $4mg \cdot cm^{-2}$)
4. Ratio of Nafion to catalyst in the electrodes (0.1-0.5)
5. GDL/MPL material (many commercial options available)

While a comprehensive study of each of these variables would help to solidify assumptions that are currently made about DFMC setups, the focus of this study had to be narrowed to be able to acquire enough data to draw larger conclusions on overall

---

[65] (Do, Spetka, & Suarez, 2012)

performance. However, we did want to test MEAs constructed in the same way, while only changing one variable. For example, have an equivalent membrane, catalyst loading in both electrodes, and GDL, but change the Nafion loading in the electrodes. To do this, the MEAs that were fabricated, and their properties, are listed in Table 8.

Table 8: Summary of selected Fabricated/Tested MEAs.

MEA Type	Anode Catalyst [Loading (mg/cm2)]	Cathode Catalyst [Loading (mg/cm2)]	GDL Material	Membrane Type	Notes
Comm. MEA	Pt/Ru on C [4mg/cm^2]	Pt/C; [2mg/cm^2]	Carbon Cloth	N117	Commercially Available
300% MEA	Pt/Ru (1:1 at.) on Opt. C; [4.56mg/cm^2]	Pt/C (XC-72); [4.42mg/cm^2]	ETEK 1*	N117	3x std. Nafion in Electrodes
MEA #7	Pt/Ru (1:1 at.) on Opt. C; [3.97mg/cm^2]	Pt/C (XC-72); [4.07mg/cm^2]	ETEK 1*	N117	Standard Fabrication
MEA #11	Pt/Ru (1:1 at.) on Opt. C; [3.71mg/cm^2]	Pt/C (XC-72); [1.39mg/cm^2]	ETEK 1*	N117	Standard Fabrication
N1035x2	Pt/Ru (1:1 at.) on Opt. C; [3.82mg/cm^2]	Pt/C (XC-72); [3.77mg/cm^2]	ETEK 1*	2x N1035	Two Half-MEAs, no hot-pressing
E.MEA 1	Pt/Ru (1:1 at.) on Opt. C; [4.72mg/cm^2]	Pt/C (XC-72); [3.66mg/cm^2]	ETEK 1*	N117	Electrospun Cathode: 18.47mg Nafion [3.08x]
E.MEA 2	Pt/Ru (1:1 at.) on Opt. C; [3.42mg/cm^2]	Pt/C (XC-72); [3.76mg/cm^2]	ETEK 1*	N117	Electrospun Cathode: 92.38mg Nafion [15.39x]
E.MEA 3	Pt/Ru (1:1 at.) on Opt. C; [3.33mg/cm^2	Pt/C (XC-72); [1.17mg/cm^2]	ETEK 1*	N117	Electrospun Cathode: 19.02Xmg Nafion [3.19x]
E.MEA Total	Pt/Ru (1:1 at.) on Opt. C; [2.45mg/cm^2	Pt/C (XC-72); [1.29mg/cm^2]	ETEK 1*	N117	Dual Electrospun electrodes C: 17.56mg Nafion [2.86x] A: 15.77mg Nafion [2.47x]

At this point, some important "pairs" of MEAs should be identified. The pairs are MEAs that are identified as comparable systems that which assumptions can be tested.

- MEA #7 and the 300% MEA are equal, with the 300% MEA containing three times as much Nafion in the electrode layers; the Nafion to catalyst ratio for #7 and 300% are 0.1 and 0.33, respectively.

- MEA#7 and N1035x2 are equivalent, with the difference being that the N1035x2 MEA is essentially MEA#7 split down the middle of the membrane; there is a complete anode hot-pressed to a Nafion membrane that is 3.5mm thick, and a cathode hot-pressed to a membrane that is 3.5mil thick. If they are aligned, they will physically represent an MEA with a 7mil thick membrane. This was done to see if individual, independent anode and cathode assemblies could be fabricated and tested, making it very easy to "swap in" an anode or cathode of known properties.

- The 300% MEA and E.MEA1 are equal, with E.MEA1 having an electrospun cathode. Despite the difference in morphology, the Nafion loading in the cathode is near equivalent.

- E.MEA1 and E.MEA2 are equal (both having electrospun cathodes), with E.MEA2 having a much higher Nafion loading.

- E.MEA3 and MEA#11 are equal, with E.MEA3 having an electrospun cathode. This pairing is the same type of pairing as the 300% and E.MEA1, but with reduced cathode catalyst loading.

- E.MEA Total is an attempt to utilize an MEA with two electrospun electrodes. Due to the fiber morphology, a lower catalyst loading needed to be used to prevent the electrode's fibers from being compacted into a thin layer. This is the first attempt of

testing an MEA with two electrospun electrodes, and could be compared to the commercial MEA that was procured and tested.

While other MEAs were manufactured, these were not listed directly as most produced results that did not reflect the proper data expected from an MEA of this type: these were not subtle, small differences, but either failures during the fabrication process or during the actual testing. Such incidents include trapping air between layers in hot pressing, rips/tears in the GDL after catching and snagging the fuel cell test block, leaching of catalyst due to over pressurization of the MeOH feed, and other general mishaps. These incidents were few and far between, and arose mostly during the first few fabrications and tests. Once familiarized with the procedural steps in fabricating the MEAs, these mistakes were very rare. The data collected from the MEAs listed above has been done in duplicate, with error bars omitted to aid in the presentation of the data in chart form. The raw data can be found in Appendix D: Raw Data, MEA Testing.

Results and Discussion

Electrospinning

Electrospinning trials were conducted using the horizontal electrospinning apparatus housed in WPI's Washburn Shops, under the direction of Professor Shivkumar and his graduate students. A schematic of this setup is seen in Figure 29; the electrically insulated box that contained the apparatus is not illustrated; it contains the spinneret, high-voltage power supply lead and the grounded collection plate[66].
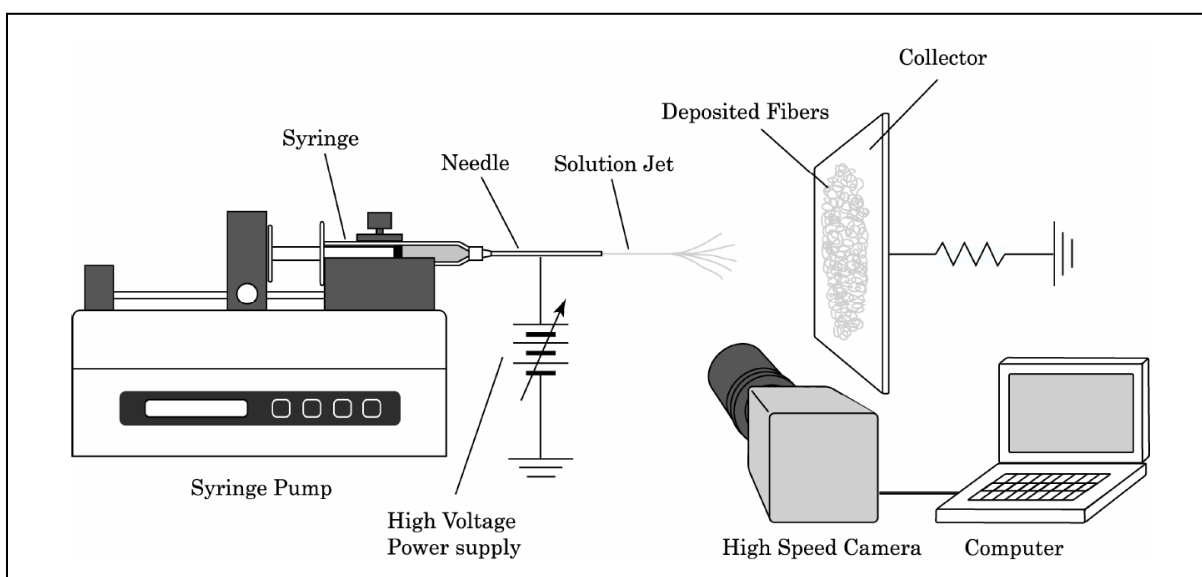
Figure 29: Schematic of electrospinning setup used for nanofiber fabrication

The electrospinning experimentation consisted of three distinct phases. First, initial solutions were tested to find solutions that were within the acceptable range of viscosity for electrospinning. Second, these initial solutions were electrospun on bare carbon cloth and imaged using scanning electron microscopy (SEM) to determine a nominal average fiber diameter. Once this was determined and a solution selected, the solution was then

---

[66] (Eda, 2006)

electrospun continuously to create a fiber mat upon a proper GDL surface. These mats, and supporting GDL, were trimmed to the proper 5cm² size and used in the single-cell test bed.

Solution Rheology

It is well known that the solution properties are vital for dictating and controlling the electrospun fiber's properties. Most importantly, there is a direct relationship between viscosity and fiber thickness. A more viscous solution will spin a thicker fiber; too thick, however, and the spinning cannot be initiated as the polymer solution cannot fit through the spinneret. Too thin a solution will cause gaps between polymer chains, thus being unable to form continuous fibers; this results in small droplets being "electrosprayed" onto the collection plate. The target for our viscosity of Nafion/PEO was between 50-150 cPs; while not being reported in the literature in many studies due to the thixotropic nature, this was given as a rule of thumb gained from experience on the electrospinning equipment at WPI.

The solutions fabricated were tested for viscosity with a Brookfield DV-III viscometer, after being calibrated using Brookfield's own 9.5 cPs calibration solution, and checked after the runs to ensure there was no error in the instrument over the duration of the testing. A build-up of polymer on the viscometer would increase the weight of the rotating plate, thus increasing the torque needed to spin, which would result in a higher viscosity. The solutions tested have been listed in Table 9.

Table 9: Nafion/PEO Solution Viscosities

Solution	Wt% Nafion	Polymer wt% PEO	Viscosity (cPs)

1a	5	1	25.3
2c	5	3	26.7
3b	10	1	34.8
4a	10	3	53.1
7a	15	3	147

From these results, solutions 4a and 7a were chosen to conduct the initial electrospinning trials. It is important to note, that higher concentrations of Nafion, while experimentally possible, were very difficult to fabricate. Because our initial polymer, Nafion in ethanol, was 13.581wt% Nafion and our PEO was solvated in a 1:1 1-propanol/2-propanol solution, the mixture was left uncapped in a fume hood and allowed to lose solvent. Using heat to advance this process caused the precipitation of what is believed to be crystalline Nafion; even gentle heating would induce this crystallization, which could not be reversed.

It is also important to note the low wt% of our carrier polymer, PEO. This PEO is 400kDa, and previous work has seen the need for up to 25polymer wt% PEO to be successfully spun. For our high-purity application, the amount of PEO was intentionally limited to below 3 polymer wt%.

SEM Analysis

Solutions 4a and 7a were electrospun to determine the fiber diameter that was produced via electrospinning. To establish the correct procedure, the flowrate of the solution and collector-to-tip distance was set. Once flowing, the voltage was increased until

electrospun fibers could be seen coming from the Taylor cone and connecting to the collection plate. If fibers were not formed, the voltage was decreased gently and then shut off, the flow ceased, and the tip-to-collector distance changed. Once the new distance was set, the experiment was repeated. While this process was not optimized, some setups would start to spin, but then either clogged the needle or produced fibers which dried too quickly, causing solid fibers to create a bridge between the needle and the collection plate. The fibers used in the SEM analysis were produced using the conditions listed in Table 10.

Table 10: Electrospinning Conditions of Fibers used for SEM

	Solution 4a	Solution 7a
Solution Viscosity [cPs]	53.1	147
Tip-to-Collector Distance [cm]	10	13
Solution Flowrate [mL/hr]	0.55	0.35
Electric Potential [kV]	13.5	12
Needle Diameter [mm]	0.413	0.413

SEM images of the resulting fibers are shown in the following pages.

Solution 4a Images
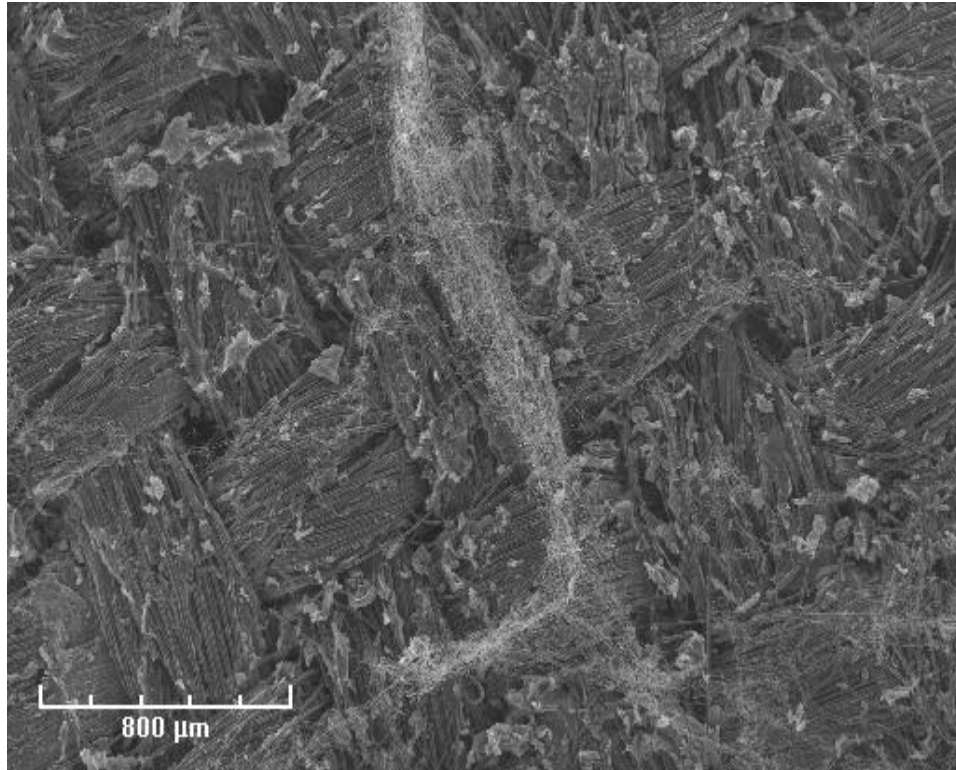
Image 1: 50x Magnification; note the carbon fiber weave of the supporting GDL, the electrospun white fibers, and the globules of material dispersed on the surface.
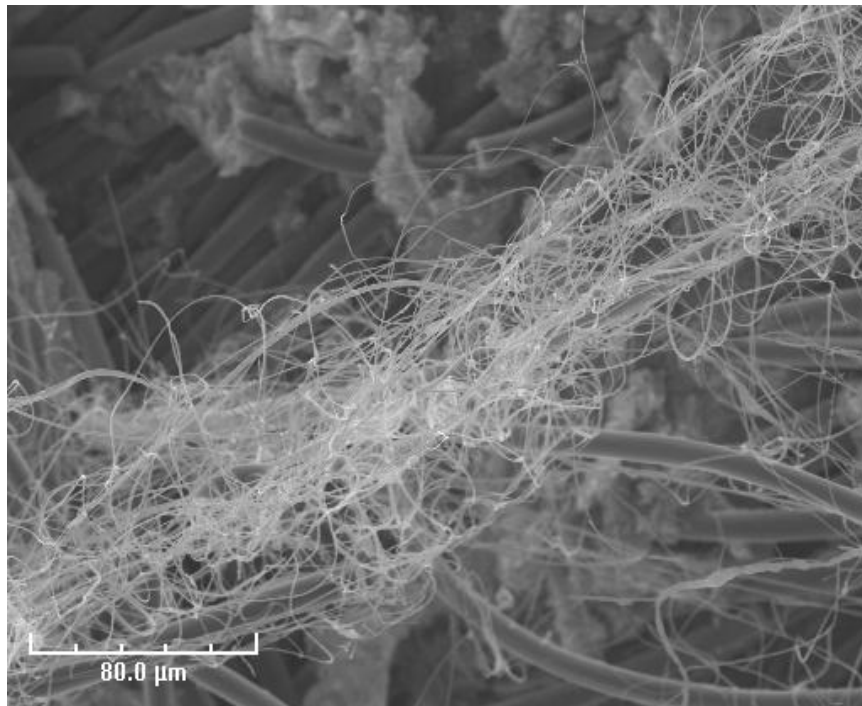
Image 2: 500x Magnification; note the relative thickness of the nanofibers to the individual carbon tows
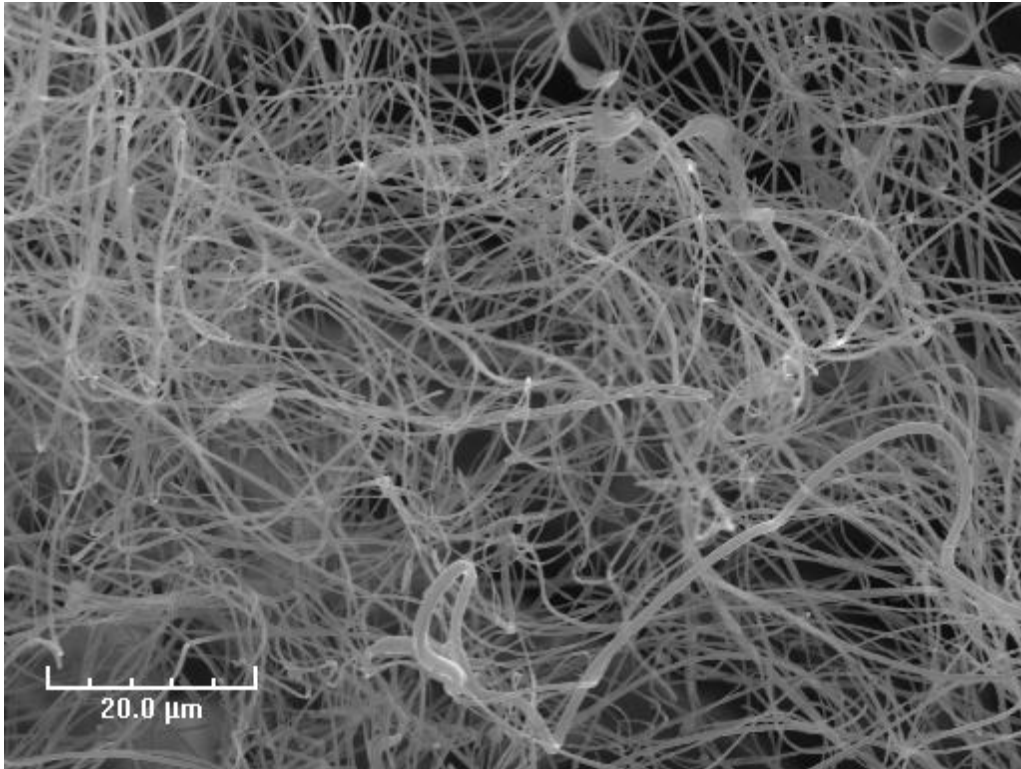
Image 3: 1000x Magnification; note the high fiber density and fairly equal fiber thickness between fibers
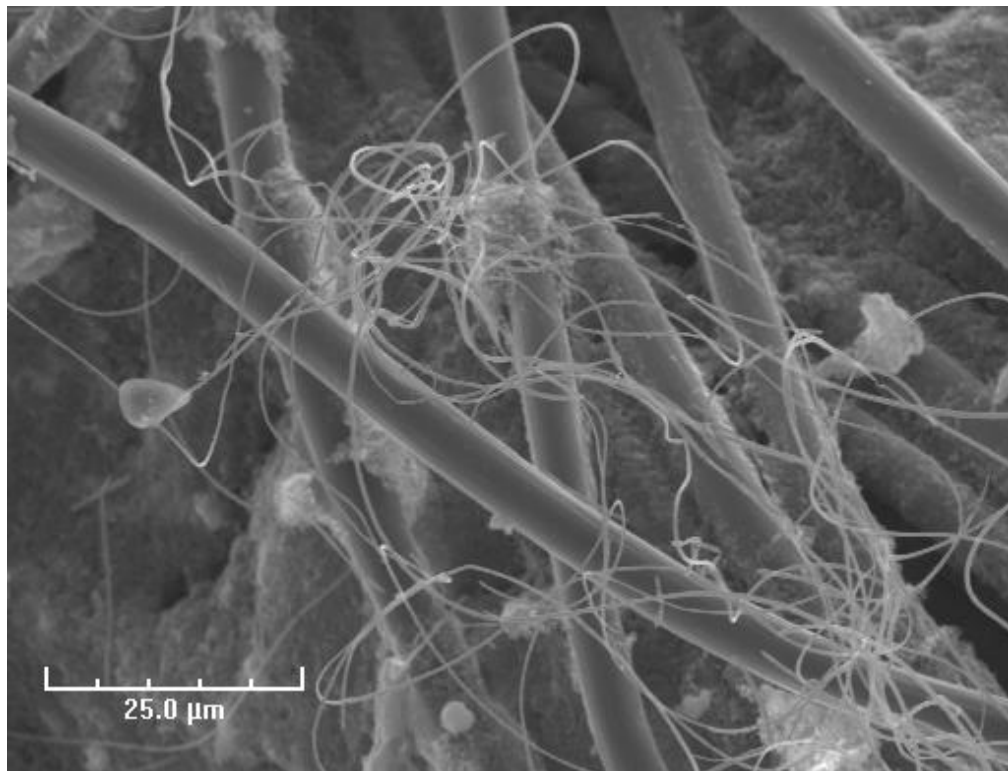
Image 4: 1000x Magnification; note the difference in diameter of the carbon and electrospun fibers, as well as the globules of polymer
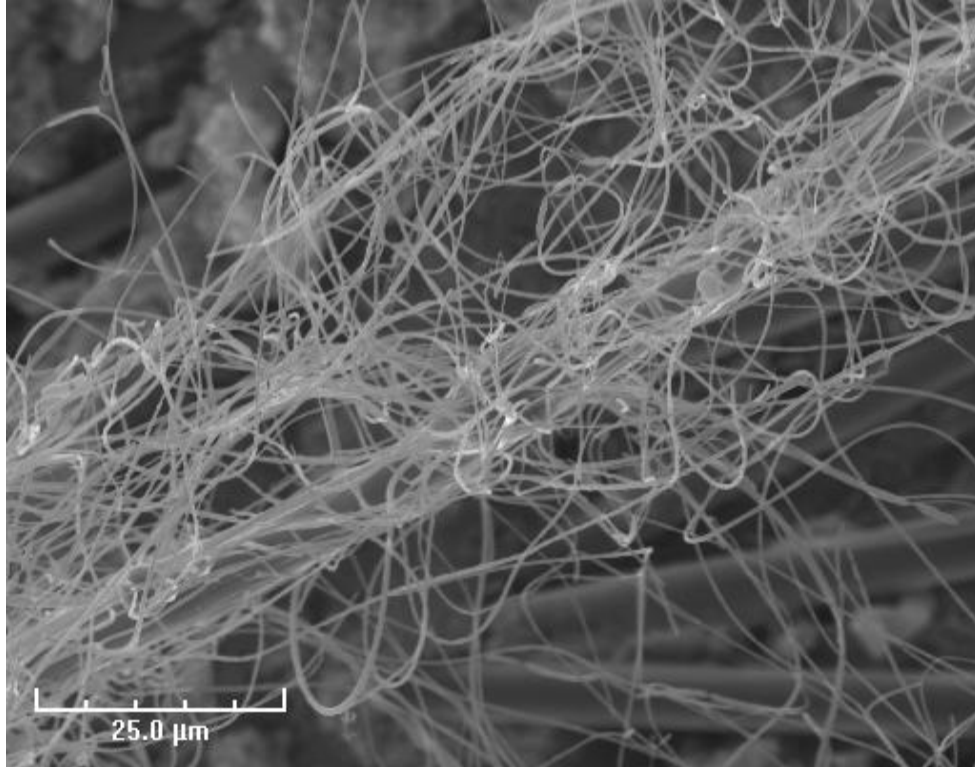
Image 5: 1000x Magnification; note the coverage of the fibers on top of the carbon cloth support
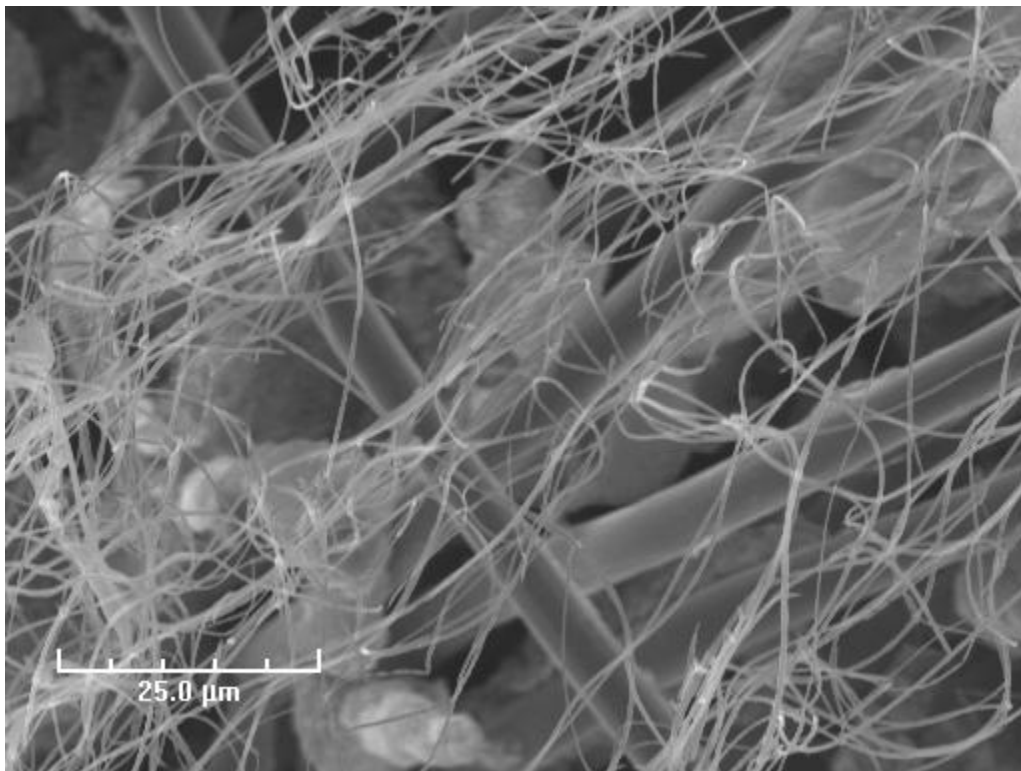
Image 6: 1000x Magnification; note how the nanofibers attach to the most raised topographical feature
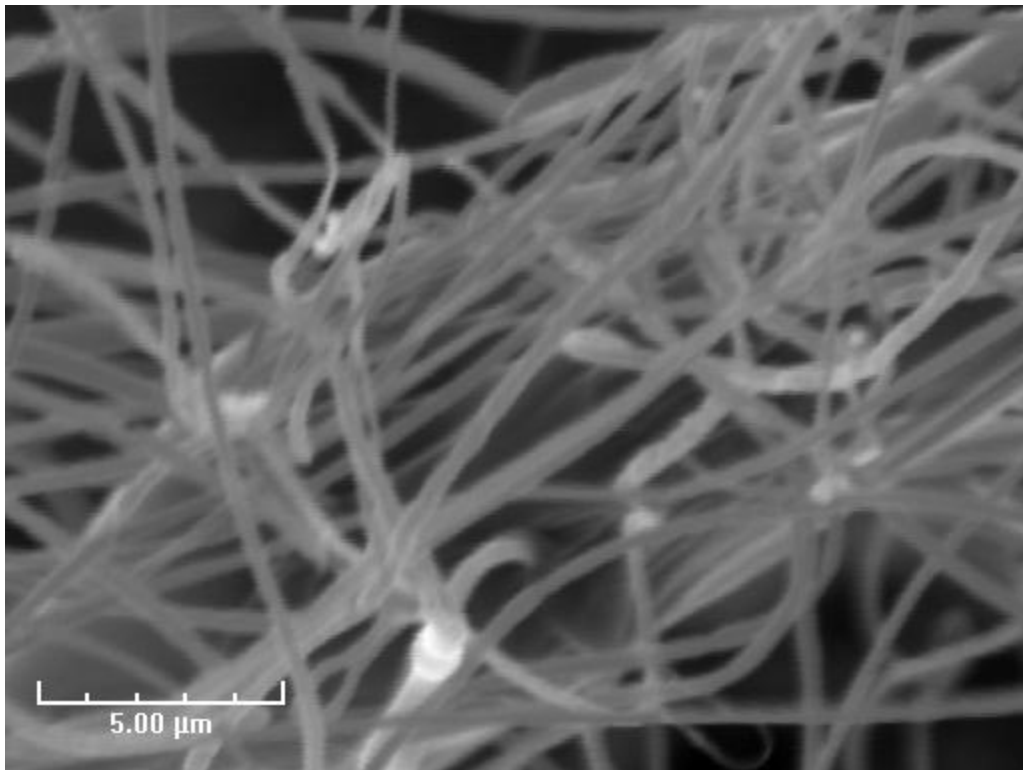
Image 7: 5000x Magnification; note smooth, continuous fiber morphology
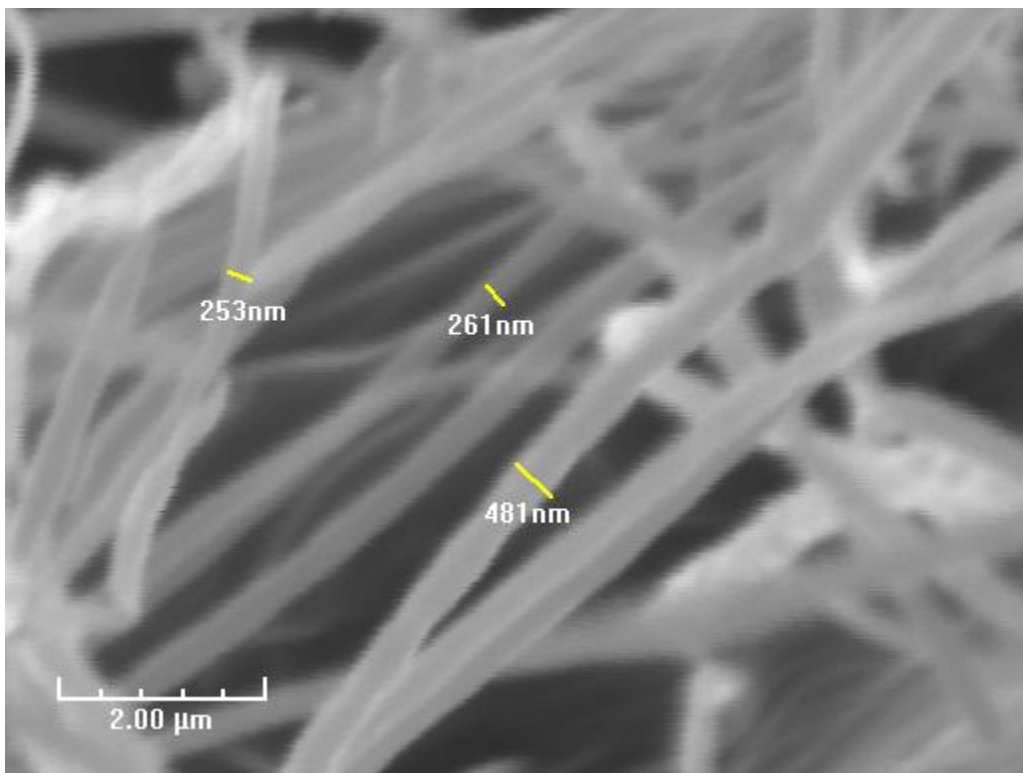
Image 8: 10000x Magnification with length estimation using SEM software and smooth fiber surfaces

Solution 7a Images
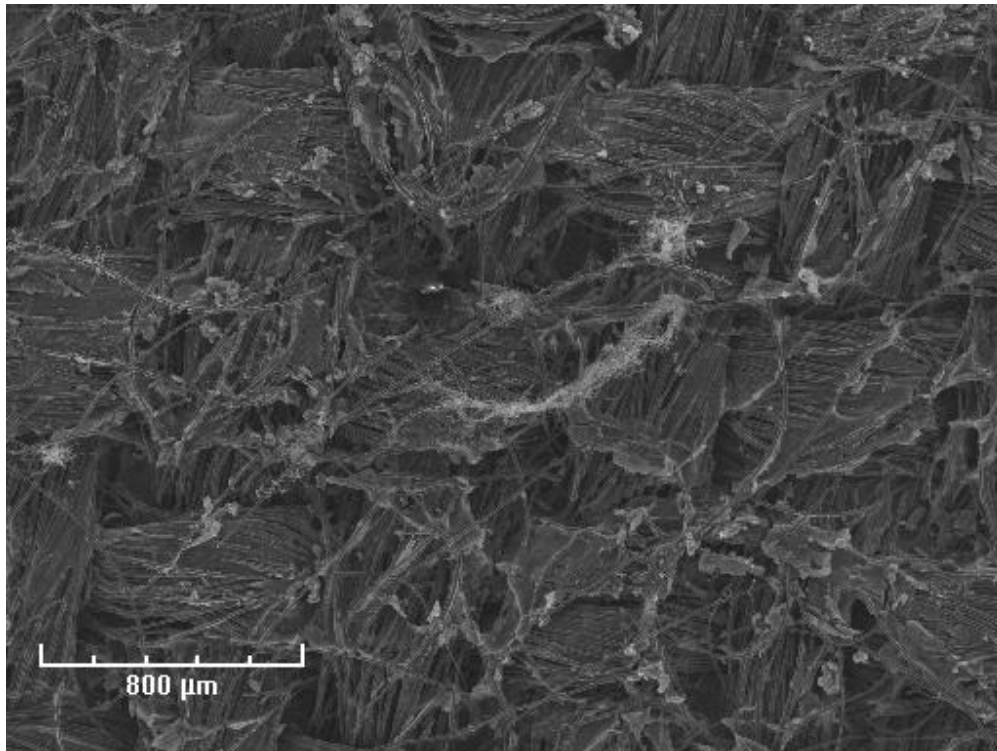
Image 9: 50x Magnification; note the size difference between electrospun fibers and carbon tows
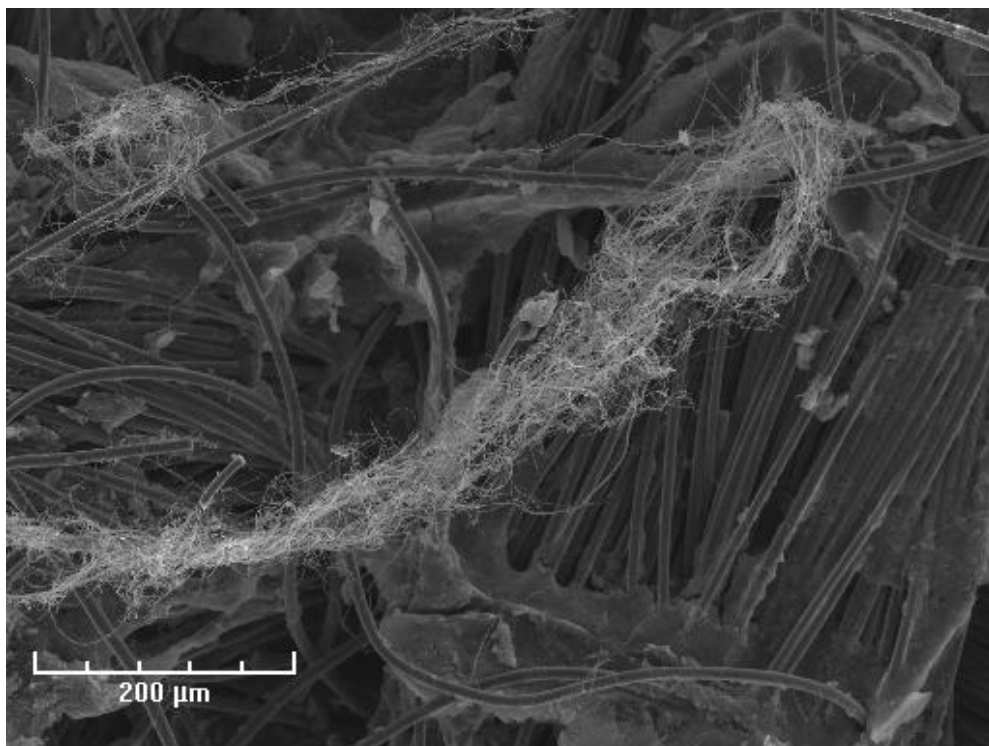
Image 10: 200x Magnification
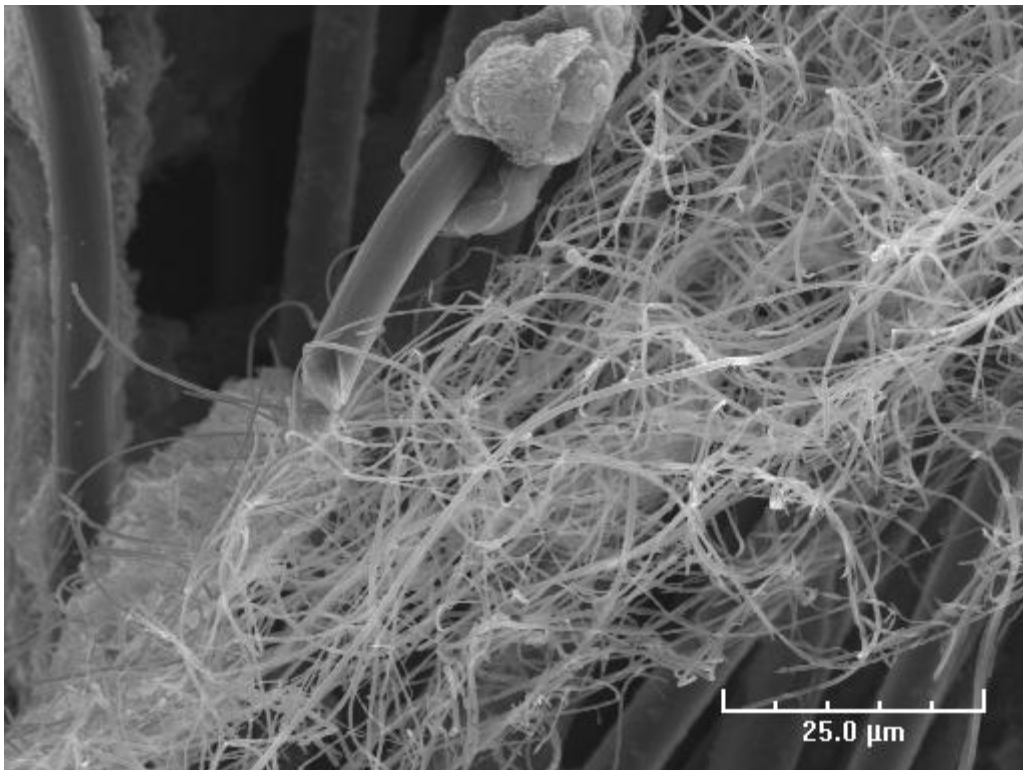
Image 11: 1000x Magnification; note tight clustering to raised carbon tows
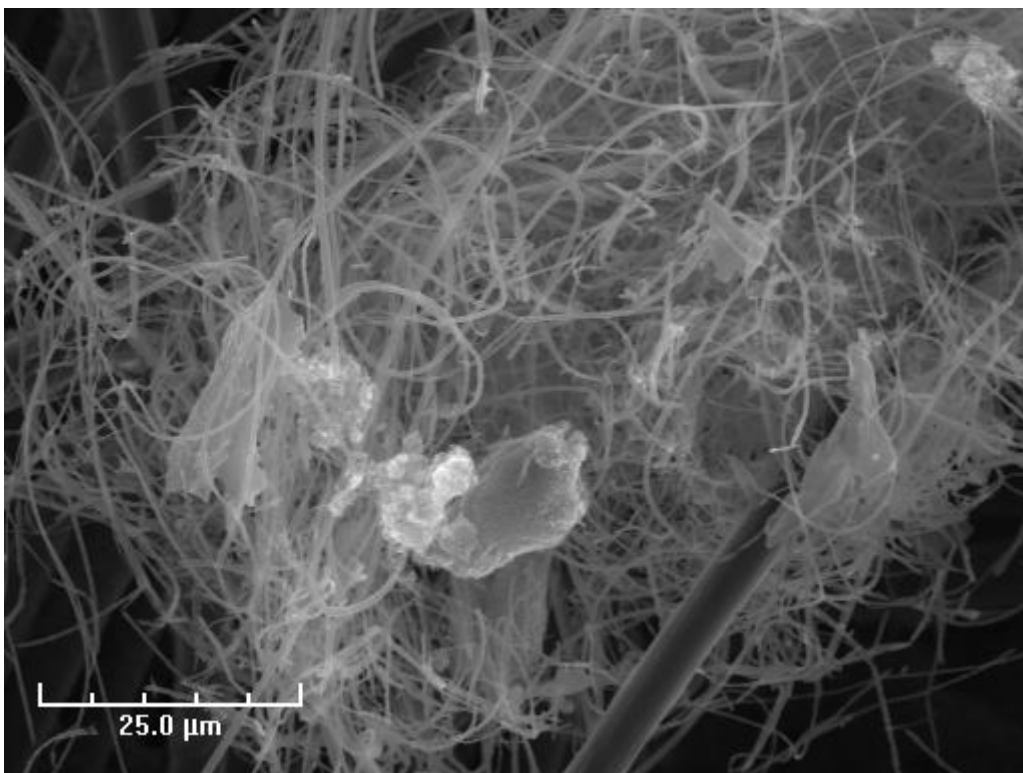
Image 12: 1000x Magnification
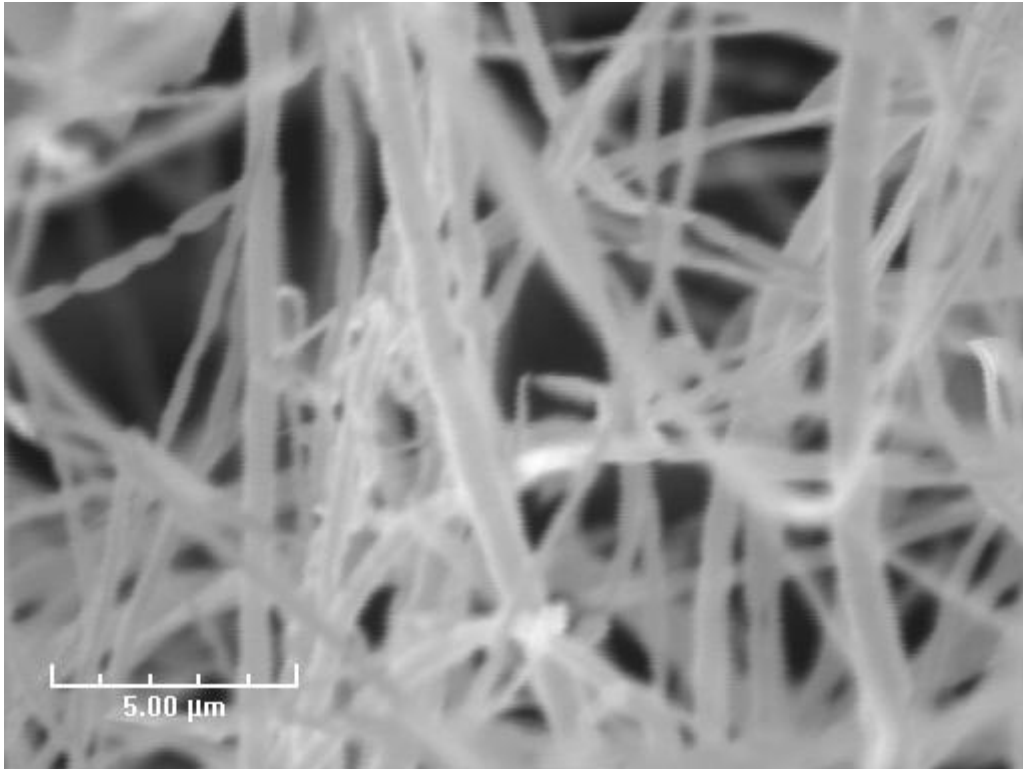
Image 13: 5000x Magnification; note smooth fibers, with some "sausage link" morphology in the left side. This could be a precursor to beaded fibers
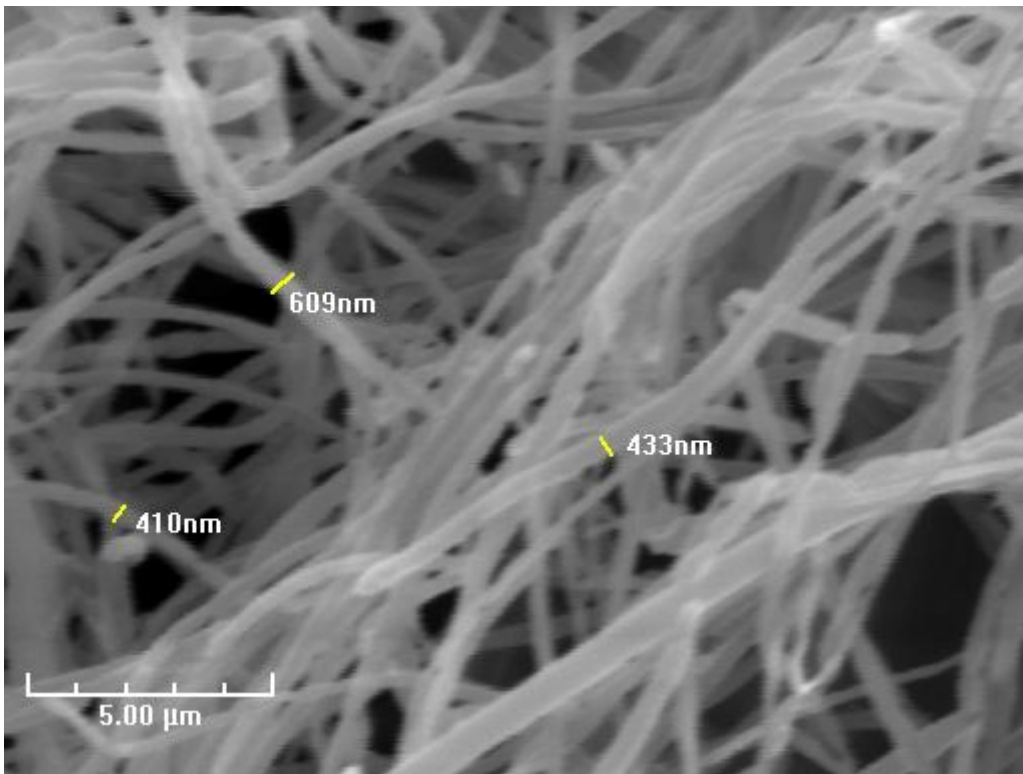
Image 14: 5000x Magnification with length measurements;

Results: Coverage

Coverage of the nanofibers over the surface, as seen in the low-magnification images, is quite low. However, these electrospinning sessions only lasted fifteen minutes; the time needed to create thick, fibrous mats would be substantially longer. However, between solution 4a and solution 7a, the thicker solution seemed to yield fibers that were more dispersed, whereas the thinner solution, 4a, had small clumps of nanofibers bundled together. It is also interesting to note the small globules of material that are much more prevalent in the images for the thinner solution, 4a. As these clumps are seen to be on top of the supporting carbon cloth but under the electrospun fibers, they very well could be Nafion/PEO material that was electrosprayed. As our methodology dictates, we slowly increase the voltage until the fibers are seen. At lower electric potential, it is reasonable to assume, as higher voltages tend to produce thicker fibers, that there was not enough energy holding the polymer chains together, and the material was sputtered out in droplet form.

Most importantly, we can see that the deposition of fiber was successful. While the fibers are in no way ordered, the fact that the fibers seem to bundle together at points of contact with the surface, and the highest topographical point on the surface at that, indicate that continuous electrospinning would produce fibers that would deposit close to each other. If we saw the fibers being evenly dispersed very sparsely over the entire surface, it would be very difficult to accumulate a fiber mat of appreciable thickness without electrospinning for days.

Results: Fiber Diameter

As fiber diameter is directly related to the proton conductivity of the material, ascertaining the average fiber diameter of the fibers that were electrospun is crucial. Using a large sampling of fibers seen in the SEM, diameters were estimated using the built-in pixel-to-length utility. While the surface of the material is not flat, the distance between the carbon surface and the electrospun fibers is not very large. While cross-sectional SEM was not conducted, it is safe to assume the fibers are very close to the surface, and there will be very little impact of this height difference on the results of the length measurements.

From the images taken and the lengths estimated, it was found that the 4a system produced fibers with an average diameter of 331nm using 30 length measurements, ranging between 200-400nm. The 7a system was also measured 30 times at various magnifications, and found to have an average fiber diameter of 496nm, with a range of fiber diameter between 450-600nm.

Comparison to Previously Studied Nafion/PEO literature

The fiber diameters that resulted seem to be line with the nearest literature research. From the literature, it was clear that we would be using a fairly short distance between the tip an collector, with a <1mL/hr flowrate with an electric potential above 10k. However, due to solution differences (solvents, PEO molecular weight, Nafion loading) direct comparisons cannot be drawn easily. For the studies using high-purity Nafion solutions, these results seem agreeable.

Electrospun Electrode Mats

From the SEM study of fiber diameter the thicker, 7a solution was chosen for the continuous electrospinning trials. The equipment was set up in the same fashion as the electrospinning trials, with the equipment variables staying the same, except for the electric potential. While the preliminary study used 12kV, the voltage was increased slightly for a few runs in order to create a stable electrospinning process.

As some time did elapse between the initial SEM testing and the need to create several electrospun mats for use as electrodes, and though the solution was kept in a sealed vial, it is assumed some solvent was lost, resulting in a slightly thicker solution. Originally 147 cPs, the viscosity of the solution when spinning mats was 166 cPs. The thicker solution did clog the needle at various points during the continuous electrospinning, but the needle was easily cleaned and the process was resumed without complication.

To assist in controlling the deposition down to a 5cm^2 area, the GDL to which the fibers were to be deposited was backed by various conducting and non conducting layers, as shown schematically in Figure 30. From the collector plate moving up, we have a sheet of aluminum foil (orange), a Teflon gasket with a 5cm^2 square cutout in the center (teal), a small 3cm x 3cm piece of aluminum foil (orange), an additional Teflon gasket (teal) and then the GDL itself.
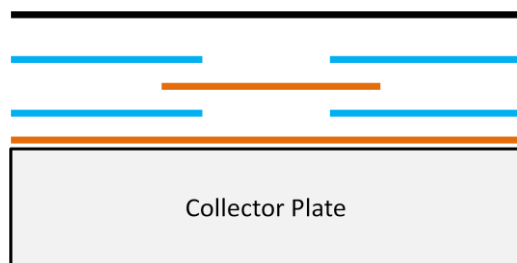
The electrospinning procedure was undertaken for 3 hours for the first mat. The mat can be seen in Image 15, with a small section of this mat used as the cathode in E.MEA1; this section is roughly outlined in the dashed red square in Image 16.

Image 15: First Electrospun Mat, using solution 7a.
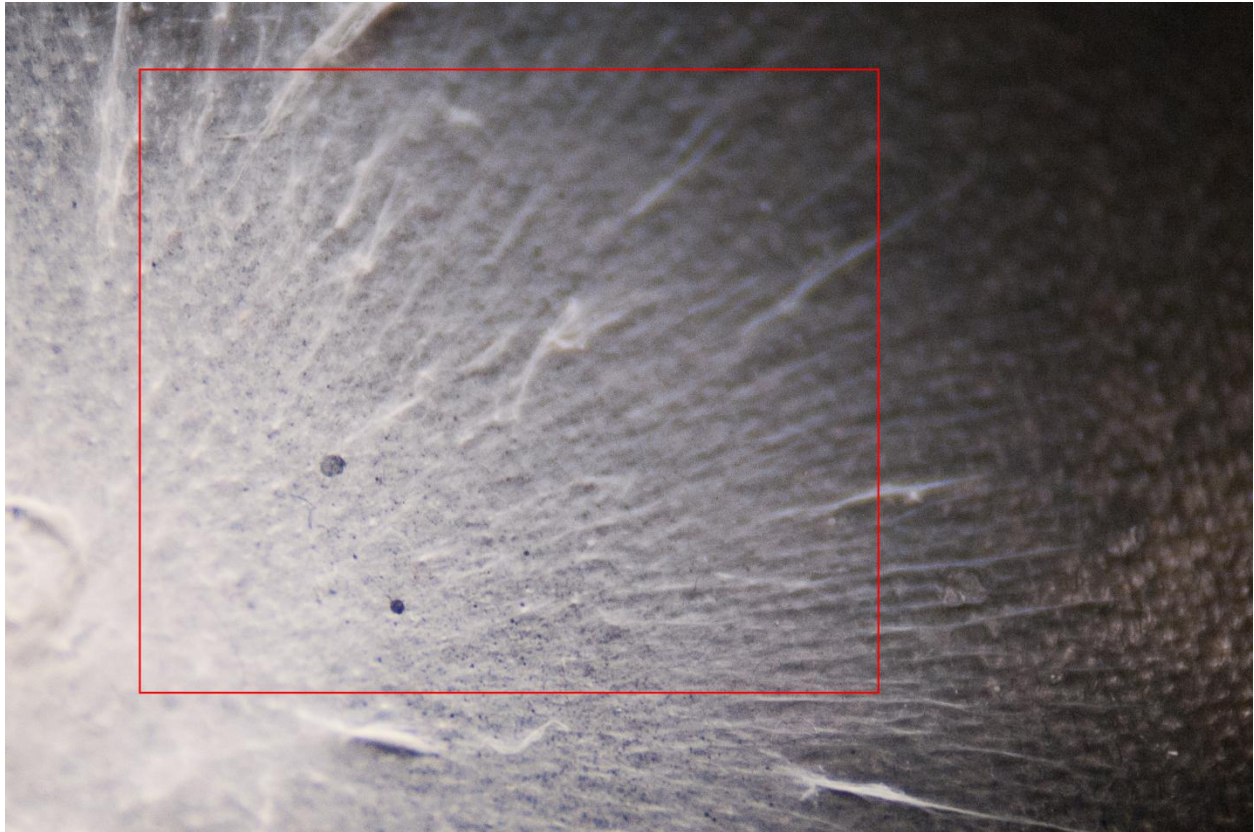
From this image, we can see that there are bulk fibers creating a "starburst" pattern around the central point of deposition. While the cause of this deposition pattern is unknown, it is believed that electrospun fibers will make contact and anchor at locations with the least electrical resistance. As there is buildup of polymer at one location, it is possible that the resistance this polymer layer contributes forces the fiber to deposit elsewhere. In addition, if a fiber does deposit in the center, the rest of the fiber, which is still electrically active, may be attracted to the surface at a different location, thus the fibers being pulled away from the center. To note, the fine line seen on the left-hand side of Image 15 is due to the fact that this is where the tape, holding down the layered assembly onto the collection plate, was placed. Upon removal of the tape, it created a fine "painter's line", as

well as removing the MPL (compare the bare carbon seen here to the MPL covered carbon on the right side of the image).

To create the cathodes for E.MEA #2, E.MEA #3 and both electrodes for E.MEA Total, the fiber spinning process was duplicated. A large mat was spun, and $5cm^2$ squares cut delicately from it to be used as the base for the electrode; this was weighed. The weight captures both the weight of the bare GDL as well as the electrospun fiber. The GDL weight can be determined from knowing the areal weight of the GDL used and the dimensions of the nearly $5cm^2$ cutout. From this, the amount of Nafion was established; if the target Nafion/catalyst ratio is 0.3, solving for the weight of catalyst that is to be added is simply found by solving the ratio.

PEMFC Performance

Performance Comparison of MEAs

Our MEAs were tested in a single-cell setup and controlled in the manner described in the experimental portion of this work. The general trends seen in literature show that the highest performance from a cell will be under humidified hydrogen conditions. Because of the small overpotential of the hydrogen reaction, and the fact that oxidation of diatomic hydrogen is much less energy intensive than that of methanol, it is known that a fuel cell will show better performance running with hydrogen than methanol. The humidification of the membrane is vital as proton conduction of the membrane itself is a function of humidity. However, too much water in the electrode layers will inhibit the mass transfer of fuel gasses to the electrode's active catalyst sites. In addition, high water content will allow for MeOH to dissolve more easily into the membrane and be transported to the opposite

side. To control humidity, the anode stream is humidified before being introduced to the anode. While this setup did not use a cathode humidifier, it is not uncommon to see both feeds humidified.

These general trends are seen when comparing MEA#7 under equal temperature, 75°C, with three different feeds. The performance curves are shown in Figure 31, with current density in diamonds and using the left axis, with power density in circles, on the right axis.
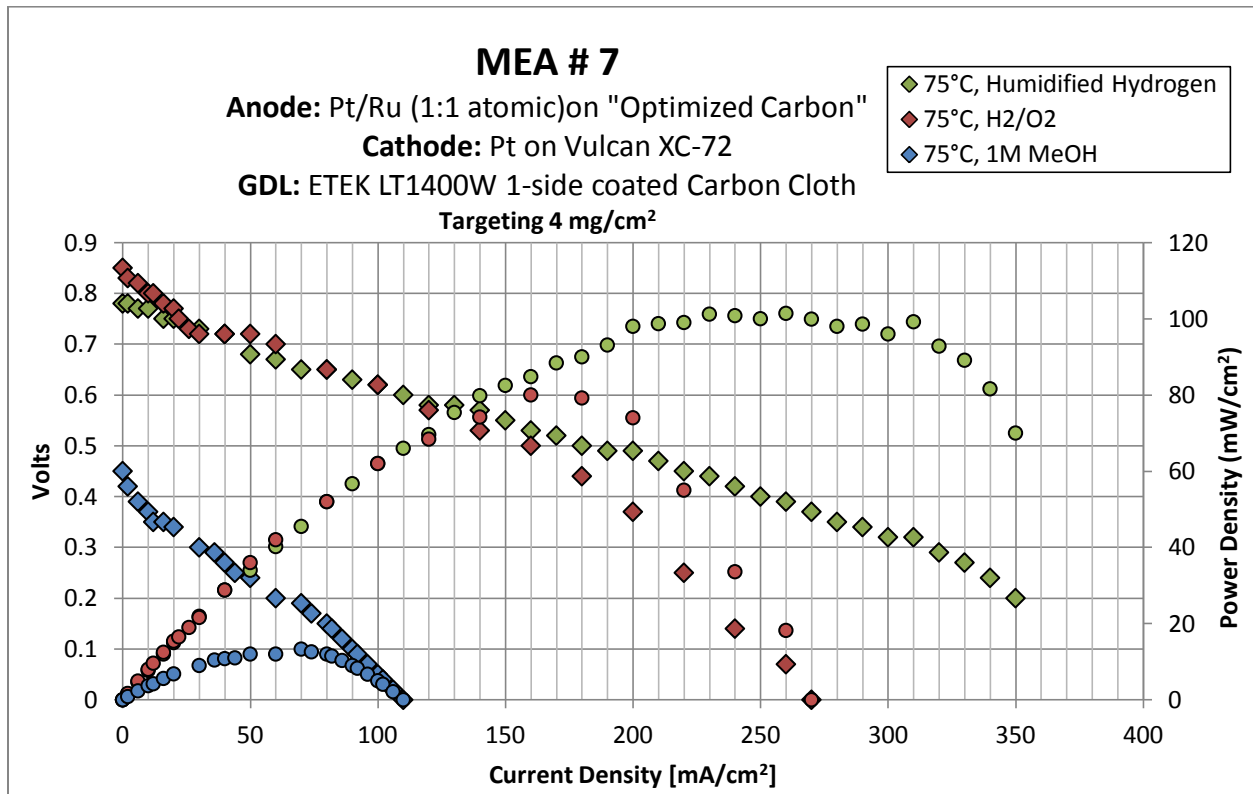
Figure 31: Effect of anode feed material on fuel cell performance

From this, it is clearly demonstrated that one can achieve a higher power density with a hydrogen feed. By separating the current density curves and their slopes into the three segments (kinetics, membrane resistance and mass transport), it is shown that the humidified hydrogen has the most gentle slope in the middle section, reflecting the least

resistance given by the membrane. It is also clear that, under non-humidified hydrogen conditions, the "mass transport knee" is much farther to the right; this indicates that the lack of water in the non-humidified run compromises the ability to transport the reactants and products to and from the catalytic sites. This set of results also indicates the trend of performance, the highest with humidified hydrogen and the least with MeOH.

A commercial MEA, bought from the Fuel Cell Store, was brought in to compare our lab-fabricated MEAs to the commercially available options. While the catalyst loading is known, the GDL material and fabrication method are not. A brief overview of its performance can be seen in Figure 32.
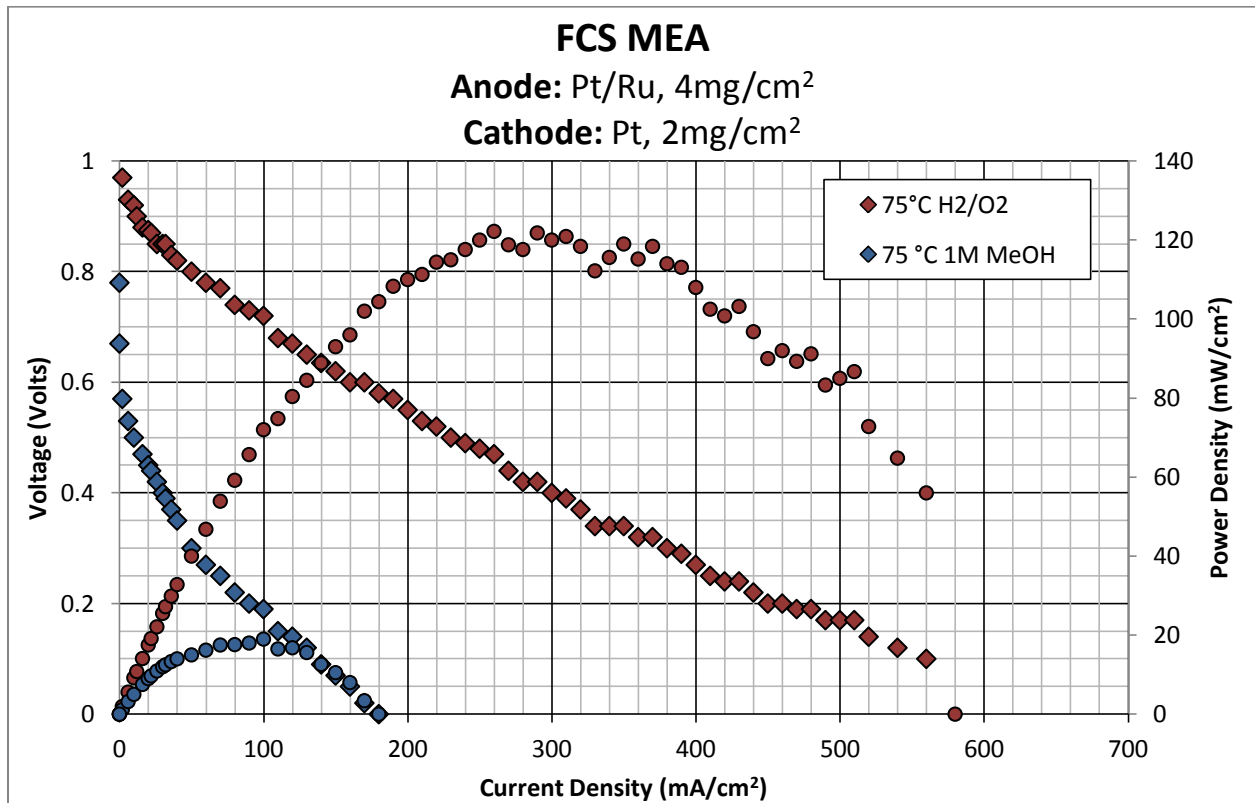
Figure 32: Fuel Cell Store MEA performance at 75°C

From this chart, it is clear the FCS MEA is more suited for a hydrogen feed; despite having a high enough loading for use in DMFC and producing a respectable maximum power density of 19mW/cm², the performance under H_2/O_2 conditions is significantly greater.

To see how the lab-based MEAs compare to a commercially viable option, MEAs of like construction can be plotted alongside the FCS MEA. Running under equal conditions, we can compare MEA#7 to the FCS MEA, as seen in Figure 33.
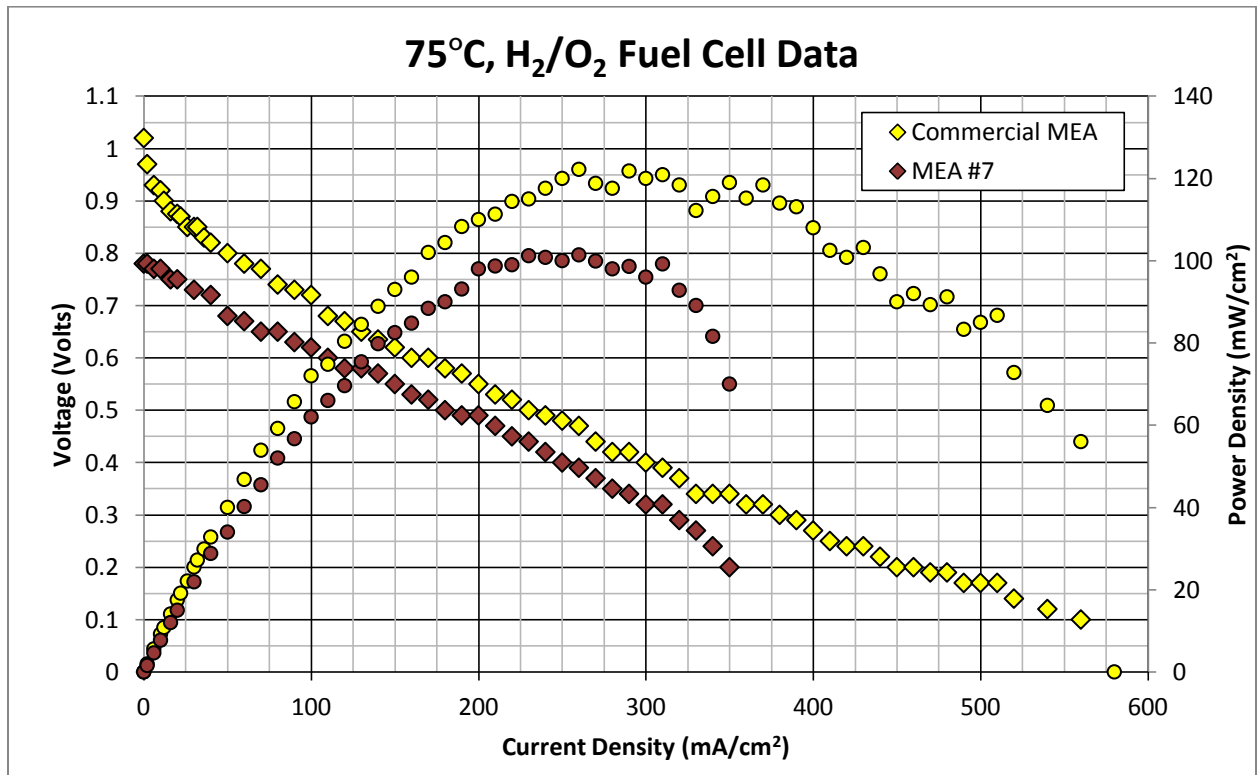
Here, it is clear that the lab-based provides nearly 80% of the performance the commercial option produces. The slopes of the current density lines have very similar slopes, with the OCV and the maximum current density of MEA #7 falling short, comparatively. The difference in peak power density is about 20 mW/cm²; while not a

large difference, 20 mW/cm^2 is 100mW over the small 5cm^2 footprint. In addition, of the maximum 500mW produced by MEA #7, 100mW is 20%. This 20% difference can be attributed to the handmade nature of the lab-based MEAs. Defects such misalignment of the GDL, membrane and feed channels, non-homogenous electrode composition, incomplete MEA activation and lack of exact humidification controls could explain lower performance, compared to a commercially viable MEA.

Nafion Loading

Before the introduction of an electrospun electrode, the effect of Nafion loading in the electrode layer was investigated. While the amount of ionic binder in the electrode of a fuel cell has been widely discussed (see the background chapter Catalyst Supports and the Electrode Layer), the affect on loading in an MEA capable of utilizing both H$_2$/O$_2$ and MeOH feeds was investigated. This comparison, between MEA#7 and the 300%MEA, has been done to elucidate what happens with our MEAs; tests using 1M methanol can be seen in Figure 34, with H$_2$/O$_2$ in Figure 35.
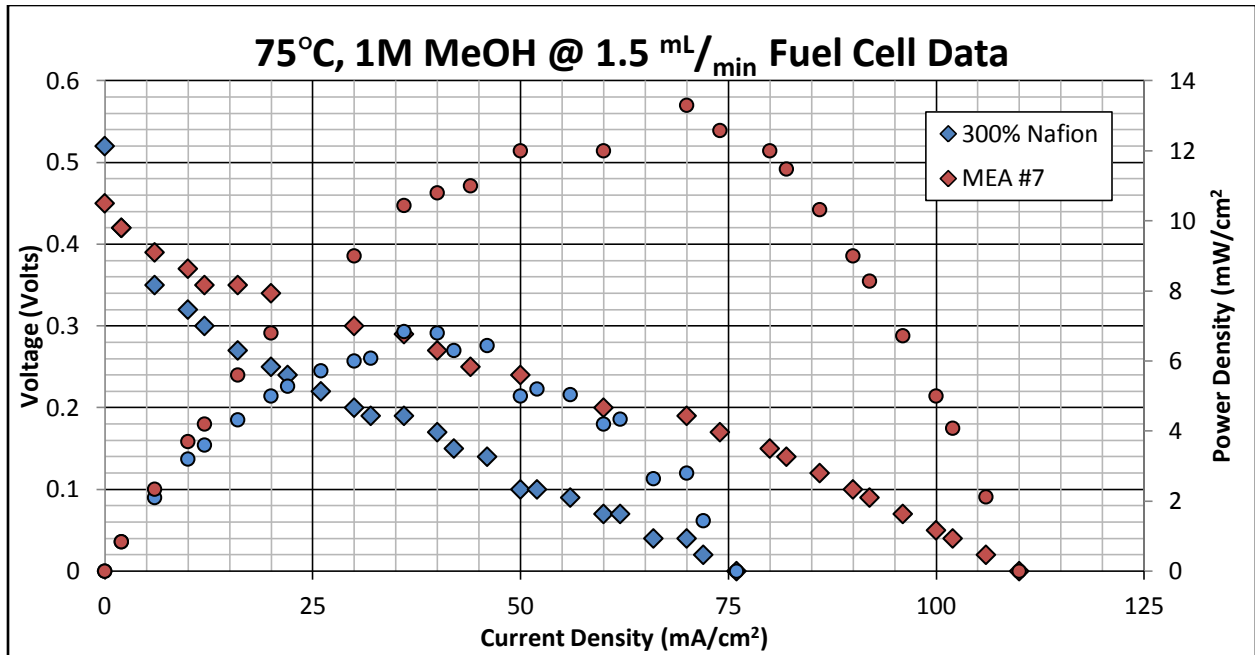
Figure 34: Fuel Cell Performance Data, 1M MeOH with varying Nafion content in the electrodes
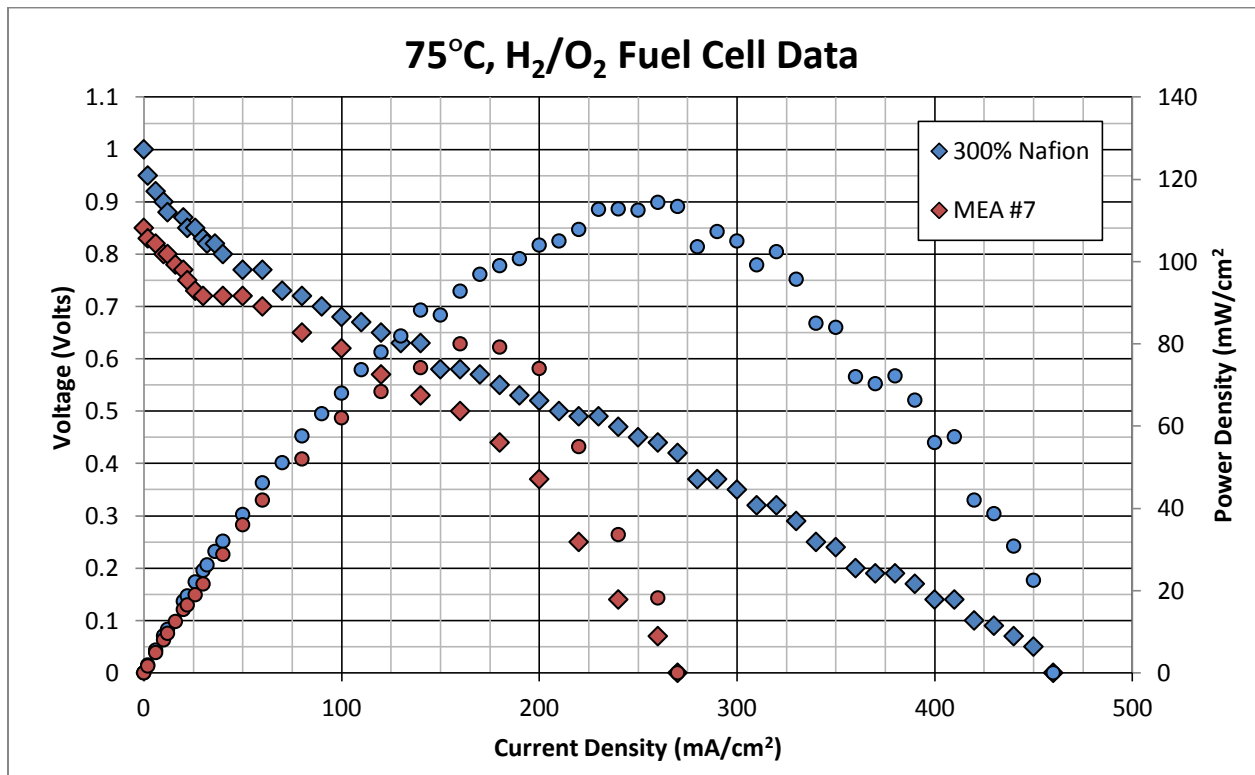
Figure 35: Fuel Cell Performance Data, H2/O2 with varying Nafion content in the electrodes

The charts clearly indicate the 300% MEA outperforming MEA #7, in H_2/O_2 conditions. To note, MEA#7 has a Nafion/catalyst ratio on 0.1, or 10wt%, to the 0.33, or

33wt% of the 300%MEA. Despite this, the 1M MeOH runs indicate the lower Nafion loading of MEA#7 yields a higher limiting current density ($110mA/cm^2$ vs. $76mA/cm^2$), showing a clear performance disparity between methanol and hydrogen fuel.

The current density plot of H_2/O_2 indicates that the 300% MEA seems to handle proton conduction better; the slope of the middle segment of the line is less steep than that of MEA#7. It is also important to note that between the two runs, the 300% MEA had the higher OCV. Under MeOH conditions, however, the drop from OCV in the first segment shows that the catalytic activity may be lower for MeOH.

One possible explanation for this is that the higher loading of ionic binder is blocking pore sites on the MPL, as well as encapsulating some catalyst particles. Due to the increase in Nafion loading, the porosity of the electrode could decrease. While this is not much of a concern for a small, diatomic hydrogen molecule which does not give off a byproduct when oxidized, it is possible for the MeOH and the off-gassing CO_2, in the presence of the water fed in the dilute methanol feed, to be limited in transport by an electrode with lower porosity.

When the 300% MEA is compared to the commercial MEA, as seen in Figure 36, we see that under equal H_2/O_2 conditions, very similar performance can be seen. This indicates that the Nafion loading, for H_2/O_2, does not limit mass transfer, especially at higher current densities where a large amount of water is being generated on the cathode side. While the difference between the current densities does diverge after ~$300mA/cm^2$, and the limiting current density is significantly lower, this may be attributed to the same phenomenon as described between H_2/O_2 and MeOH. At higher current densities, more water is being

generated. If this water is not managed on the cathode side, the excess water will add resistance to mass transfer of oxygen to the catalyst sites in the cathode. With additional Nafion, especially if the Nafion is compacted onto the GDL, the rate that water can be removed at is limited, thus saturating the electrode and limiting gaseous diffusion.

300% MEA
Anode: Pt/Ru (1:1 atomic)on "Optimized Carbon"
0.33g Nafion / 1g Catalyst
Anode Catalyst Loading: 4 mg/cm²
Cathode: Pt on Vulcan XC-72
GDL: ETEK LT1400W 1-side coated Carbon Cloth

Legend:
- FCS 75 °C H2/O2 SOP
- FCS 75 °C 1M MeOH
- 75 °C H2/O2
- 50 °C H2/O2
- 75 °C 1M MeOH
- 50 °C 1M MeOH

X-axis: Current Density (mA/cm²)
Y-axis: Voltage (Volts)
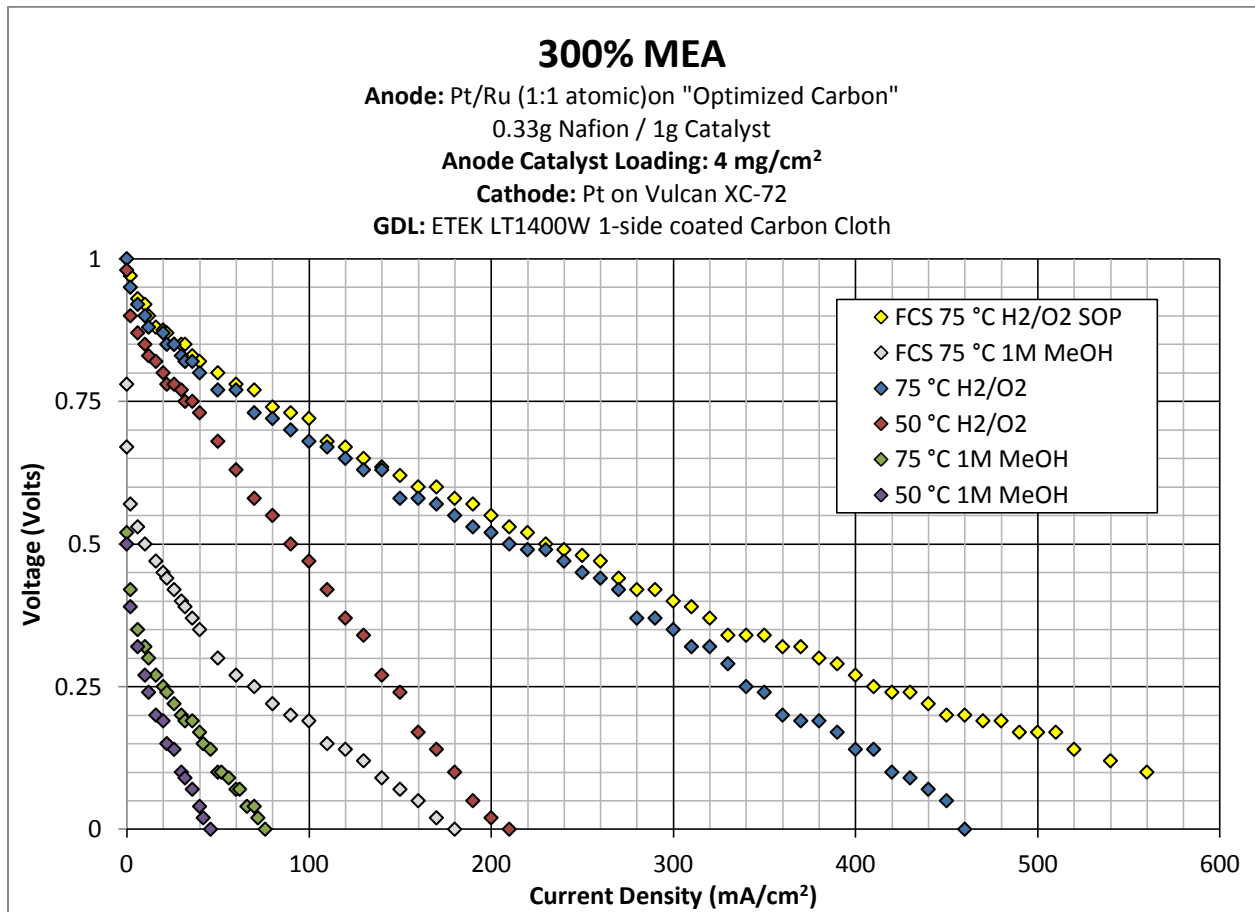
The difference between the MeOH performance curves makes this phenomenon even more likely. While the H_2 feed is humidified, one can assume there is more water being fed when the fuel is dilute methanol. This would cause the anode to become saturated with water, limiting the active surface sites for catalysis, as well as providing a solvent for the exhaust CO_2 to dissolve in. To prevent this from occurring, one would need

to ensure the solution being airbrushed is both homogenous and prevented from agglomerating into large clusters.

Catalyst Loading

Catalyst loading in a fell cell electrode significantly changes the performance capabilities. The more catalyst is present, the more active sites are available for the reduction and oxidation reactions to take place. However, too much catalyst can decrease the porosity of the electrode, causing mass diffusion limitations; there may be an increased number of reaction sites, but little availability to utilize them. MEA #7 and MEA #11 were made in the same conventional method, with varied catalyst loadings, used to directly compare with the electrospun MEAs. Compared side by side, as seen in Figure 37 and Figure 38, it is clear that the higher loading of catalyst has a significant impact on performance over the entire range of current densities the MEA will be run at. A higher peak power density and limiting current density demonstrates this. The tradeoff is, of course, cost. With all else remaining the same between the two MEAs, inspection of the catalyst loading reveals that MEA #7 uses 1.57 times the amount of catalyst that MEA #11 does, including the additional catalyst initial solution used in airbrushing to make up for the 20% lost during deposition. With the current cost of catalyst being the driving force for much of the research in fuel cell optimization, it is important to balance cost and performance when deciding if a fuel cell is viable in a commercial application.
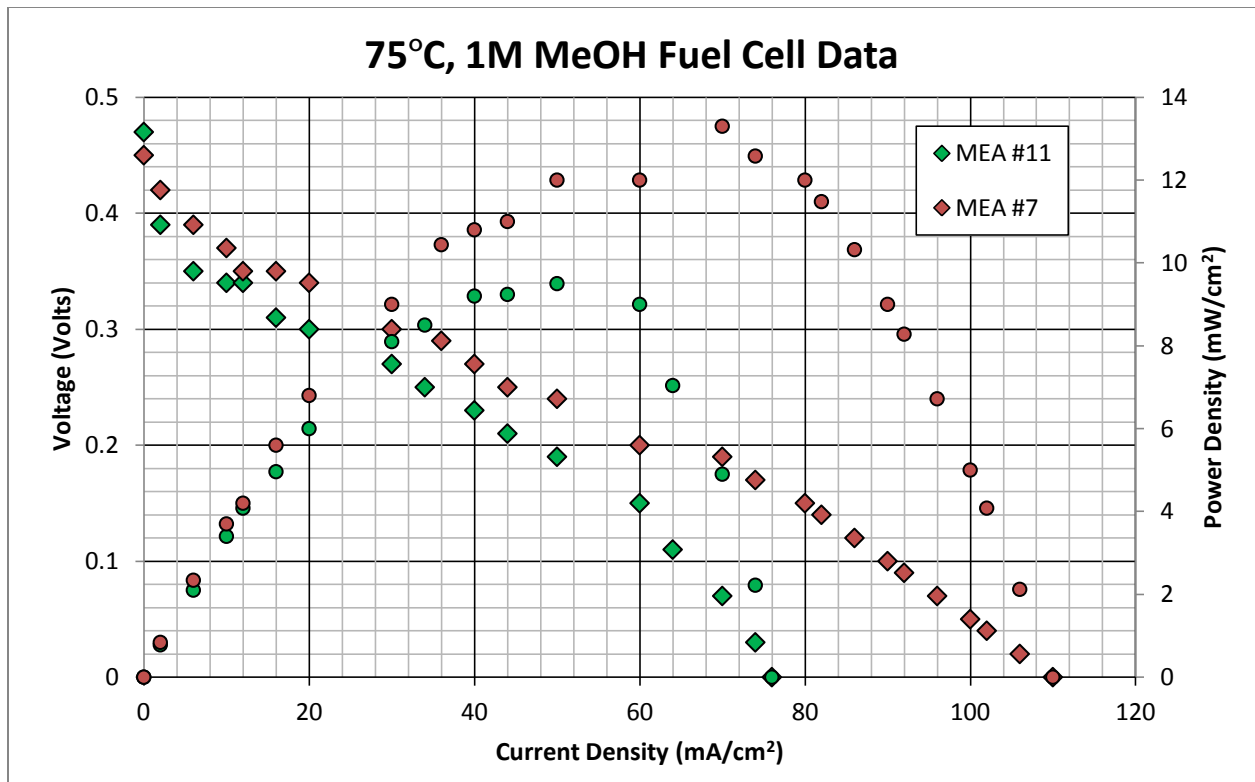
Figure 37: Fuel Cell Performance; effect of cathode catalyst loading
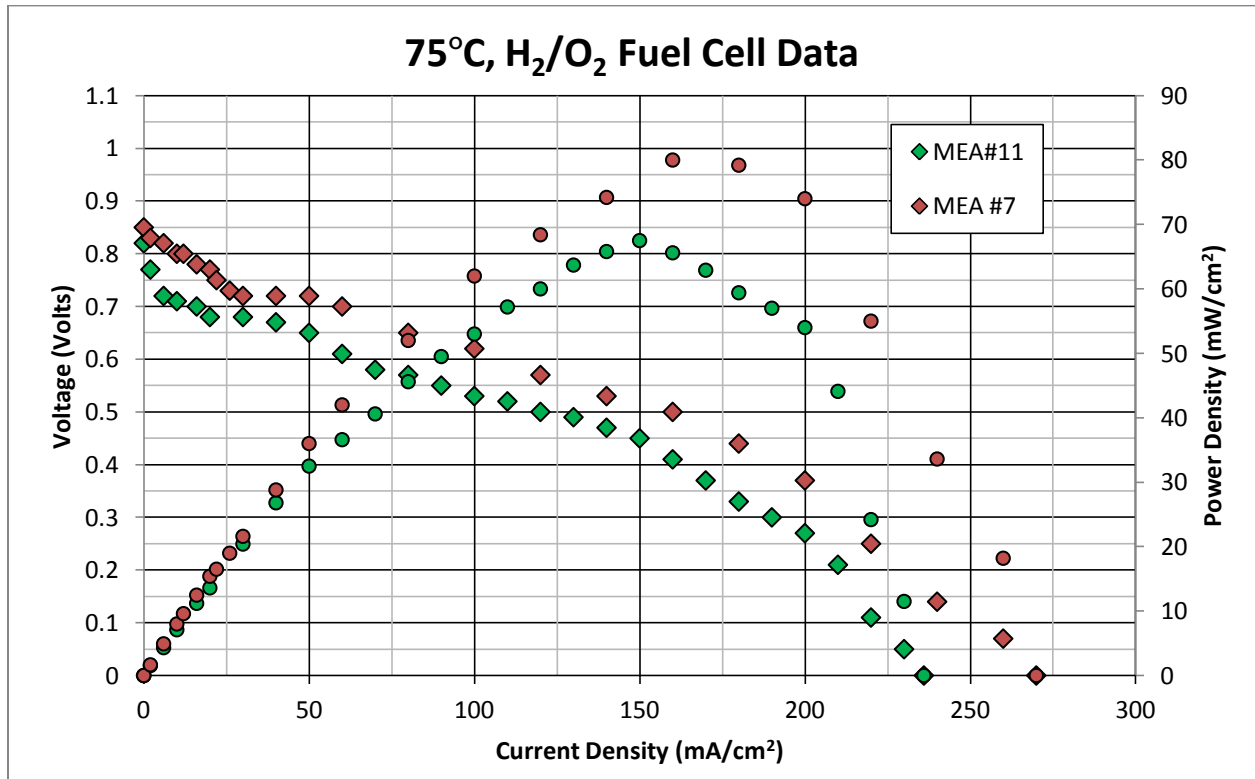
Figure 38: Fuel Cell Performance; effect of cathode catalyst loading in H2/O2

Electrode Type

MEAs fabricated with a novel electrospun electrode would need to be tested and compared against equivalent traditional MEAs as a baseline. By keeping the catalyst loading, Nafion loading, fabrication techniques and test bed variables consistent, the effect on electrode catalyst support morphology could be studied. In most cases, the Nafion catalyst support was electrospun, the weight of the Nafion used was measured, and a cathode was made in the traditional manner, targeting to use the same amount of Nafion. As the traditional electrode procedure includes catalyst in the ink, the amount of catalyst used for the traditional electrode was recorded, and this amount of catalyst was deposited on the electrospun support. Because the fabrication and weight measurement steps are separate, the loading between the two comparable MEAs are not perfect; however, it is believed that they are close enough to not represent or induced a significant change n performance.

The first two MEAs to be compared are the 300% MEA and E.MEA #1. Both have a Nafion-to-catalyst weight ratio near 0.33, and have cathode catalyst loadings close to 4 mg·cm^{-2}, with near identical anodes. These were tested in both H_2/O_2, with the same break-in procedure, and the results are seen in Figure 39.
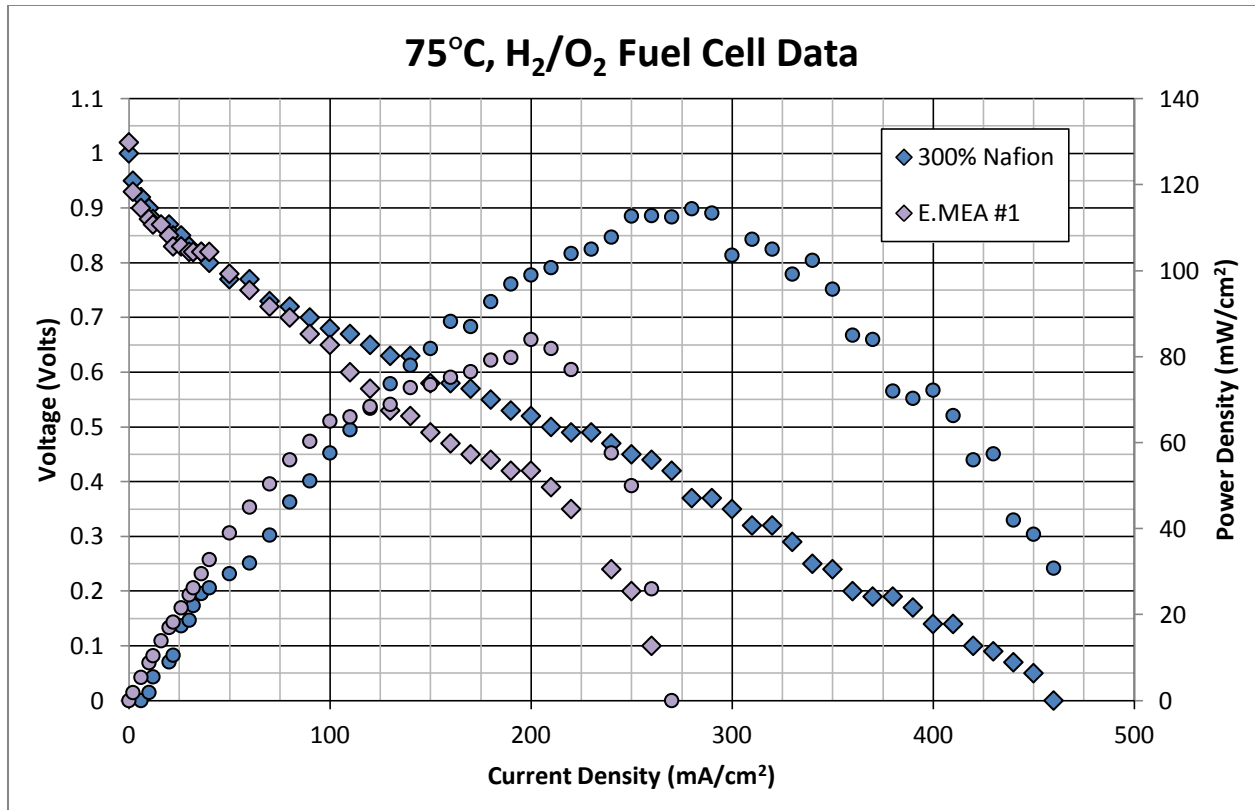
Figure 39: Fuel Cell Performance Comparison, H2/O2, 300% MEA vs. E.MEA1

The results produced under hydrogen fuel use raise two main important points. First, the OCV of both MEAs are near each other, and both greater than one. This reveals that both MEAs are well fabricated; the electrospun support does not, in any way, completely block active catalyst sites. The drop in performance between 0 and 40 mA/cm^2, which looks to be the range of which activation/ kinetics are limiting, is fairly similar between both of these MEAs. In theory, the electrospun material could "utilize" more reaction sites, as the airbrushed Nafion could cover some catalyst sites. At this high anode and cathode catalyst loading, however, we may be in a region where catalyst is in such excess, a large change will not bee seen.

Second, and most apparently, the E.MEA seems to suffer from a very apparent and immediate drop after the mass transport knee; in this case, right around 220mA/cm^2. This

drop, commonly attributed to mass transport limitations, is interesting. While this should be the advantageous property of the electrospun electrode, it is not clear as to how much Nafion is needed in the electrode in this new morphology. It is quite possible that the lack of uniformity of the fiber mat is limiting access to catalyst sites. E.MEA #2, which used a much thicker mat made up of more macro-fibers, resulting in weight five times more than E.MEA #1, failed to perform. While an OCV of 0.2V was recorded, there was a complete lack of ability to draw current from E.MEA #2. This high loading of Nafion could support the theory in which the catalyst sites are not only being encapsulated or buried within the electrospun material, but also the fact that there s very little, to any, ability for water to be generated and wicked away from the reaction sites on the cathode. This build-up of water could over-hydrate the membrane, leading to an increased amount of fuel crossover, and potentially leading to catalyst leaching, especially ruthenium. While Nafion loading was not varied over a wide range, it could be a future point of focus, as it clearly has an effect (with E.MEA #2 failing at a very large loading) but has not been studied. It is possible that E.MEA #2 did not show any performance due to a mechanical defect, such as a pinhole or delamination between the membrane and electrode.

After testing these MEAs in H_2/O_2, it would be expected for the performance trends to be similar for the dilute MeOH trials. However, as seen in Figure 40, this is not the case.
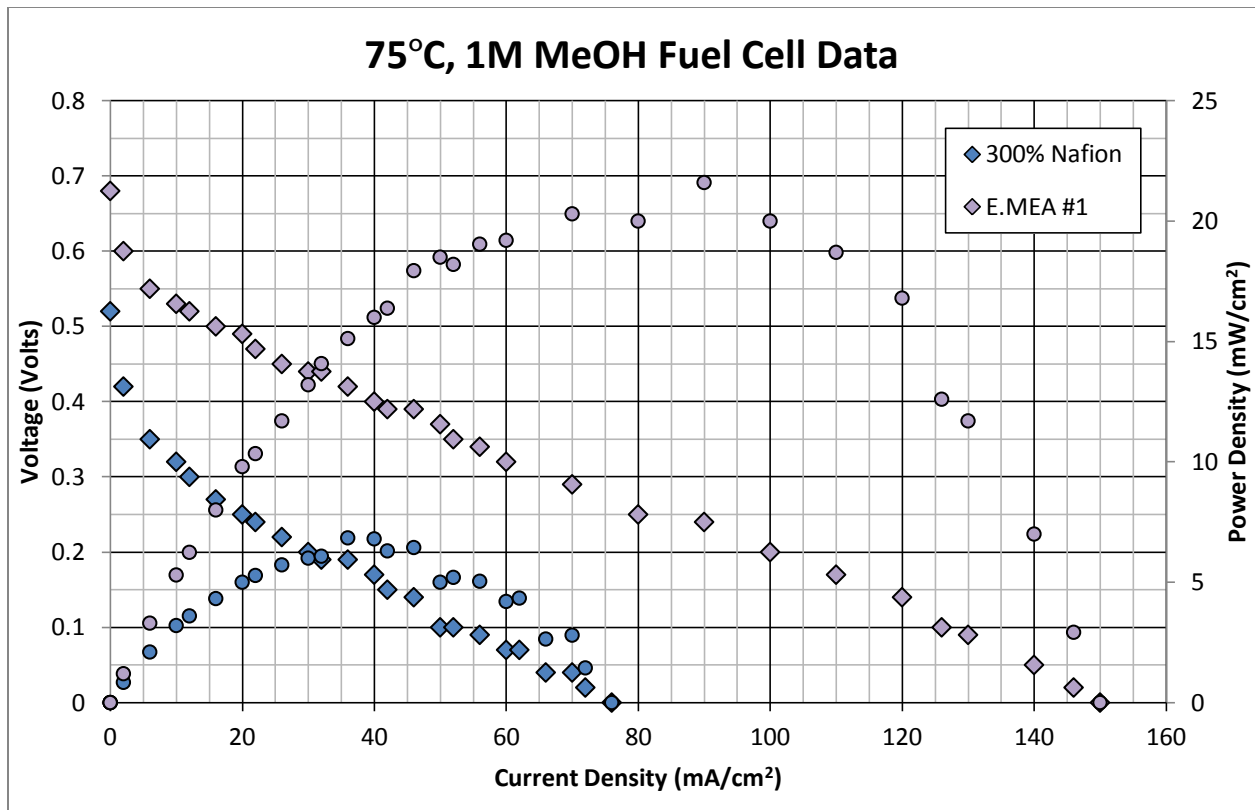
Figure 40: Fuel Cell Performance Comparison, 1M MeOH, 300% MEA vs. E.MEA1

Not only do we see a much higher OCV, limiting current density and peak power density, there is smooth performance over the whole range of current drawn form the cell. This result brings forth a plethora of questions, in both the phenomena occurring as well as the ramifications. The most apparent would be that the 300% MEA has already been shown to perform poorly in dilute MeOH; outperforming it is normal test of a cell's ability. However, it was assumed to perform poorly due to the excess Nafion causing mass transfer limitations. The fact that the electrospun morphology is the only real difference between the 300% MEA and E.MEA #1, is both exciting and difficult to fathom. Perhaps the fibrous Nafion, even when compacted, is still more porous than the compacted micro-globules formed during the airbrushing. The airbrushed construction, as Nafion and catalyst are sprayed at the same time, may lead to catalyst encapsulation, whereas the electrospun

support, made up of solid fibers, cannot physically absorb the catalyst particles. Without SEM images of the two surfaces after airbrushing catalyst, there is no definitive answer.

While these are the apparent explanations, there are others that could be possible. The increase in performance between these two looks as though E.MEA#1 is suffering from much less crossover. Crossover occurs when there is methanol in the electrode layer that is unused, dissolves into water that is present, and is carried across the membrane. Limiting crossover would be done by either decreasing the amount of free MeOH (use it up more quickly) With an electrospun morphology, it may be that, with the catalyst being attached to the walls of the fibers as well as inside the pores created by the fibers overlapping, that the methanol is used up more quickly, and thus a smaller amount makes it through the length of the electrode to the membrane. With equivalent catalyst loading, the nanofiber morphology may provide a more efficient use of the catalyst, as seen by the better performance and higher OCV. However, SEM images of the electrode surfaces, cross sections of the electrode, and further testing using higher and lower MeOH flow rates would need to be conducted to make these claims anything more than a hypothesis.

Upon fabricating E.MEA #2, it was noted that that high catalyst loading in the cathode seemed to compact the fibers and build a layer of just catalyst on top of it. While this was not as apparent in E.MEA #1, it was agreed that a lower cathode loading may aid in performance, as there is not creation of separate layers. E.MEA #3 was then made, using a lower cathode loading ($1.17 \text{mg} \cdot \text{cm}^{-2}$). To compare directly to a traditional MEA, MEA #11 was fabricated to have equal catalyst loading and Nafion weight in the cathode, with both

having the same type of anode. The resulting performance is seen in Figure 41 and Figure 42.
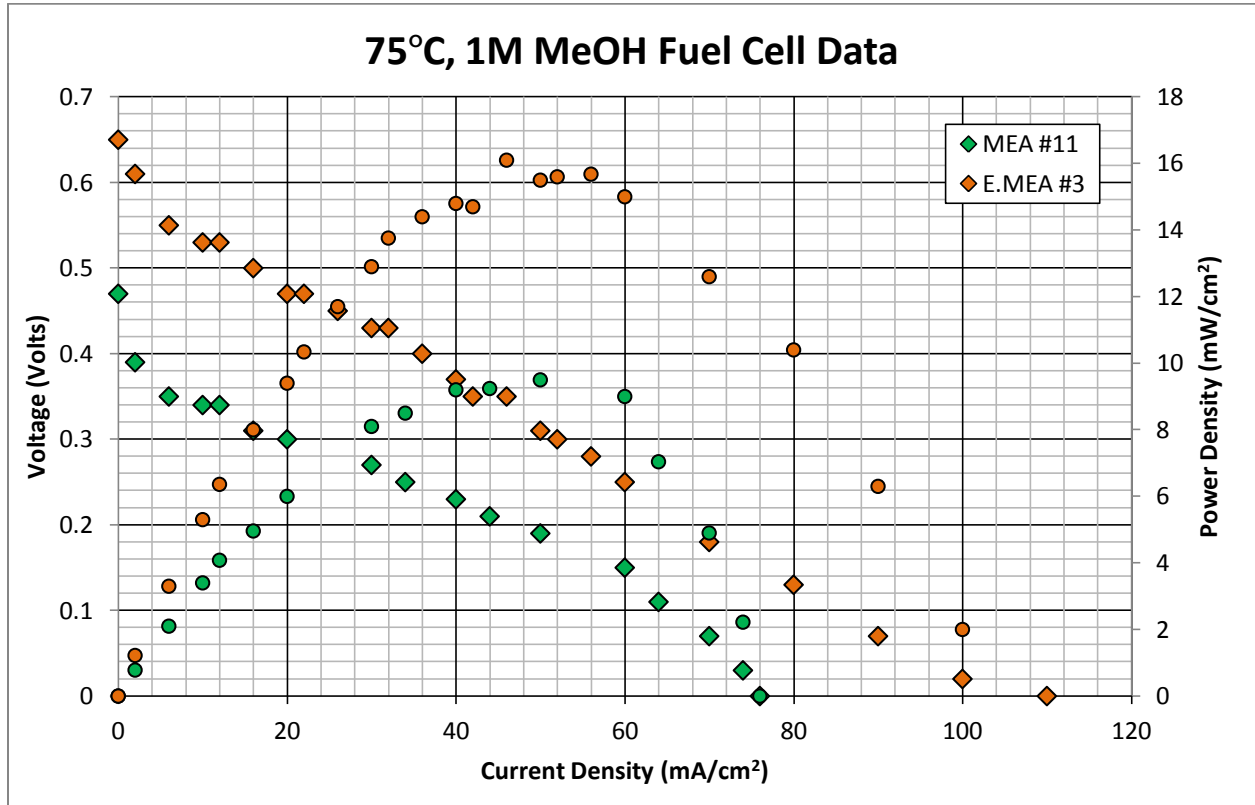
Figure 41: Fuel Cell comparison; effect of cathode morphology in MeOH
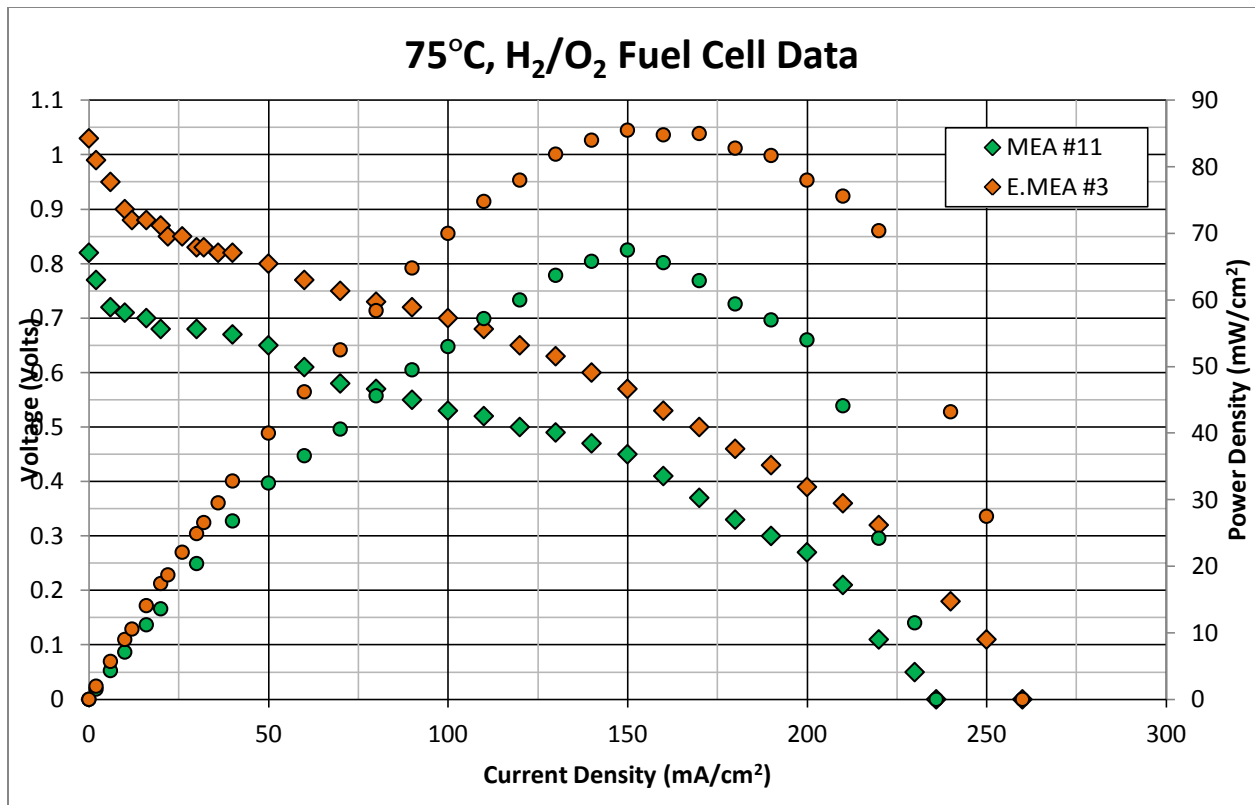
Figure 42: Fuel Cell comparison; effect of cathode morphology in H_2/O_2.

The data seen here shows very similar trends to those found between E.MEA #1 and the 300% MEA; there is a profound increase in performance in MeOH, where the difference is less apparent in H_2/O_2 conditions. In this case, it is clear that the electrospun MEA outperforms the equivalent traditional MEA in both fuel conditions. While the OCVs are different, the slopes between both setups is well defined and very similar; the internal resistances, either for proton or electron conduction, seem to be equal. This should be the case, as the membrane is the same thickness in both MEAs, assuming it to be the dominant resistance although proton transfer resistance in the electrode layer will also contribute.

The changes that are seen, as a result of this test, is that the mass-transport knee is not as visible in E. MEA #3 as it is in MEA #11. In addition, the initial decrease from OCV to the stable slope is less aggressive in the E.MEA #3 plot; this could be due to a more efficient

use of the available catalyst due to the electrospun morphology. The decrease in MEA #11 is sharper in MeOH, but not as bad in H_2/O_2. This could be a result of the compacted globules in the traditional airbrushing causing limitations in diffusion, especially for the larger MeOH molecules and the off-gassing CO_2.

Dual Electrospun Electrodes

In total, there were three viable MEAs that were fabricated with at least one electrospun electrode. E.MEA #1 and E.MEA #3 had electrospun cathodes, whereas E.MEA Total has both an electrospun anode and cathode. Referring back to Table 8, E.MEA #1 has a higher catalyst loading (A: $4.72mg \cdot cm^{-2}$; C: $3.66\ mg \cdot cm^{-2}$) than the others, whereas E.MEA #3 and E.MEA Total have similar loadings. Performance of each is seen in Figure 43 and Figure 44.
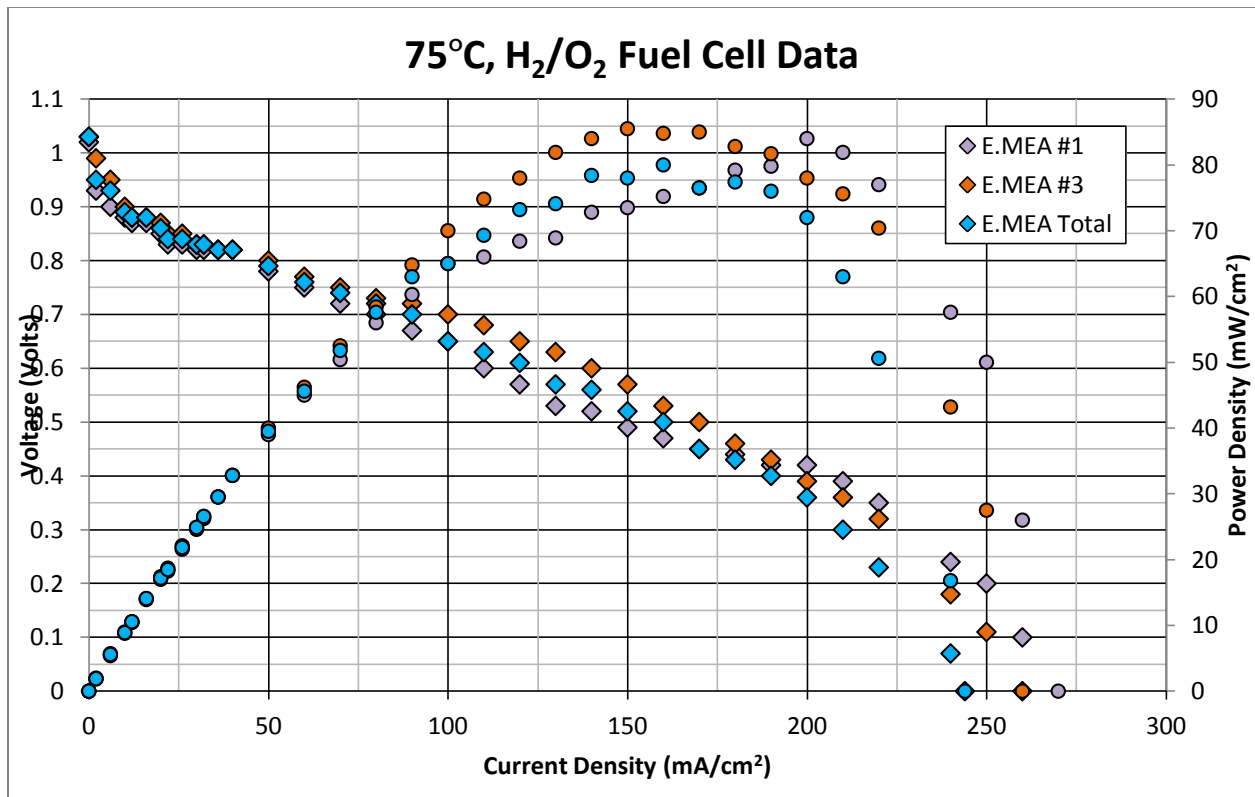
Figure 43: Fuel Cell comparison; MEAs with electrospun electrodes in H2/O2.
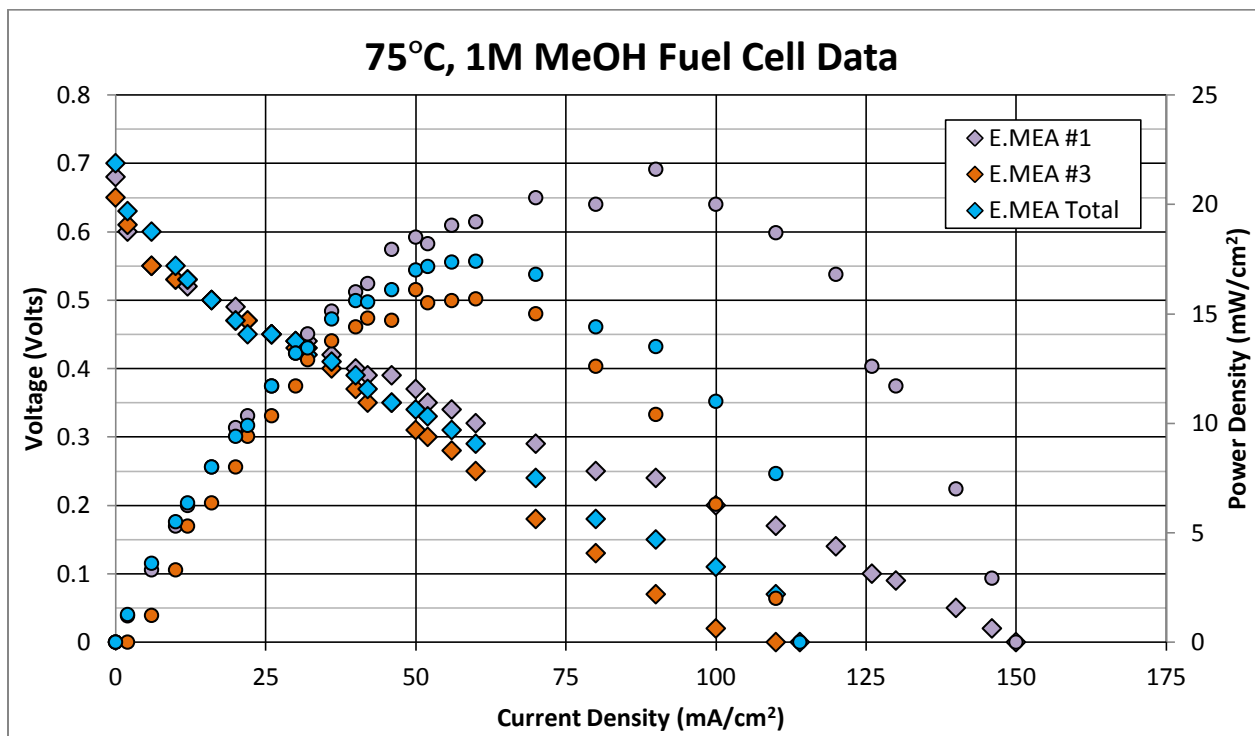
Figure 44: Fuel Cell Comparison; MEAs with electrospun electrodes in 1M MeOH

From both figures, it is clear that, based upon performance, E.MEA #1 is the strongest candidate, having the highest power density, as well as the highest limiting current density. However, in having the highest catalyst loading, these results must be observed with care. Between E.MEA #3 and E.MEA Total, where the major difference is the presence of an electrospun anode, we see a slight increase in performance with H_2 as a fuel, while having nearly identical performance in MeOH; despite falling short in current density and power density, E.MEA Total had the highest OCV in both fuel cases.

Reflecting upon the data gained from the experimentation with Nafion loading in the electrodes, there are comparable results with the electrospun morphology. It was noted that one potential reason the higher Nafion loadings performed better in H_2/O_2 conditions was due to an increased utilization of catalyst, most likely due to the reduction in resistance to proton conduction through the electrode. The lack of superior performance under MeOH conditions was most likely due to the restriction of the rate of mass transfer through the electrode; the increased physical mass of Nafion caused blockage of pores, which affected the liquid MeOH, now off-gassing CO_2, more than the H_2/O_2 runs.

Here, it is apparent that the dual-electrospun MEA can produce electricity; the OCV is the highest of the bunch. However, the steeper slope down to the limiting current density, as compared to E.MEA #1, is indicative of increased resistance in the cell. While there is no apparent mass-transport "knee", the fall to a limiting current density is very sudden, further indicating a limited ability to process the fuel in a timely manner.

The slight increase in performance seen using dual electrospun electrodes indicates that there is, indeed, potential for the further increase of power and current densities with

better preparation methods. While the MEA construction is identical, there are several points in the preparation of an MEA that are hard to control. With electrospun electrodes, there is the inherent non-homogeneity of the electrode's Nafion dispersion, at least at this phase of development. Electrodes have been constructed with a bi-layer construction, with two layers having different loadings of Nafion[67]. The resulting data indicates there may, indeed, be a penalty for having too high of a loading of Nafion at the electrode-GDL interface, but they were able to get higher performance than the traditional "pristine" MEA with a dual-layer gradient. If this is true, the electrospun mat will be very dense, or have a high effective loading, of Nafion at the electrode-GDL interface, as this is where the nanofibers are attached. In addition, compaction in the hot-pressing step will compact the nanofibers, leading to a more distinct layer of fibers. Dense layers can lead to more electrical resistance, as well as limitations of mass flow through the electrode.

Comparing the data between the three MEAs with electrospun electrodes, the disparity between the data mainly lies in the operation with MeOH. As these tests were all done with a dilute feed (1M MeOH), an increase in feed concentration may have a profound impact on performance, as water management in the electrode seems to be a major limitation with these dense, electrospun mats.

The comparison between equivalently loaded MEAs, in terms of Nafion and catalyst, can indicate how much, if any, improvement the electrospun electrodes have upon fuel cell performance. While not identical in loading, the commercial Fuel Cell Store MEA, MEA #11

---

[67] (Kim K. , et al., 2008)

and the dual-electrospun MEA, E.MEA Total, can be compared on a somewhat level playing field. This is seen in Figure 45.
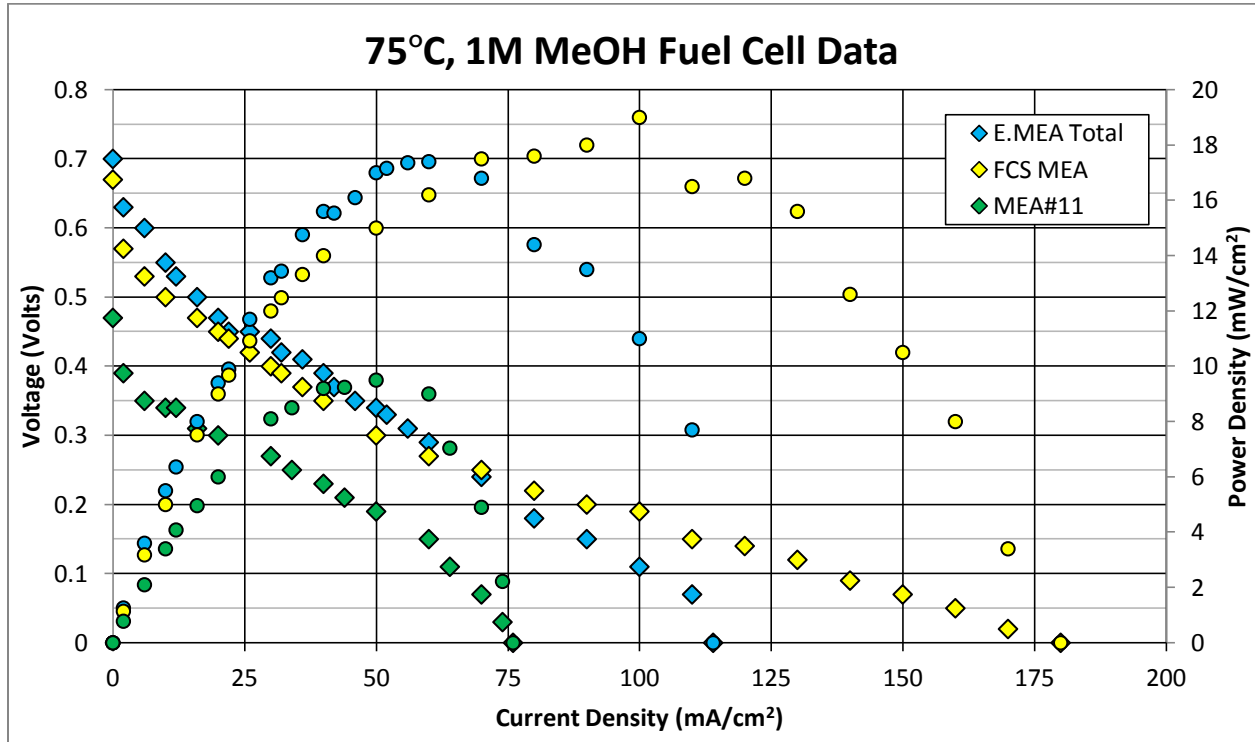
The comparison between these three shows that, in this dilute MeOH case, the electrospun MEA not only has the highest OCV, but outperforms the lab-fabricated MEA (MEA #11) over the entire range of current densities. While there are no major defects in the lab-fabricated samples, the process is not perfect, and is not controlled to the level at which the FCS MEA is created in, as it is in a well-controlled manufacturing environment. Despite this, the lab-made E.MEA Total does show slightly better performance at low current densities, i.e in the kinetic region. While not providing the same peak power density as the FCS, as well as having a limiting current density roughly 60mA/cm² less, the fact that it is close to the same performance is a very good sign, especially when equivalent MEAs with traditional electrodes are performing well under that of the commercial MEA.

Fabrication Comparisons

Difficultly/Cost

While both electrode types are fabricated in the lab, both lab procedures are rife with opportunities for both error and causing irreparable damage to the MEA. While the GDL preparation for both the conventional and electrospun cathodes are simply cutting the piece to the proper size, the electrospun cathodes already have electrostaticly active fiber on the surface. When cutting out a square from the larger electrospun mat, there is a very possible chance that the scissors, when opening back up, will pull the fibers from the surface. When the fibers are mechanically forced together, they become inseparable macro fibers, and tend to detach from the carbon surface.

The airbrushing of catalytic ink onto the GDL to create the electrode is a source of error, as the ink can run off from the surface if applied too liberally. The use of "active drying", drying the sample continuously as the ink is sprayed, mitigates these losses, but the process is still inexact. The airbrushing of the electrospun fibers must be done much slower, by as using a much lower air pressure to eject the solution from the tip of the airbrush. Too high a velocity of air/solution, and the fibers will be ripped from the surface. The steps past here, the hot pressing and use in the test bed, are identical.

The cost of fabricating each has not been quantified; however, the cost of the electrospinning equipment (quotes can be found in Appendix E: Quotes for Lab-Bench Electrospinning Equipment) is quite prohibitive. The time for creating an electrospun electrode is also much higher, and there is always a period of time before the actual electrospinning takes place. Not only do the solutions have to be fabricated carefully and

stored immaculately, even the same solution in the electrospinning equipment at the same conditions may not spin correctly. The time taken adjusting parameters and the physical setup (to keep the GDL flat on the collection plate is one prime example) can be long and arduous. On a lab scale, both types use the same amount of material, but the electrospinning electrodes take up much more time and have more opportunity to fail during fabrication. However, it does appear that fibrous Nafion, however it can be fabricated, improves performance of the catalyst layers for DMFC.

Effect on performance

From the data collected, it is clear that the lab-fabricated MEAs are not up to the commercial standard. However, despite the small defects and limitations picked up through the fabrication process, these MEAs are still competitive.

More importantly, the comparisons between like lab-based MEAs shows there are clear advantages to certain constructions and run conditions. Once fabricated successfully, there is a clear trend that shows the electrospun MEAs performing better in MeOH conditions. In addition, the H2/O2 results show a competitive OCV, indicating these fuel cells are still functional in either case, not requiring a water-saturated electrode layer to successfully operate. The overall results are seen in Table 11 and Table 12, with the maximum performance figures in bold.

Table 11: Summary of Limiting Current Density, Peak Power Density, and OCV in H2/O2

MEA	Limiting Current Density (mA/cm2)	Peak Power Density (mW/cm2)	OCV (V)
Comm. MEA	**580**	**119**	**1.02**
300% MEA	460	114	**1.02**
MEA #7	350	101	0.71

MEA			
MEA #11	235	68	0.82
N1035x2	145	38	0.98
E.MEA 1	270	84	**1.02**
E.MEA 2	20	0	0.2
E.MEA 3	260	86	**1.03**
E.MEA Total	245	80	**1.03**

Table 12: Summary of Limiting Current Density, Peak Power Density, and OCV in 1M MeOH

MEA	Limiting Current Density (mA/cm2)	Peak Power Density (mW/cm2)	OCV (V)
Comm. MEA	**180**	19	0.67
300% MEA	75	7	0.52
MEA #7	110	14	0.45
MEA #11	75	10	0.47
N1035x2	60	5	0.58
E.MEA 1	150	**22**	0.68
E.MEA 2	N/A	N/A	0
E.MEA 3	110	16	0.65
E.MEA Total	115	18	**0.7**

These results, while very informative, cannot be used to interpret advanced phenomena without a great deal of speculation. If water management is truly the limiting factor as we approach high current densities, getting an idea of what the electrode looks like is crucial; a high density layer of compacted fibers on the GDL-electrode interface could cause an excess amount of water in the electrode, therefore over-humidifying the membrane as well as hampering gaseous diffusion, as not it must go through a liquid media. However, while we see this sort of behavior between E.MEA #1 and the 300% MEA, it is less clear between E.MEA #3 and MEA#11. Due to the lower catalyst loading, perhaps the fibers are less compacted, but it is not clear without a cross-sectional SEM.

In addition, it is unclear as to how the catalyst is depositing in the electrode. In theory, one would think that the catalyst, when sprayed onto the fibrous surface, it would pass by the fibers, with some catalytic material adhering to the fiber surface, resulting in long fibers being covered, or doped, with catalyst particles. However, it is unclear if this occurs. If the catalyst bypasses the fibers and simply builds up on the surface of the MPL, we would expect to see poor kinetics (low OCV) as the catalyst sites are not physically open to the fuel. Additionally, there is little Nafion to allow for proton conduction. On the other hand, the catalyst might be trapped by the fibers, not allowing it to penetrate into the electrode layer. This would result in an electrode with little catalyst at the GDL-electrode layer, and a heavy concentration between the membrane-electrode interface. This, also, would result in poor kinetics (difficulty in accessing the catalyst, as it is packed up into the membrane) and potentially a limited amount of performance as the water generated at the electrode would have so much further to travel in order to diffuse out.

In general, it is clear that the experimentation done here has proven the electrospun electrodes as a concept that has some potential to improve electrode construction. While a dual-electrospun MEA does not match up to the commercial standard, it is clear that even just an electrospun cathode can increase performance in dilute MeOH conditions. To test this further, one should investigate different concentrations and flowrates, as well as varying the electrospun Nafion content in the electrode layer. Additional future work can be found in Future Work.

Conclusions

We have been able to successfully electrospin Nafion® nanofibers continuously, creating fiber mats with fiber diameters near 400nm as verified by SEM. These mats were tested in a direct methanol fuel cell (DMFC) application as cathodes, and showed improved performance with a dilute methanol feed compared to conventional MEAs with equivalent Nafion and catalyst loading. An MEA fabricated with twin electrospun electrodes was compared against an equivalent conventional MEA, showing the same performance enhancement using a dilute methanol fuel. While the electrospinning process is difficult to control and potentially unattractive to commercial applications, the fibers can be spun into a mat and be used in the electrodes of a fuel cell MEA. The presence of these mats appears to improve the performance of catalyst layers in DMFC.

Future Work

Electrospinning

Inclusion of catalyst particles in electrospun solution

The main focus in utilizing the electrospun morphology of Nafion is to decrease the mass diffusion limitations of both fuel and product species in the electrode layer, while increasing the proton conduction and availability of active catalyst sites. While this study has focused on the electrospinning and catalyst deposition steps separately, the inclusion of the catalyst nanoparticles into the Nafion solution used for electrospinning may be a viable alternative.

The airbrushing of catalyst upon the electrospun fibers can be detrimental to the electrode; if one does not control the airflow out of the airbrush correctly, the fibers, which are weakly bound to the MPL surface of the GDL, can be ripped from the surface entirely. In addition, there is some potential for the fibers to be matted down, with the catalyst building upon previously deposited catalyst and making a separate catalyst layer in the electrode. To promote active catalytic areas and homogeneity, a post-doctoral student at Vanderbilt was able to successfully create electrospun Nafion fibers containing catalyst particles with an unreported carrier polymer, as seen in Figure 46.
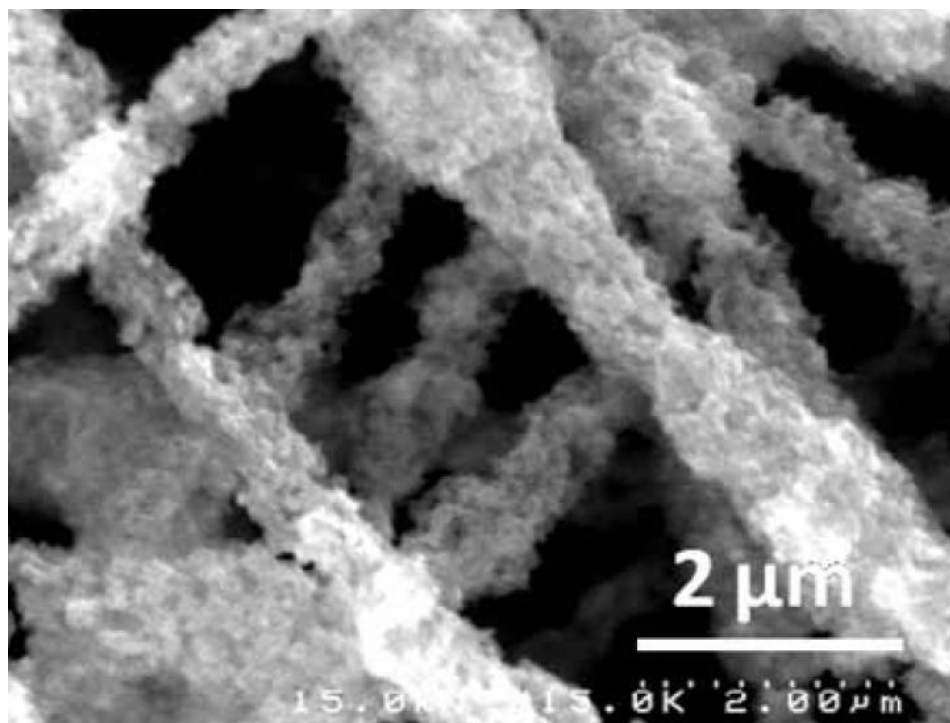
Figure 46: SEM images of electrospun Nafion fibers containing Pt/C catalyst particles

With these mats created, they were employed as an electrode on the cathode side of a single-cell MEA of unreported size and unreported Nafion loading. It was seen that, with a 4 $mg \cdot cm^{-2}$ catalyst loading, the electrospun cathode was able to produce 1080 mA/cm² at 0.6V, wheras an equivalent cathode prepared by the decal method was only able to produce 866 mA/cm². The maximum power density achieved by the MEA with the composite electrospun cathode was 705 mW/cm²; the traditional decal method, 550 mW/cm². These results are for an H_2/O_2 system, with anode humidification unreported[68]. While these results are promising, there have been no further publications from the Vanderbilt research group on the subject.

One concern of utilizing this technique is the potential encapsulation of particles. Even if one can achieve a homogenous mixture of catalyst particles in the solution and they

---

[68] (Zhang W. , 2010)

do not agglomerate into larger clusters, which is the main concern with suspensions such as this, there is a likelihood of the particles being encapsulated in the fiber. As the catalyst particles are typically very small (5nm diameter particles on 30nm diameter carbon supports) as compared to the diameter of the polymer fiber (nominally 400nm), there is a chance the catalyst particles could reside inside the fiber. This encapsulation would render the catalyst particle much less effective, as there is no avenue for direct contact between a Pt atom and either the electrons or protons in the cathode layer. Perhaps there is no need for direct metal-to-atom interaction; if there is, this reduction in active catalyst sites results in a less efficient use of catalys, adding a cost penalty to this type of construction.

In addition, there is a distinct change of rheometry of the solution may pose an issue for electrospinning. Adding particulate matter to a solution will change the viscosity, and may turn the solution into behaving with fixotropic properties. A colloid solution is rarely homogenous, and this difference will affect viscosity. To compensate, a thinner solution would have to be used. However, due to the delicate nature of electrospinning, this may not be feasible for a Nafion-PEO system. If possible to be electrospun, this type of solution would require very careful control to ensure the fibers created are of the correct composition and loading of both Nafion and catalyst.

Fuel Cell Application

Longevity / Durability

One important facet of a fuel cell assembly is longevity. Due to the high cost of fabrication (primarily due to catalyst cost), and the prohibitive time an energy requirements to successfully recycle catalyst, an MEA must have a long, useful lifespan to

be economically feasible. While MEA longevity was not a focus of this research, it must be established for our electrode material. The nanofibers, already somewhat fragile, are being subjected to material it is soluble in (alcohol, in this case methanol, and water) at low to medium temperatures. While this is certainly not the most caustic environment a fuel cell can see, the electrospun nanofibers have not be tested for long-term stability in the presence of water or alcohol solvents.

To test this, a set of nearly identical electrospun mats could be submerged in water, methanol, or any mixture of the two. They could then be removed at various times (if there are five mats, we can remove one after one hour, another at 2 hours, another at 4 hours, one at 8 hours and the last after 24 hours) and take SEM images of the surface. IF the nanofibers are unstable, there should be very discernible morphological changes that the fibers undergo; the fibers can break, swell, shrivel, melt, or seem to dissolve, based upon the interaction with the solvent. If no change is seen over 24 hours, longer times can be tested. While these times will not be equivalent to the useful life of the MEA (as the MEA is not fully saturated in liquid feed; rather, it is a mixed-phase stream, mostly saturated vapor), it will elucidate a general trend, and knowledge of what environments the electrospun material is stable in.

In addition to the simple test above for mechanical, morphological changes, it would be a good use of time to test an MEA using electrospun electrodes for long durations of time, under either constant current draw or continuous sweeping (from OCV to a set current) for long-term testing. While the surfaces are unable to be tested via SEM (or any other analytical measurement, such as cyclic voltammetry, surface energy or electrical

impedance spectroscopy), a more fundamental understanding of the lifespan of an MEA utilizing this new catalyst support can be gained. The long term tests can be done for various methanol concentrations, as well as flowrates and feed conditions, chosen to emulate real-world situations of current draw and feed conditions.

Additional Fabrication Techniques

As was seen when trying to deposit a high loading of catalyst upon the electrospun fiber mat, the catalyst covered the fibers, was able to wet the surface, and as able to build up so the fibers were then submerged and compressed beneath a layer of just catalyst particles. If this occurs, it is assumed that there is very little Nafion present in the membrane side of the electrode layer. While this was mitigated by using a lower catalyst loading, it gave rise to thoughts of different ways of applying the catalyst to promote homogeneity of the catalyst over both the area and the depth of the electrode layer.

One idea is to alternate the electrospinning and catalyst deposition steps. As the electrode Nafion content is targeted during electrospinning, it can be broken up into four segments. After each segment of time, some amount of catalyst can then be airbrushed onto deposited nanofibers. The amount deposited could be controlled by either the weight added (mass), or the amount of catalyst ink used (volume). Once the catalyst has been deposited, the second segment of the electrospinning could then commence, and this process alternated until a full-thickness electrode could be used.

This process, however, would have to be thought through before use, especially due to safety. As a solution is electrospun, it is conducting electricity between the grounded plate and the charged spinneret. The voltage of this electricity can be as high as 20kV,

though at a fairly low current. Even so, it is a tremendous amount of energy, and discharging such a flow of electricity upon Pt/Ru metal may pose a safety concern, especially as the ink used to airbrush contains ethanol. If this was to be undertaken, a study could be done by spraying a solution of either Nafion or other stable polymer (such as polystyrene) onto a GDL surface which has a light loading of catalyst. The electric potential and the catalyst loading can be increased in small amounts to ensure it is safe to continue.

Electrospun Nafion Loading in Electrodes

While touched upon when comparing performance of electrospun MEAs, there was no direct study between the Nafion loading in the electrodes using electrospun supports. While E.MEA #2 likely failed due to excessive loading, the lower bound of loading was not studied. The electrodes were constructed to have equivalent Nafion loading in the electrodes as compared to traditional MEAs in order to compare directly. However, as the surface area of the Nafion structures in a fibrous form is much greater than in micro-globules found when airbrushed, perhaps the amount of Nafion required is reduced. To study this, mats of electrospun fibers would need to be fabricated with the same solution and equipment variables, with the time of electrospinning varied. For example, spinning for 0.5, 1, 2, 4 and 8 hours would create mats of varied loading. By applying the same amount of catalyst to each, assembling them into MEAs with the same GDL, anode and membrane, it could be possible to see a trend. From the data gather thus far, it would be expected that very low amounts of Nafion would perform like a traditionally made MEA, with the intermediate loadings performing identically and the higher loadings perform poorly. However, this is just a hypothesis, and testing this would prove to be useful in understanding the limiting factors in an electrode's construction.

Modeling of Electrospinning

One of the most important aspects of continuing this work is to be able to achieve repeatable electrospinning sessions which yield very similar fiber mats. As Nafion is so difficult to electrospin, and very slight perturbations and changes can have a large effect on not only fiber diameter but also the area the fibers are deposited upon, the ability to control each variable, especially the solution variables, is vital.

The methodology used to electrospin fibers in this project was adapted from previous studies; the variables set and used by others were taken as the initial guess of a very long, iterative process. While much of the existing literature showed similar trends between variable setpoint and the resulting fiber diameter, the actual values were not the same. This is not uncommon in systems which has multiple variables that are linked together.

One way around this trial-and-error approach would be to undergo a serious modeling study of Nafion nanofiber diameter and deposition area, with respect to the solution and equipment variables. While the existing modeling of electrospinning is highly theoretical and varied (some studies work of a foundation of finite element analysis of one section of fiber; others work from conservation equations), a simple model could be developed to assist future researchers in applying the electrospinning of Nafion into their own use. As of now, the process to determine fiber diameter is to prepare a solution for electrospinning carefully (to keep track of solution variables) and electrospin, take the resulting fiber, and use SEM micrographs to determine fiber size. If we could predict this

with some semblance of accuracy, it would cut down on much of the time put into establishing the first solution's properties.

This type of modeling, however, would require either extensive empirical relations to be gathered, or a precise theoretical model developed, presumably from one of the existing methods currently being pursued. Even if a model were to be produced, the differences between individual electrospinning setups would incur error or unaccounted variation; while the variables of the solution and equipment are known, the electrostatic instability of the fiber as it is spun is hard to quantify. As the fiber is small and has a small charge, small, unseen and unaccounted for variances in the space between the spinneret and the collection plate can make the fibers act chaotically. While very stable polymers such as polystyrene can be electrospun and even ordered into precise alignments, the inherent difficulty of the Nafion polymer makes these types of external manipulations unpredictable. Until this is understood more fundamentally, the modeling of an electrospinning device for a high-purity Nafion solution is a long way off.

Modeling of PEMFC Performance

One aspect of modeling is the performance of the fuel cell itself. While current models are abound, and have been briefly reviewed in the modeling chapter, application of such a model to our exact system has not been done. If a modeling effort is pursued, it may be able to indicate which resistances to current conduction are the highest. Identifying these types of ohmic resistances could point to areas in which the fuel cell could be improved; while the variables of the system are known, the magnitude of the effect they

have when changed is somewhat unique between systems, and it would be very useful to

know these types of limitations the fuel cell developed here is constrained to.

Acknowledgements

First and foremost, I want to thank Professor Ravindra Datta for his tireless attention to my studies. Between critiques during weekly meetings, an easy, welcoming approachability and the ability to always keep the big picture in mind was undeniably crucial to my ability complete this stage of the research done here.

My WPI Fuel Cell Center Colleagues, Susan Yen, Ph.D; Nick Devau, Ph.D; Drew Martino, Ph.D; Jason Morgan, Ph.D; Neal Rosenthal, M.S '11, and Dan Knox. M.S were, in many ways, my family during my duration of study in the WPI Fuel Cell Center. Between finding parts, talking through theory, scraping up mutual encouragement and occasionally lamenting about the infrequency of seeing direct sunlight, the team worked together to further everyone's research as a whole.

The WPI Fuel Cell MQP Students, Samantha Do, Kaitlyn Spetka, Matt Suarez, Casey Rivera and Diego Lugo were also instrumental in making things work around the lab and really fleshing out the concepts. Between troubleshooting test stations, modifying test beds for improved functionality, talking our way through data and watching each other's experiments every so often, the skills gained and lessons learned helped all parties involved. As they say, the best way to learn is to teach.

Professor Satya Shivkumar and his graduate students, Haikun Xu, M.S and Yukun Tao, M.S, deserve a great deal of thanks for the introduction and supervision of the electrospinning trials. Without them, there could be no electrospinning, which is the crux of this work.

The chemical engineering department here at WPI has been my place of study for both a B.S and M.S; from the first time learning about material balances to employment as an instructor for the senior level Unit Operations lab, everyone, from teachers to staff to students, has always been professional, kind and understanding for the better part of six years I've spent in Goddard's hallowed halls.

In particular, I'd like to thank Professor DiBiasio, Dept. Head for his leadership, as well as my MQP advisor Susan Zhou as well as Nikolaos Kazantzis, my undergraduate advisor. Felicia Vidito and Tiffany Royal deserve more thanks than they can ever receive for making the department run so smoothly, and never letting us forget about a single meeting, seminar or colloquium, no matter how hard we try. Jack Ferraro and Doug White, the staff of the machine and tech shop, hold this department together, literally and figuratively; between their work, the lab facilities and equipment are promptly attended, always up and running, and they will always take time to fabricate a custom solution. As well, the chemical engineering faculty and my fellow grad students deserve thanks for all the help and support given over the years.

And last, but not least, mom and dad (B.S EE, WPI '67). Without their upbringing, I would simply be a shell of the person I am proud to say that I am today. Thank you, truly, for everything, and giving me the chance to pursue my own goals in life.

Works Cited

Ahn, S.-Y., Lee, Y.-C., Heung, Y.-H., Hong, S.-A., & Oh, I.-H. (2004). Effect of the ionomers in the electrode on the performance of PEMFC under non-humidifying conditions. *Electrochemica Acta , 50*, 673-675.

Antolini, E. (2009). Carbon supports for low-temperature fuel cell catalysts. *Applied Catalysis B: Environmental , 88*, 1-24.

Antolini, E., Giorgi, L., Pozio, A., & Passalacqua, E. (1999). Influence of Nafion loading in the catalyst layer of gas-diffusion electrodes for PEFC. *Journal Of Power Sources , 77*, 136-142.

Bajon, R., Balaji, S., & Guo, S. (2009). Electrospun Nafion Nanofiber for Proton Exchange Membrane Fuel Cell Application. *Journal of Fuel Cell Science and Technology , 6*.

Ballengee, J. B., & Pintauro, P. N. (2010). Morphological Control of Electrospun Nafion Nanofiber Mats. *Electrochemical Society Transactions , 33* (1), 647-658.

Ballengee, J., & Pintauro, P. (2011). Composite Fuel Cell Membranes from Dual-Nanofiber Electrospun Mats. *Macromolecules , 44*, 7307-7314.

Barral, S., & Kowalewsi, T. (2006). *Numerical Modeling of Electrospinning.* Retrieved 4 1, 2012, from http://fluid.ippt.gov.pl/seminar/text/sbarral120406.pdf

Carmo, M., Paganin, V., Rosolen, J., & Gonzalez, E. (2005). Alternative supports for the preparation of catalysts for low-temperature fuel cells: the use of carbon nanotubes. *Journal of Power Sources , 142*, 169-176.

Celebioglu, A., & Uyar, T. (2012). Electrospinning of nanofibers from non-polymeric systems: polymer-free nanofibers from cyclodextrin derivatives. *Nanoscale , 4* (2), 621-31.

Choi, J. (2010). High Conductivity Perfluorosulfonic Acid Nanofiber Composite Fuel-Cell Membranes. *ChemSusChem Communications , 3*, 1245 – 1248.

Choi, J., Wycisk, R., Pintauro, P., Lee, K., & Mather, P. (2010). Nanofiber composite membranes with low equivalent weight perfluorosulfonic acid polymers. *Journal of Materials Chemistry , 20*, 6282–6290.

Choi, J., Wycisk, R., Zhang, W. J., Pintauro, P. N., & Lee, K. M. (2010). High Conductivity Perfluorosulfonic Acid Nanofiber Composite Fuel-Cell Membranes. *ChemSusChem , 3* (11), 1245-1248.

Choi, J., Wycisk, R., Zhang, W., Pintauro, P., Lee, K., & Mather, P. (2010). High Conductivity Perfluorosulfonic Acid Nanofiber Composite Fuel-Cell Membranes. *ChemSusChem , 3*, 1245-1248.

Do, S., Spetka, K., & Suarez, M. (2012). *Effect of Temperature on the Performance of Direct Methanol Fuel Cells.* Worcester Polytechnic Institute, Chemical Engineering. Worcester: WPI.

Dong, B., Gwee, L., Salas-de la Cruz, D., Winey, K. I., & Elabd, Y. A. (2010). Super Proton Conductive High-Purity Nafion Nanofibers. *Nano Letters , 10* (9), 3785-3790.

Dong, Z., Kennedy, S., & Wu, Y. (2011). Electrospinning materials for energy-related applications and devices. *Journal of Power Sources* , Electronic Publication Only.

Dotti, F., Varesano, A., Montarsolo, A., Aluigi, A., Tonin, C., & Mazzuchetti, G. (2007). Electrospun Porous Mats for High Efficiency Filtration. *Journal of Industrial Textiles , 37* (2), 151-162.

Eda, G. (2006). *Effects of Solution Rheology on Electrospinning of Polystyrene.* Master's Thesis, Worcester Polytechnic Institute, Material Science, Worcester, MA.

Garland, N. L., & Kopasz, J. P. (2007). The United States Department of Energy's high temperature, low relative humidity membrane program. *Journal of Power Sources , 172* (1), 94–99.

Gottesfeld, S., & Wilson, M. (1992). Thin-film catalyst layers for fuel cell electrodes. *JOURNAL OF APPLIED ELECTROCHEMISTRY , 22*, 1-7.

Hill, J. M. (2003). Study of Platinum/Ruthenium Catalysts for Methanol Oxidation in Direct Methanol Fuel Cells. *NACS Presentation.*

Hsin, Y., Hwang, K., & Yeh, C. (2007). Poly(vinylpyrrolidone)-Modified Graphite Carbon Nanofibers as Promising Supports for PtRu Catalysts in Direct Methanol Fuel Cells. *J. AM. CHEM. SOC , 129*, 9999-10010.

Huang, Z.-M., Zhang, Y.-Z., Kotaki, M., & Ramakrishna, S. (2003). A review on polymer nanofibers by electrospinning and their applications in nanocomposites. *Composites Science and Technology , 63*, 2223-2253.

Hyeon, T., Han, S., Sung, Y., Park, K., & Kim, Y. (2003). High-Performance Direct Methanol Fuel Cell Electrodes using Solid-Phase-Synthesized Carbon Nanocoils. *Angew. Chem , 115*, 4488-4492.

Khajeh-Hosseini-Dalasm, N., Kermani, M., Moghaddam, D., & Stockie, J. (2010). A parametric study of cathode catalyst layer structural parameters on the performance of a PEM fuel cell. *International Journal of Hydrogen Energy , 35*, 2417-2427.

Kim, K., Kim, H., Lee, K., Jang, J., Lee, S., Cho, E., et al. (2008). Effect of Nafion gradient in dual catalyst layer on proton exchange membrane fuel cell performance. *International Journal of Hydrogen Energy , 32*, 2783-2789.

Kim, K., Kim, H., Lee, K., Jang, J., Lee, S., Cho, E., et al. (2008). Effect of Nafion(r) gradient in dual catalyst layer on proton exchange membrane fuel cell performance. *International Journal of Hydrogen Energy , 33*, 2783-2789.

Kim, K., Lee, K., Kim, H., Cho, E., Lee, S., Lim, T., et al. (2010). The effects of Nafion ionomer content in PEMFC MEAs prepared by a catalyt-coated membrane (CCM) spraying method. *International Journal of Hydrogen Energy , 35*, 2119-2126.

Kosek, J. (1994). *Patent No. 5523177.* USA.

Kowalczyk, T., & Barral, S. K. (2009). *Modeling Electrospinning of Nanofibers.* IUTAM Symposium on Modelling Nanomaterials and Nanosystems.

Kowalewski, T. B. (2005). Experiments and modelling of electrospinning process. *Bulletin of the Polish Academy of Sciences , 53* (4).

Krishnan, N., Prabhuram, J., Hong, Y., Kim, H.-J., Yoon, K., Ha, H.-Y., et al. (2010). Fabrication of MEA with hydrocarbon based membranes using low temperature decal method for DMFC. *International Journal of Hydrogen Energy , 35* (11), 5647-5655.

Kulikovsky, A. (2011). A model for carbon and Ru corrosion due to methanol depletion in DFMC. *Electrochemical Acta , 56*, 9846-9850.

Laforgue, A., Robitaille, L., Mokrini, A., & Ajji, A. (2007). Fabrication and characterization of ionic conducting nanofibers. *Macromolocules Materials Engineering , 292* (12), 1229-1236.

Lai, C., Lin, J., Ting, F., San-Der, C., & Hsueh, K. (2008). Contribution of Nafion loading to the activity of catalysts and the performance of PEMFC. *International Journal of Hydrogen Energy , 33*, 4132-4137.

Lee, D., & Hwang, S. (2008). Effect of loading and distributions of Nafion ionomer in the catalyst layer of PEMFCs. *International Journal of Hydrogen Energy , 33*, 2790-2794.

Lee, S., Mukerjee, S., McBreen, J., Rho, Y., Kho, Y., & Lee, T. (1998). Effects of Nafion impregnation on performances of PEMFC electrodes. *Electrochemcial Acta , 43* (24), 3693-3701.

Lee, Y. (2011). Preparation and Performance of IPMC Actuators with electrospun Nafion-MWCNT Composite Electrodes. *Actuators B* , Electronic Distribution.

Li, G., & Pickup, P. (2003). Ionic Conductivity of PEMFC Electrodes. *Journal of the Electrochemical Society , 150* (11), C745-C752.

Lin, H.-L., Wang, S.-H., Chiu, C.-K., Yu, T., Chen, L.-C., Huang, C.-C., et al. (2010). Preparation of Nafion/poly(vinyl alcohol) electro-spun fiber composite membranes for direct methanol fuel cells. *Journal of Membrane Science , 365*, 114-122.

Ortiz-Pivera, E., Reyer-Hernandez, A., & Febo, R. (2007). Understanding the History of Fuel Cells. *2007 IEEE Conference onthe History of Electric Power*, (pp. 117-122).

Park, J., Ju, Y., Park, S., Jung, H., Yang, K., & Lee, W. (2009). Effects of electrospun polyacrylonitrile-based carbon nanofibers as catalyst support in PEMFC. *J Appl Electrochem , 39*, 1229-1236.

Passalacqua, E. L. (2001). Nafion content in the catalyst layer of polymer electrolyte fuel cells: effects on structure and performance. *Electrochemical Acta , 46*, 799-805.

Piela, P., Eickes, C., Brosha, E., Garzon, F., & Zelenay, P. (2004). Ruthenium Crossover in Direct Methanol Fuel Cell with Pt-Ru Black Anode. *Journal of The Electrochemical Society , 151* (12), A2053-A2059.

Pintauro, P., Wycisk, R., & Lee, K. (2005). Sulfonated Polyphosphazene-Polybenzimidazole Membranes for DMFCs. *J. Electrochem. Soc , 152* (5), A892-A898.

Poltarzewski, Z. S. (1992). Nation Distribution in Gas Diffusion Electrodes for Solid-Polymer-Electrolyte-Fuel-Cell Applications. *Journal of the Electrochemical Society , 139*, 761-766.

Qi, Z. K. (2003). Low Pt loading high performance cathodes for PEM fuel cells. *Journal of Power Sources* (113), 37-43.

Rosenthal, N. (2009). *A Home-Made Passive Direct Methanol Fuel Cell.* WPI, Chemical Engineering. Worcester, MA: Worcester Polytechnic Institute.

Saha, M., Paul, D., Peppley, B., & Karan, K. (2010). Fabrication of catalyst-coated membrane by modified decal transfer technique. *Electrochemistry Communications , 12* (3), 410-413.

Sasikumar, G. I. (2004). Optimum Nafion Content in PEM fuel cell electrodes. *Electrochemica Acta , 50*, 601-605.

Sasikumar, G., Ihm, J., & Ryu, H. (2004). Optimum Nafion content in PEM fuel cell electrodes. *Electrochemica Acta , 50*, 601-605.

Shutov, A., & Astakhov, E. (2006). Formation of Fibrous Filtering Membranes by Electrospinning. *Technical Physics , 51* (11), 1093–1096.

Song, J. C. (2001). Optimal composition of polymer electrolyte fuel cell electrodes determined by the AC impedance method. *Journal of Power SOurces , 94*, 78-84.

Song, J., Cha, S., & Lee, W. (2001). Optimal composition of polymer electrolyte fuel cell electrodes determined by the AC impedance method. *Journal of Power Sources , 94*, 78-84.

Staiti, P., Poltarzewski, Z., Alderucci, V., Maggio, G., & Giordano, N. (1994). Solid polymer electrolyte fuel cell (SPEFC) research and development at the institute CNR-TAE of messina. *International Journal of Hydrogen Energy , 19* (6), 523–527.

Subramanian, C., Weiss, R., & Shaw, M. (2010). Electrospinning and characterization of highly sulfonated polystyrene fibers. *Polymer , 51*, 1983-1989.

Szajdzinska-Pietek, E., Wolszczak, M., Plonka, A., & Schlick, S. (1999). Structure and Dynamics of Micellar Aggregates in Aqueous Nafion Solutions Reported by Electron Spin Resonance and Fluorescence Probes. *Macromolecules , 32*, 7454-7460.

Thompson, C. C. (2007). Effects of parameters on nanofiber diameter determined from electrospinning model. *Polymer , 48*, 6913-6922.

Thostenson, E., Ren, Z., & Chou, T.-W. (2001). Advances in the science and technology of carbonnanotubes and their composites: a review. *Composites Science and Technology , 61* (13), 1899-1912.

Ticianelli, E., Derouin, C. R., Redondo, A., & Srinivasan, S. (1988). Methods to Advance Technology of Proton Exchange Membrane Fuel Cells. *Journal of the Electrochemical Society , 135* (9), 2209-2214.

W. Gebrial, R. J. (2006). Non-contact imaging of carbon composite structures using electric potential (displacement current) sensors. *Measurement Science and Technology , 17* (6), 1470.

Xu, L. (2009). A mathematical model for electrospinning process under coupled field forces. *Chaos, Solitons & Fractals , 42* (3), 1463-1465.

Yarin, A., Kataphinan, W., & Reneker, D. (2005). Branching in electrospinning of nanofibers. *J. Applied Physics , 98*.

Yuan, T., Kang, Y., Chen, J., Du, C., Qiau, Y., Zue, X., et al. (2011). Enhanced performance of a passive direct methanol fuel cell with decreased Nafion aggregate size within the anode catalytic layer. *International Journal of Hydrogen Energy , 36*, 10000-10005.

Zhang, N. K. (2002). Surface modification of superparamagnetic magnetite nanoparticles and their intracellular uptake. *Biomaterials , 23* (7), 1553–1561.

Zhang, W. (2010). Electrospinning Pt/C Catalysts into a nanofiber Fuel Cell Cathode. *The Electrochemical Society Interface* , 51.

Zhani, M., Gharibi, H., & Kakaei, K. (2010). Optimization of Nafion content in Nafion-polyaniline nano-composite modified cathodes for PEMFC applications. *International Journal of Hydrogen Energy , 35*, 9261-9268.

Zhou, C. S., Liu, Z., Dai, J. Y., & Xiao, D. (2010). Electrospun Ru(bpy)32+-doped nafion nanofibers for electrochemiluminescence sensing. *Analyst , 135* (5), 1004–1009.

Appendices

Appendix A: Fuel Cell Test Bed Operation

A.1: Syringe Pump

Current Flow Rate

Pressure

Amount in Pump

Run Time

"A"

"Run", "Stop", "Refill" buttons

Numeric Keypad
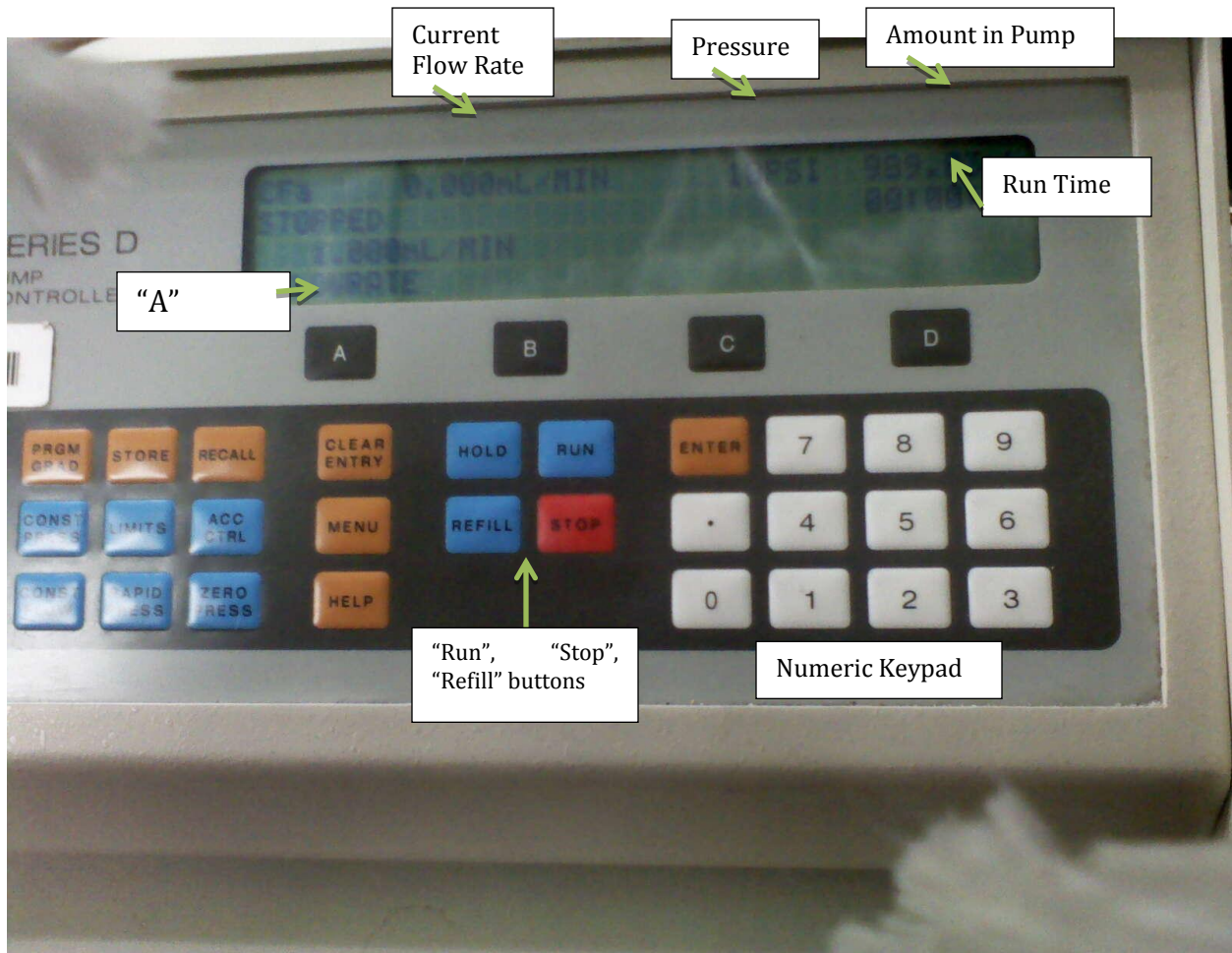
Figure 47: Syringe Pump Interface

Filling

1. If the pump is not on, turn on the power for the pump and then the power for the controller.
2. Detach the fitting connecting the plastic tubing to the insulated metal tubing.
3. Place end of plastic tubing in container and submerge with methanol/DI water.
4. Push "A" button (below display).

5. Enter flow rate (###.#) using numeric keypad.
6. Press "Enter".
7. Press "Refill".
8. Wait for pump to take in as much liquid as it can.
   a) Be careful when using less than 1L of liquid to fill pump because pump will take in air when there is no more water or methanol.
9. Run the pump (repeat steps 4-6 and then press "Run") until some liquid returns to the storage container in order to produce suction head, and then reattach the plastic line.

Running/Emptying

1. If the pump is not on, turn on the power for the pump and then the power for the controller.
2. If the pump is being emptied, detach the fitting that connects the plastic tubing to the insulated metal tubing and place it in the storage container. If the pump will be sending methanol to the cell, open the methanol feed valve.
3. Push "A" button (below display).
4. Enter flow rate (###.#) using numeric keypad.
5. Press "Enter".
6. Press "Run".

Warnings/Hints

- Refilling the pump at too high a flow rate can cause too much air to be taken in. 150-200 mL/min is usually fine and does not take excessively long to refill.
- After filling pump, it is a good idea to run at a relatively high flow rate (ex: 15 mL/min) to remove air bubbles.
- The pressure in the pump should not exceed 30 psi. The normal operating pressure appears to be around 18 psi.
- When emptying the pump, higher flow rates result in higher pressure. Exceeding flow rates of about 150 mL/min can make the pressure too high.
- Rinse the pump out between methanol concentrations (ex: when going from 10M to 3M methanol, remove the 10M methanol, fill the pump with DI water, remove the water, and then fill the pump with the 3M methanol) to prevent cross contamination.

A.2: Flow Controller
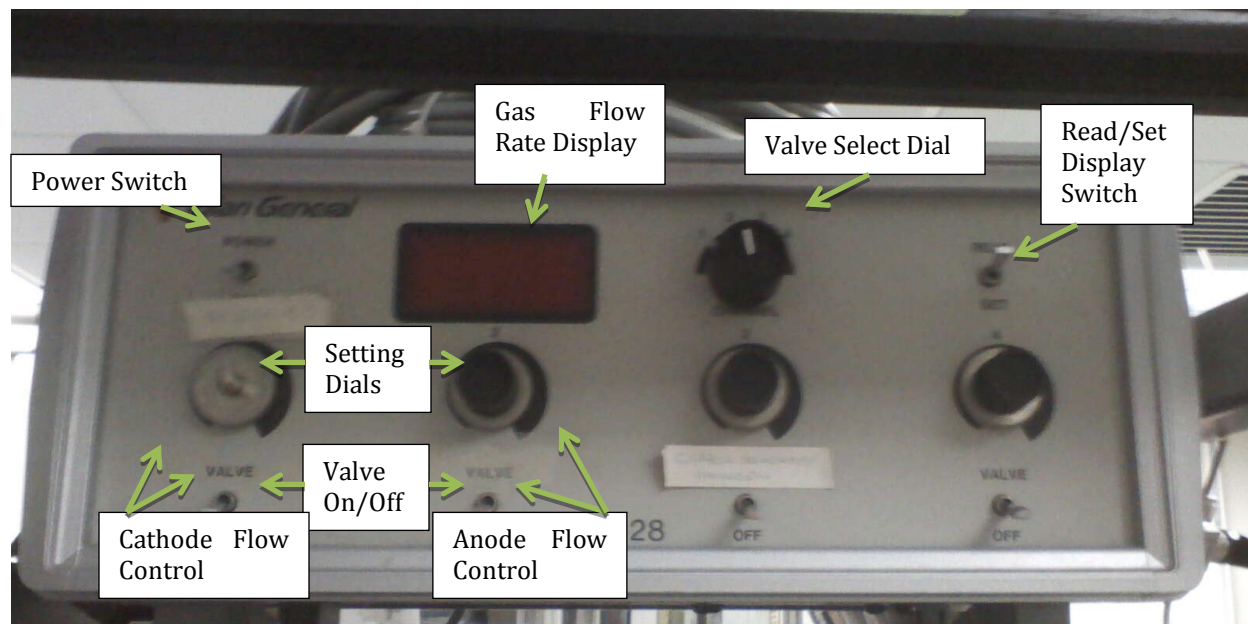
Figure 48: Flow Controller Interface

Start/Stop

1. When using the flow controller, turn on the power and then open the desired valve (valve 1 for the cathode, valve 2 for the anode).
2. When the flow controller is no longer needed, close the active valves before turning off the power.

Setting Flow Rates

1. Turn the valve select dial to the number of the valve being used (valve 1 for cathode, valve 2 for anode)
2. Turn the setting dial for the desired valve until the necessary flow rate is reached. There is a calibration curve taped to the top left corner of the test station.

A.3: Temperature Controllers
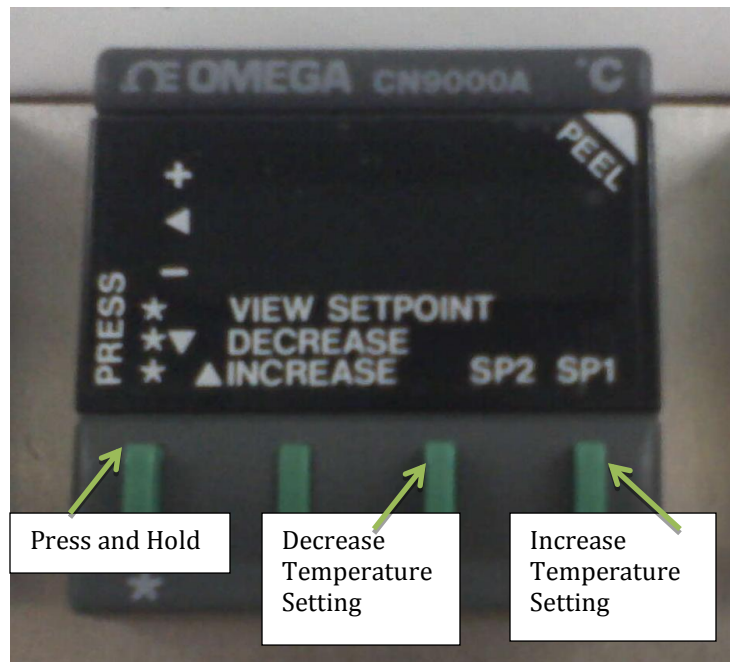
Figure 49: Omega Thermocouple Controller Interface

- There are three temperature controllers on the test station. The leftmost one controls the upper section of the methanol feed. The middle one (pictured) controls the temperature of the assembly. The rightmost one controls the lower section of the methanol feed.
- These controllers control heating only, cooling must be done through conduction and convection.
- Temperature controls are only on when power strip in back is also on.

A.4: Load Box
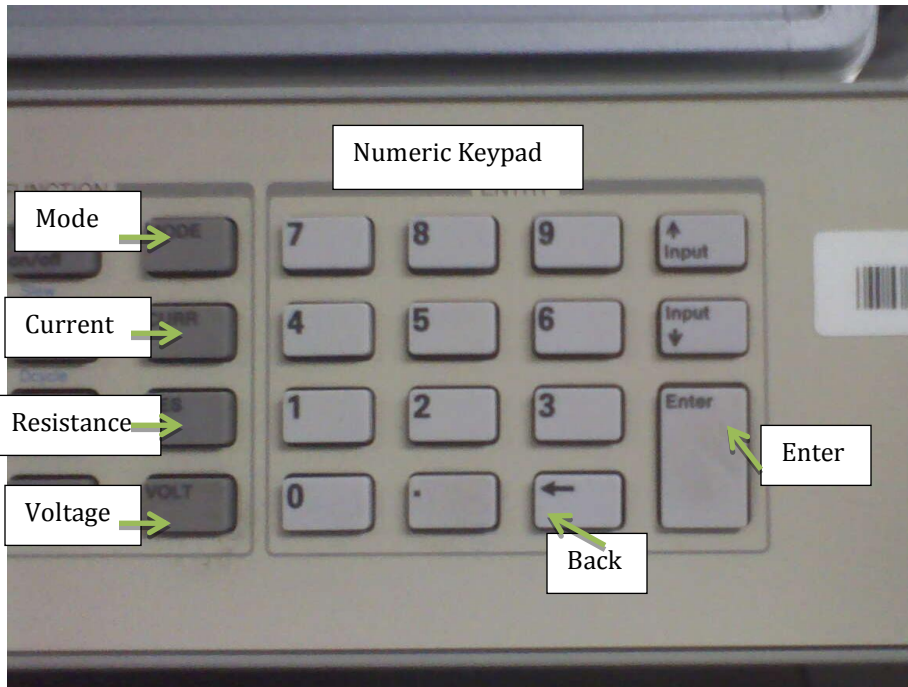
Figure 50: Load Box Interface

1. Turn on load box.
2. To specify the current (and record corresponding voltage), press "Curr"; to specify the voltage (and record the corresponding current), press "Volt"
3. Enter desired value using numeric keypad.
4. Press "Enter".
5. For subsequent settings, press "Curr" or "Volt" and then repeat steps 3 and 4.

A.5: Feed Instructions

In order to switch from any set of conditions to any other set of conditions, stop the current feed and then start the next feed.

Figure 51: Test Station Piping Diagram, Upstream of Fuel Cell

A.5.1: Hydrogen to the Anode

Starting Feed

1. Open the globe valve on the hydrogen tank.
2. Adjust pressure regulator to desired stream pressure.
3. Open the first and second check valves, following the line leading from the hydrogen tank.
4. If humidifying the hydrogen stream, turn the first and second three way valves so that the arrows on both handles point toward the humidifier. If not humidifying the hydrogen stream, turn the first and second three way valves so that the arrows on both sides point toward the bypass (away from the humidifier).
5. If using the flow controller, follow the instructions above for the use of the flow controller. If not using the flow controller, open the bypass check valve. **Do not use the flow controller with a humidified hydrogen stream.** The flow controller does not like water.
6. Open the remaining check valve.
7. If using the flow controller, open the back pressure regulator completely. If not using the flow controller, use the back pressure regulator to adjust the pressure and flow rate of the stream as desired.

Stopping Feed

1. Close the globe valve on the hydrogen tank.
2. Adjust pressure regulator to low/no pressure.
3. Close the first and second check valves, following the line leading from the hydrogen tank.
4. Return the first and second three way valves to neutral.
5. If using the flow controller, close valve 2 and then turn off power. If not using the flow controller, close the bypass check valve.
6. Close the remaining check valve.
7. Close the back pressure regulator.

A.5.2: Oxygen to the Cathode

Starting Feed

1. Open the globe valve on the oxygen tank.
2. Adjust pressure regulator to desired stream pressure.
3. Open the needle valve.
4. Open the check valve.
5. If using the flow controller, follow the instructions above for the use of the flow controller. If not using the flow controller, open the bypass check valve.

6. <u>If using the flow controller</u>, open the back pressure regulator completely. <u>If not using the flow controller</u>, use the back pressure regulator to adjust the pressure and flow rate of the stream as desired.

<u>Stopping Feed</u>

1. Close the globe valve on the oxygen tank.
2. Adjust pressure regulator to low/no pressure.
3. Close the needle valve.
4. Close the check valve.
5. <u>If using the flow controller</u>, close valve 1 and turn off the flow controller. <u>If not using the flow controller</u>, close the bypass check valve.
6. Close the back pressure regulator completely.

A.5.3: Nitrogen to the Anode

<u>Starting Feed</u>

1. Open the globe valve on the nitrogen tank.
2. Adjust pressure regulator to desired stream pressure.
3. Open the needle valve.
4. Open the check valve.
5. Follow the lines to the check valve that intersects with the hydrogen pathway. Open the check valve that leads to the hydrogen lines. This check valve has a green handle.
6. <u>If using the flow controller</u>, follow the instructions above for the use of the flow controller. <u>If not using the flow controller</u>, open the bypass check valve.
7. Open the remaining check valve.
8. <u>If using the flow controller</u>, open the back pressure regulator completely. <u>If not using the flow controller</u>, use the back pressure regulator to adjust the pressure and flow rate of the stream as desired.   If leaving the cell running with nitrogen overnight, a flow controller setting of about 10 is sufficient.

<u>Stopping Feed</u>

1. Close the globe valve on the nitrogen tank.
2. Adjust pressure regulator to little/no pressure.
3. Close the needle valve.
4. Close the check valve.
5. Follow the lines to the check valve that intersects with the hydrogen pathway. Close the check valve that leads to the hydrogen lines. This check valve has a green handle.
6. <u>If using the flow controller</u>, close valve 2 and turn off the flow controller. <u>If not using the flow controller</u>, close the bypass check valve.

7. Close the remaining check valve.
8. Close the back pressure regulator completely.

A.5.4: Nitrogen to the Cathode

<u>Starting Feed</u>

1. Open the globe valve on the nitrogen tank.
2. Adjust pressure regulator to desired stream pressure.
3. Open the needle valve.
4. Open the check valve.
5. Follow the lines to the check valve that intersects with the oxygen pathway. Open the check valve that leads to the hydrogen lines. This check valve has a red handle.
6. <u>If using the flow controller</u>, follow the instructions above for the use of the flow controller. <u>If not using the flow controller</u>, open the bypass check valve.
7. <u>If using the flow controller</u>, open the back pressure regulator completely. <u>If not using the flow controller</u>, use the back pressure regulator to adjust the pressure and flow rate of the stream as desired. If leaving the cell running with nitrogen overnight, a flow controller setting of about 10 is sufficient.

<u>Stopping Feed</u>

1. Close the globe valve on the nitrogen tank.
2. Adjust pressure regulator to little/no pressure.
3. Close the needle valve.
4. Close the check valve.
5. Follow the lines to the check valve that intersects with the oxygen pathway. Close the check valve that leads to the hydrogen lines. This check valve has a red handle.
6. <u>If using the flow controller</u>, close valve 1 and turn off the flow controller. <u>If not using the flow controller</u>, close the bypass check valve.
7. Close the back pressure regulator completely.

A.5.5: Methanol to the Anode (Nafion®)

<u>Starting Feed</u>

1. Check that there is enough methanol in pump.
2. Follow directions for filling the pump if necessary.
3. Adjust temperature for bottom section of feed line.
4. Open methanol feed check valve.
5. Follow directions for running methanol feed from pump.

Stopping Feed

1. Stop syringe pump.
2. Return temperature setting to room temp or below.
3. Close methanol feed check valve.

Appendix B: Experimental Procedure, Fabrication of a Membrane-Electrode Assembly

GDL and Electrode Preparation

The GDL material used, ETEK LT1400, already has an MPL deposited. To use, the GDL was simply cut into the proper shape and size before being used.

Membrane Activation

The PEM used was a Nafion membrane obtained from ElectroChem, Inc. More specifically, the Nafion membrane, manufactured by DuPont, is a transparent nonreinforced film based on Nafion PFSA polymer, a perfluorosulfonic acid/PTFE copolymer in acid form. The thickness of the Nafion membrane used was one of the following:

- Nafion membrane N1035, (1000EW, 3.5 mil thick)
- The EC-NM-115 N115 membrane (1100 EW, 5 mil thick)
- Nafion membrane N117 (1100 EW, 7 mil thick)
- Nafion membrane N1110, (1100EW, 10 mil thick)

The Nafion membrane was cut into 5 cm by 5 cm squares with scissors. Using tweezers, the Nafion membrane was inserted into a Pyrex® beaker with deionized water at a low boil for about an hour. The Nafion membrane is then transferred to a beaker with 3 wt% hydrogen peroxide for 0.5 hours at a low boil. This was to allow for hydrogen peroxide to oxidize the organic impurities upon the surface the Nafion membranes. Following the hydrogen peroxide treatment was another half-hour of deionized water at a low boil, then 1 hour in 0.5 M sulfuric acid at a low boil. The sulfuric acid protonates the sulfonic acid sites in the Nafion, allowing proton transport to occur. Afterwards, the Nafion membrane was once again submerged in deionized water at a low boil for another hour. It was critical to maintain a low boil throughout the entire process; rapid boiling causes damage to the membrane surface.

Hot-Pressing

After preparing the Nafion membranes, an optional step is to press them, bookended by Kim Wipes, in the Carver hot press without heat or excess force for five minutes. This was done to flatten out the Nafion membranes and ease the process of the electrode addition.

After the Nafion membranes were pressed, the Carver hot press was heated up to 275°F (130°C). The Nafion membranes, along with the anode and cathode electrodes, were sandwiched by two Teflon sheets and then placed in the hot press for two minutes with an applied force ranging from 1 to 5 tons.

After that time, the newly created MEAs were allowed to cool for 10 minutes before being properly stored (sealed, labeled plastic bag in a dark, cool place) for future use.

Appendix C: Experimental Procedure, Electrospinning

Solution Fabrication

The solution fabrication method is described in the methodological text; however, it will be briefly summarized here. First, define the targets of the solution; namely, wt% Nafion and polymer wt% PEO. These two characteristics will be the main factors in preparing this solution.

1. Set a basis, of either 10g or 10mL of solution. 5g is the minimum suggested initial target.
2. Calculate how much Nafion will be needed, understanding that the Nafion in the lab is in ethanol at 13.581wt%.
3. Once this is calculated, we know the mass of Nafion and ethanol in the system. The PEO, in solution (0.025g PEO / 1g solution [1:1 1-propanol/HOH]) that is needed can then be calculated, knowing the set polymer wt% of this solution.
4. This brings us to have a solution containing ethanol, 1-propanol, water, the correct weight of Nafion and the correct weight of PEO.
5. To obtain the proper Nafion wt%, solvent (of your choice/design) will either needed to be added, or to be removed. Adding solvent is straightforward. To remove solvent, mix all the components, weighed out, in an 8-dram vial.
6. Take the mass of this; if the mass is known, and the components are known, we have a value for mass corresponding to a wt%.
7. Cap, and shake well for 3 minutes.
8. To drive off solvent, uncap the vial and leave standing. Measure the mass over time; as it decreases, it is assumed that ethanol, if not 1-propanol and water, are leaving the system.
9. Assuming all ethanol evaporation, once can, based on a new weight, calculate the amount of solvent lost and, therefore, the new wt%. Do not try to accelerate this process with heat; it forms a precipitate, thought to be crystalline Nafion even at gentle temperatures.
10. Once the proper weight is achived, cap the solution and use for the electrospinning trials as soon as practical. Before use, weigh the sample to check how much additional solvent has evaporated.

GDL/Collection Plate Preparation

The collection plate must be covered, to protect it and prevent any buildup from compromising the flat surface. This can be done with aluminum foil, or, in the case of making an electrode, GDL material. There are two main focuses here: the surface to be electrospun onto must be 1) flat and 2) connected to the collection plate with a clear conduction path to the surface. If

either one of these criteria is not met, the electrospun jet will discharge to the closest grounded surface, which could be the inner faces of the box or back towards the syringe pump.

The 10cm x 10cm collection plate can be covered with the material to be spun on, or layered with gasket material to limit the area that will have proper conduction. The layers, as well as with the top layer, should be tapped down along the edges of the collection plate to ensure it is both flat and secured correctly. The green lab tape was used, but clear Scotch-brand tape can also be used. Once affixed, it can be loaded into the chamber and used. Once the run is done, untape the surface and be careful not to disrupt the fibers on the surface.

Electrospinning Apparatus

The electrospinning apparatus consists of a syringe pump, DC power supply, circuit breaker, collection plate and encasing plexiglass box, as well as sectioned-off electronic wiring.

Syringe Pump Operation

The syringe pump in the lab will depress a syringe at a certain, defined rate down to 0.05 mL/hr. When the syringe pump is in operation, a small arrow will blink, indicating there is flow. To set a flowrate, scroll through the options using the "A" key until you see rate. Pressing the up and down arrow keys will increase the value of the rate, displayed in mL/hr. When a flowrate is set, depressing the "Run" key will start the pump operation. The pump will move the large, solid, black piece from left to right. To properly load the syringe, place the needle facing to the right, and nest it into the space provided. The body of the syringe should be flat, with the end of the syringe, the part that tapers/flares out, should be forced tightly, pushing to the right, against the pump body

Once loaded, the unit can be maneuvered to fit into the hole drilled into the plexiglass box. When electrospinning, the needle inside the box will be hooked up to the alligator clip that conducts

the electricity generated by the DC generator, so be sure to load at least two inches of needle into the box.

Voltage Regulator

The voltage regulator, or DC power generator, has an on/off switch as well as a twisiting top that acts as the potentiometer, controlling the amount of voltage generated. Before the first run, twist the top both clock and counter clockwise to understand both how the unit works as well as where the chock is for zero volts generated; this is also marked on the body of the unit.

Run Protocol

1. Open up the plexiglass box, and affix the GDL to the aluminum ground plate.
2. Set the correct distance to the collection plate. This can be fine-tuned later on, once the needle is in the correct position.
3. Obtain and, if necessary, clean a 22-gauge needle tip with proper solvent (compatible with the system to be spun)
4. Attach to a syringe, flush with water to ensure proper syringe and needle tip operation, checking for any blockages or leaks between the needle-syringe interface
5. Draw ~2-3 mL of solution into the syringe, ensuring no air is entrapped. This will take several attempts due to the high viscosity of the sample
6. Ensure the main 30 amp circuit breaker is in the "Off" position; if on, the light bulb will be on.
7. Secure the syringe firmly into the syringe pump, and lock down the syringe.
8. Move the syringe pump to ensure the needle is inside the plexiglass box, and is aligned correctly with the collector plate.
9. Check the tip-to-collector distance, and modify if needed.
10. Gently depress the syringe plunger to force a small amount of solution out of the needle. A small droplet on the tip is needed.
11. Attach, by hand, the alligator-clip lead to the middle of the needle.
12. Set the flow rate desired on the syringe pump, and set to "run". As indicated in the instructions above, the small arrow on the Home screen will start to blink when running
13. Ensure the voltage generator is turned to produce 0 V, and turn on the multimeter.
14. Turn on the main breaker.
15. Slowly increase the voltage by turning the top of the DC power supply clockwise. Monitor the voltage level on the multimeter. When the fibers start to spin from the Taylor cone, stop increasing the voltage and take note of the value.
16. Watch the run carefully. If fibers stagnate and dry, or do not form at all, the flowrate, applied electric potential or the tip-to-collector distance will need to be modified.
17. When done, decrease the electric potential, turn off the main breaker, and wait for the applied voltage to wind down to zero.
18. Turn off the syringe pump, and gently open the plexiglass box.

19. With the screwdriver, touch the spinneret tip to ensure proper discharge has completed.
20. Remove the alligator clip lead, and remove the GDL from the collector plate.

Safety

There are a number of key safety points to be made when using the electrospinning equipment.

- Don't go in alone: always have the supervision of one of the graduate students well-versed in the electrospinning process in the room.
- Verify with Rita, the secretary of the Material Science Department, that you are using the setup.
- Make sure to shake the solution well before drawing a sample. Non-homogeneity in the solution will cause the spun fibers to be different compared to those spun with a solution with the value on the vial.
- Make sure that the main breaker is off, and the DC generator is set to zero at all times other than during the run.
- Make very small perturbations to the electric potential applied. Large changes can damage the equipment.
- Never exceed 20 kV on the current electrospinning setup.
- Always close the box fully before operation.
- Always have the multimeter on, to ensure that there is no loose electricity coursing through the circuitry.

Appendix D: Raw Data, MEA Testing

All tests performed at standard procedures (1M MeOH @ 1.5mL/min or H_2/O_2 at 7 psig) unless otherwise noted.

MEA #11							
H2/O2				**MeOH**			
Voltage	**Current**	**Current Density**	**Power Density**	**Voltage**	**Current**	**Current Density**	**Power Density**
0	0.82	0	0	0	0.47	0	0
0.01	0.77	2	1.54	0.01	0.39	2	0.78
0.03	0.72	6	4.32	0.03	0.35	6	2.1
0.05	0.71	10	7.1	0.05	0.34	10	3.4
0.08	0.7	16	11.2	0.06	0.34	12	4.08
0.1	0.68	20	13.6	0.08	0.31	16	4.96
0.15	0.68	30	20.4	0.1	0.3	20	6
0.2	0.67	40	26.8	0.15	0.27	30	8.1
0.25	0.65	50	32.5	0.17	0.25	34	8.5
0.3	0.61	60	36.6	0.2	0.23	40	9.2
0.35	0.58	70	40.6	0.22	0.21	44	9.24
0.4	0.57	80	45.6	0.25	0.19	50	9.5
0.45	0.55	90	49.5	0.3	0.15	60	9
0.5	0.53	100	53	0.32	0.11	64	7.04
0.55	0.52	110	57.2	0.35	0.07	70	4.9
0.6	0.5	120	60	0.37	0.03	74	2.22
0.65	0.49	130	63.7	0.38	0	76	0
0.7	0.47	140	65.8				
0.75	0.45	150	67.5				
0.8	0.41	160	65.6				
0.85	0.37	170	62.9				
0.9	0.33	180	59.4				
0.95	0.3	190	57				
1	0.27	200	54				
1.05	0.21	210	44.1				
1.1	0.11	220	24.2				
1.15	0.05	230	11.5				
1.18	0	236	0				

E. MEA Total							
H2/O2				MeOH			
Voltage	Current	Current Density	Power Density	Voltage	Current	Current Density	Power Density
1.03	0	0	0	0.7	0	0	0
0.95	0.01	2	1.9	0.63	0.01	2	1.26
0.93	0.03	6	5.58	0.6	0.03	6	3.6
0.89	0.05	10	8.9	0.55	0.05	10	5.5
0.88	0.06	12	10.56	0.53	0.06	12	6.36
0.88	0.08	16	14.08	0.5	0.08	16	8
0.86	0.1	20	17.2	0.47	0.1	20	9.4
0.84	0.11	22	18.48	0.45	0.11	22	9.9
0.84	0.13	26	21.84	0.45	0.13	26	11.7
0.83	0.15	30	24.9	0.44	0.15	30	13.2
0.83	0.16	32	26.56	0.42	0.16	32	13.44
0.82	0.18	36	29.52	0.41	0.18	36	14.76
0.82	0.2	40	32.8	0.39	0.2	40	15.6
0.79	0.25	50	39.5	0.37	0.21	42	15.54
0.76	0.3	60	45.6	0.35	0.23	46	16.1
0.74	0.35	70	51.8	0.34	0.25	50	17
0.72	0.4	80	57.6	0.33	0.26	52	17.16
0.7	0.45	90	63	0.31	0.28	56	17.36
0.65	0.5	100	65	0.29	0.3	60	17.4
0.63	0.55	110	69.3	0.24	0.35	70	16.8
0.61	0.6	120	73.2	0.18	0.4	80	14.4
0.57	0.65	130	74.1	0.15	0.45	90	13.5
0.56	0.7	140	78.4	0.11	0.5	100	11
0.52	0.75	150	78	0.07	0.55	110	7.7
0.5	0.8	160	80	0	0.57	114	0
0.45	0.85	170	76.5				
0.43	0.9	180	77.4				
0.4	0.95	190	76				
0.36	1	200	72				
0.3	1.05	210	63				
0.23	1.1	220	50.6				
0.07	1.2	240	16.8				
0	1.22	244	0				

E. MEA 1							
H2/O2				**MeOH**			
Voltage	Current	Current Density	Power Density	Voltage	Current	Current Density	Power Density
1.02	0	0	0	0.68	0	0	0
0.93	0.01	2	1.86	0.6	0.01	2	1.2
0.9	0.03	6	5.4	0.55	0.03	6	3.3
0.88	0.05	10	8.8	0.53	0.05	10	5.3
0.87	0.06	12	10.44	0.52	0.06	12	6.24
0.87	0.08	16	13.92	0.5	0.08	16	8
0.85	0.1	20	17	0.49	0.1	20	9.8
0.83	0.11	22	18.26	0.47	0.11	22	10.34
0.83	0.13	26	21.58	0.45	0.13	26	11.7
0.82	0.15	30	24.6	0.44	0.15	30	13.2
0.82	0.16	32	26.24	0.44	0.16	32	14.08
0.82	0.18	36	29.52	0.42	0.18	36	15.12
0.82	0.2	40	32.8	0.4	0.2	40	16
0.78	0.25	50	39	0.39	0.21	42	16.38
0.75	0.3	60	45	0.39	0.23	46	17.94
0.72	0.35	70	50.4	0.37	0.25	50	18.5
0.7	0.4	80	56	0.35	0.26	52	18.2
0.67	0.45	90	60.3	0.34	0.28	56	19.04
0.65	0.5	100	65	0.32	0.3	60	19.2
0.6	0.55	110	66	0.29	0.35	70	20.3
0.57	0.6	120	68.4	0.25	0.4	80	20
0.53	0.65	130	68.9	0.24	0.45	90	21.6
0.52	0.7	140	72.8	0.2	0.5	100	20
0.49	0.75	150	73.5	0.17	0.55	110	18.7
0.47	0.8	160	75.2	0.14	0.6	120	16.8
0.45	0.85	170	76.5	0.1	0.63	126	12.6
0.44	0.9	180	79.2	0.09	0.65	130	11.7
0.42	0.95	190	79.8	0.05	0.7	140	7
0.42	1	200	84	0.02	0.73	146	2.92
0.39	1.05	210	81.9	0	0.75	150	0
0.35	1.1	220	77				
0.24	1.2	240	57.6				
0.2	1.25	250	50				
0.1	1.3	260	26				
0	1.35	270	0				

E. MEA 3							
H2/O2				**MeOH**			
Voltage	**Current**	**Current Density**	**Power Density**	**Voltage**	**Current**	**Current Density**	**Power Density**
1.03	0	0	0	0.65	0	0	0
0.99	0.01	2	1.98	0.61	0.01	2	1.22
0.95	0.03	6	5.7	0.55	0.03	6	3.3
0.9	0.05	10	9	0.53	0.05	10	5.3
0.88	0.06	12	10.56	0.53	0.06	12	6.36
0.88	0.08	16	14.08	0.5	0.08	16	8
0.87	0.1	20	17.4	0.47	0.1	20	9.4
0.85	0.11	22	18.7	0.47	0.11	22	10.34
0.85	0.13	26	22.1	0.45	0.13	26	11.7
0.83	0.15	30	24.9	0.43	0.15	30	12.9
0.83	0.16	32	26.56	0.43	0.16	32	13.76
0.82	0.18	36	29.52	0.4	0.18	36	14.4
0.82	0.2	40	32.8	0.37	0.2	40	14.8
0.8	0.25	50	40	0.35	0.21	42	14.7
0.77	0.3	60	46.2	0.35	0.23	46	16.1
0.75	0.35	70	52.5	0.31	0.25	50	15.5
0.73	0.4	80	58.4	0.3	0.26	52	15.6
0.72	0.45	90	64.8	0.28	0.28	56	15.68
0.7	0.5	100	70	0.25	0.3	60	15
0.68	0.55	110	74.8	0.18	0.35	70	12.6
0.65	0.6	120	78	0.13	0.4	80	10.4
0.63	0.65	130	81.9	0.07	0.45	90	6.3
0.6	0.7	140	84	0.02	0.5	100	2
0.57	0.75	150	85.5	0	0.55	110	0
0.53	0.8	160	84.8				
0.5	0.85	170	85				
0.46	0.9	180	82.8				
0.43	0.95	190	81.7				
0.39	1	200	78				
0.36	1.05	210	75.6				
0.32	1.1	220	70.4				
0.18	1.2	240	43.2				
0.11	1.25	250	27.5				
0	1.3	260	0				

300% MEA							
H2/O2				MeOH			
Voltage	Current	Current Density	Power Density	Voltage	Current	Current Density	Power Density
1	0	0	0	0.52	0	0	0
0.95	0.01	2	1.9	0.42	0.01	2	0.84
0.92	0.03	6	5.52	0.35	0.03	6	2.1
0.9	0.05	10	9	0.32	0.05	10	3.2
0.88	0.06	12	10.56	0.3	0.06	12	3.6
0.87	0.1	20	17.4	0.27	0.08	16	4.32
0.85	0.11	22	18.7	0.25	0.1	20	5
0.85	0.13	26	22.1	0.24	0.11	22	5.28
0.83	0.15	30	24.9	0.22	0.13	26	5.72
0.82	0.16	32	26.24	0.2	0.15	30	6
0.82	0.18	36	29.52	0.19	0.16	32	6.08
0.8	0.2	40	32	0.19	0.18	36	6.84
0.77	0.25	50	38.5	0.17	0.2	40	6.8
0.77	0.3	60	46.2	0.15	0.21	42	6.3
0.73	0.35	70	51.1	0.14	0.23	46	6.44
0.72	0.4	80	57.6	0.1	0.25	50	5
0.7	0.45	90	63	0.1	0.26	52	5.2
0.68	0.5	100	68	0.09	0.28	56	5.04
0.67	0.55	110	73.7	0.07	0.3	60	4.2
0.65	0.6	120	78	0.07	0.31	62	4.34
0.63	0.65	130	81.9	0.04	0.33	66	2.64
0.63	0.7	140	88.2	0.04	0.35	70	2.8
0.58	0.75	150	87	0.02	0.36	72	1.44
0.58	0.8	160	92.8	0	0.38	76	0
0.57	0.85	170	96.9				
0.55	0.9	180	99			From H2/O2	
0.53	0.95	190	100.7	0.29	1.65	330	95.7
0.52	1	200	104	0.25	1.7	340	85
0.5	1.05	210	105	0.24	1.75	350	84
0.49	1.1	220	107.8	0.2	1.8	360	72
0.49	1.15	230	112.7	0.19	1.85	370	70.3
0.47	1.2	240	112.8	0.19	1.9	380	72.2
0.45	1.25	250	112.5	0.17	1.95	390	66.3
0.44	1.3	260	114.4	0.14	2	400	56
0.42	1.35	270	113.4	0.14	2.05	410	57.4
0.37	1.4	280	103.6	0.1	2.1	420	42
0.37	1.45	290	107.3	0.09	2.15	430	38.7
0.35	1.5	300	105	0.07	2.2	440	30.8
0.32	1.55	310	99.2	0.05	2.25	450	22.5
0.32	1.6	320	102.4	0	2.3	460	0

FCS MEA (Commercial, Fuel Cell Store)							
H2/O2				**MeOH**			
Voltage	**Current**	**Current Density**	**Power Density**	**Voltage**	**Current**	**Current Density**	**Power Density**
1.02	0	0	0	0.67	0	0	0
0.97	0.01	2	1.94	0.57	0.01	2	1.14
0.93	0.03	6	5.58	0.53	0.03	6	3.18
0.92	0.05	10	9.2	0.5	0.05	10	5
0.9	0.06	12	10.8	0.47	0.08	16	7.52
0.88	0.08	16	14.08	0.45	0.1	20	9
0.875	0.1	20	17.5	0.44	0.11	22	9.68
0.87	0.11	22	19.14	0.42	0.13	26	10.92
0.85	0.13	26	22.1	0.4	0.15	30	12
0.85	0.15	30	25.5	0.39	0.16	32	12.48
0.85	0.16	32	27.2	0.37	0.18	36	13.32
0.83	0.18	36	29.88	0.35	0.2	40	14
0.82	0.2	40	32.8	0.3	0.25	50	15
0.8	0.25	50	40	0.27	0.3	60	16.2
0.78	0.3	60	46.8	0.25	0.35	70	17.5
0.77	0.35	70	53.9	0.22	0.4	80	17.6
0.74	0.4	80	59.2	0.2	0.45	90	18
0.73	0.45	90	65.7	0.19	0.5	100	19
0.72	0.5	100	72	0.15	0.55	110	16.5
0.68	0.55	110	74.8	0.14	0.6	120	16.8
0.67	0.6	120	80.4	0.12	0.65	130	15.6
0.65	0.65	130	84.5	0.09	0.7	140	12.6
0.635	0.7	140	88.9	0.07	0.75	150	10.5
0.62	0.75	150	93	0.05	0.8	160	8
0.6	0.8	160	96	0.02	0.85	170	3.4
0.6	0.85	170	102	0	0.9	180	0
0.58	0.9	180	104.4				
0.57	0.95	190	108.3				
0.55	1	200	110				
0.53	1.05	210	111.3				
0.52	1.1	220	114.4				
0.5	1.15	230	115				
0.49	1.2	240	117.6				
0.48	1.25	250	120				
0.47	1.3	260	122.2				
0.44	1.35	270	118.8				
0.42	1.4	280	117.6				

0.42	1.45	290	121.8
0.4	1.5	300	120
0.39	1.55	310	120.9
0.37	1.6	320	118.4
0.34	1.65	330	112.2
0.34	1.7	340	115.6
0.34	1.75	350	119
0.32	1.8	360	115.2
0.32	1.85	370	118.4
0.3	1.9	380	114
0.29	1.95	390	113.1
0.27	2	400	108
0.25	2.05	410	102.5
0.24	2.1	420	100.8
0.24	2.15	430	103.2
0.22	2.2	440	96.8
0.2	2.25	450	90
0.2	2.3	460	92
0.19	2.35	470	89.3
0.19	2.4	480	91.2
0.17	2.45	490	83.3
0.17	2.5	500	85
0.17	2.55	510	86.7
0.14	2.6	520	72.8
0.12	2.7	540	64.8
0.1	2.8	560	56
0	2.9	580	0

MEA #7							
H2/O2				**MeOH**			
Voltage	**Current**	**Current Density**	**Power Density**	**Voltage**	**Current**	**Current Density**	**Power Density**
0.85	0	0	0	0.45	0	0	0
0.83	0.01	2	1.66	0.42	0.01	2	0.84
0.82	0.03	6	4.92	0.39	0.03	6	2.34
0.8	0.05	10	8	0.37	0.05	10	3.7
0.8	0.06	12	9.6	0.35	0.06	12	4.2
0.78	0.08	16	12.48	0.35	0.08	16	5.6
0.77	0.1	20	15.4	0.34	0.1	20	6.8
0.75	0.11	22	16.5	0.3	0.15	30	9
0.73	0.13	26	18.98	0.29	0.18	36	10.44
0.72	0.15	30	21.6	0.27	0.2	40	10.8
0.72	0.2	40	28.8	0.25	0.22	44	11
0.72	0.25	50	36	0.24	0.25	50	12
0.7	0.3	60	42	0.2	0.3	60	12
0.65	0.4	80	52	0.19	0.35	70	13.3
0.62	0.5	100	62	0.17	0.37	74	12.58
0.57	0.6	120	68.4	0.15	0.4	80	12
0.53	0.7	140	74.2	0.14	0.41	82	11.48
0.5	0.8	160	80	0.12	0.43	86	10.32
0.44	0.9	180	79.2	0.1	0.45	90	9
0.37	1	200	74	0.09	0.46	92	8.28
0.25	1.1	220	55	0.07	0.48	96	6.72
0.14	1.2	240	33.6	0.05	0.5	100	5
0.07	1.3	260	18.2	0.04	0.51	102	4.08
0	1.35	270	0	0.02	0.53	106	2.12
				0	0.55	110	0

MECC MECC CO., LTD.
196-1 FUKUDO, OGORI-SHI, FUKUOKA 838-0137 JAPAN

Phone: +81-942-41-2200
Fax: +81-942-41-2205

Quotation

To:	Worcester Polytechnic Institute		Date:	2011/9/1
	Mr.Matthew S. Perrone		No.	QSD11-032

Dear Sir / Madam,

We have the pleasure in quoting you as follows:

Item No.	Description	Q'ty	Unit Price	Amount
1	Electrospinning Setup Main unit Model : SD-02 (Mechanical unit,Plate collector) Except HV PS UNIT,Syringe pump Options	1	US$6,000.00	US$6,000.00
2	HV PS UNIT	1	US$5,000.00	US$5,000.00
3	Syringe pump	1	US$3,500.00	US$3,500.00
4	Plate collector	1	US$2,000.00	US$2,000.00
5	Clip Spinnneret	1	US$4,000.00	US$4,000.00
6	Transportation cost(without Tax)	1	US$3,000.00	US$3,000.00
	Note.Not include Draft chamber Note;Not include installation fee			
	SUB TOTAL		US$23,500.00	US$23,500.00
			US$23,500.00	US$23,500.00

End User:	-
Payment Terms:	L/C at sight with 100% value
Place of Delivery	-
Shipment:	CIF
Ship to:	As Designated
Ship via:	As Designated
Packing:	Standard Export Packing
Validity:	90 Days from this Date
Time of Shipments	2month ARO
Warranty:	

Best Regards,

Chikashi   Naito

E-mail;   naitoh@mecc.co.jp

Electrospinz Limited
44 Lee Street
Blenheim 7201
New Zealand

Electrospinz
nanofibre engineering

5 October 2011

<u>**Quotation Number 110062**</u>

For:

Matthew S Perrone

Qty	Description	Unit Price	Total
1	ES1a Electrospinning Platform	$14,000.00	$14,000.00
1	Packing and freight (via DHL) for ES1a	$1,500.00	$1,500.00
	Total for ES1a		$15,500.00
1	ES4 Electrospinning Platform	$25,000.00	$25,000.00
1	Packing and freight (via DHL) for ES4	$2,500.00	$2,500.00
	Total for ES4		$27,500.00

All prices are expressed in New Zealand dollars ($NZ).
All taxes and duties outside New Zealand are to be to be paid by the Customer.
Lead time to manufacture is 6 to 8 weeks from receipt of the order.
This Quote is subject to the Terms and Conditions of Trade as attached.

Quotation prepared by:
    Neil (CJ) Buunk,
    Director,
    Electrospinz Limited.

Appendix F: Applicable MSDS Forms